2007

Error equivalence theory for manufacturing process control

Hui Wang
University of South Florida

Error Equivalence Theory for Manufacturing Process Control

by

Hui Wang

A dissertation submitted in partial fulfillment of
the requirements for the degree of
Doctor of Philosophy
Department of Industrial and Management Systems Engineering
College of Engineering
University of South Florida

Major Professor: Qiang Huang, Ph.D.
Shekhar Bhansali, Ph.D.
Tapas K. Das, Ph.D.
Yuncheng You, Ph.D.
José L. Zayas-Castro, Ph.D.

Date of Approval:
April 17, 2007

Keywords: error cancellation, process modeling, root cause identification, automatic process adjustment, statistical quality control

Dedication

To my parents.

Acknowledgements

I would like to express my sincere gratitude to Prof. Qiang Huang, my advisor, for sharing his insightful ideas in research, for providing continual encouragement and critical mentoring. Prof. Huang's innovative ideas, broad and in-depth knowledge in manufacturing and applied statistics have been a great inspiration to me. Without him, I would not be able to accomplish what I have accomplished. Throughout my four-year PhD studies, he has always been wholeheartedly supporting me to steer through countless difficulties in all aspects of my life.

I want to thank my dissertation committee members, Prof. Tapas K. Das, Prof. José Zayas-Castro, Prof. Shekhar Bhansali, and Prof. Yuncheng You for their valuable suggestions and assistance. I wish to thank Prof. Louis Martin-Vega and Prof. A.N.V. Rao for their constructive suggestions when they were my dissertation committee members. I am also grateful to Dr. Reuven Katz from the University of Michigan for his advice on clarifying several vague concepts in Chapter Two.

Special thanks are given to all other faculty members, Ms. Gloria Hanshaw, Ms. Jackie Stephens, and Mr. Chris Paulus in the IMSE department for their kind help during my Ph.D. studies.

In addition, I would like to express my sincere appreciation to my friends, Mr. Shaoqiang Chen, Mr. Xi Zhang, Ms. Diana Prieto, Mr. Yang Tan, and other fellow IMSE graduate students.

Finally, I am forever indebted to my wonderful parents Zulin Chen and Yongkang Wang. I would have never finished this dissertation without their endless love, encouragement and unconditional support. I owe them so much.

Table of Contents

List of Tables

List of Figures

Error Equivalence Theory For Manufacturing Process Control

Hui Wang

ABSTRACT

Due to uncertainty in manufacturing processes, applied probability and statistics have been widely applied for quality and productivity improvement. In spite of significant achievements made in causality modeling for control of process variations, there exists a lack of understanding on error equivalence phenomenon, which concerns the mechanism that different error sources result in identical variation patterns on part features. This so called error equivalence phenomenon could have dual effects on dimensional control: significantly increasing the complexity of root cause identification, and providing an opportunity to use one error source to counteract or compensate the others.

Most of previous research has focused on analyses of individual errors, process modeling of variation propagation, process diagnosis, reduction of sensing noise, and error compensation for machine tool. This dissertation presents a mathematical formulation of the error equivalence to achieve a better, insightful understanding, and control of manufacturing process.

The first issue to be studied is mathematical modeling of the error equivalence phenomenon in manufacturing to predict product variation. Using kinematic analysis and analytical geometry, the research derives an error equivalence model that can transform

different types of errors to the equivalent amount of one base error. A causal process model is then developed to predict the joint impact of multiple process errors on product features.

Second, error equivalence analysis is conducted for root cause identification. Based on the error equivalence modeling, this study proposes a sequential root cause identification procedure to detect and pinpoint the error sources. Comparing with the conventional measurement strategy, the proposed sequential procedure identifies the potential error sources more effectively.

Finally, an error-canceling-error compensation strategy with integration of statistical quality control is proposed. A novel error compensation approach has been proposed to compensate for process errors by controlling the base error. The adjustment process and product quality will be monitored by quality control charts. Based on the monitoring results, an updating scheme is developed to enhance the stability and sensitivity of the compensation algorithm. These aspects constitute the “Error Equivalence Theory”. The research will lead to new analytical tools and algorithms for continuous variation reduction and quality improvement in manufacturing.

Chapter 1

Introduction

The intense global competition has been driving the manufacturers to continuously improve quality in the life cycle of product design and manufacturing. Vital to the competition success is the product variation reduction to achieve the continuous manufacturing process improvement. However, variation reduction for the process improvement has been an extremely challenging issue because of the following reasons:

- *Prediction of quality performance with process variation.* Due to the uncertain nature of the manufacturing process, probabilistic models and statistics have been widely applied to depict the process variation. However, there exists a lack of understanding on "error equivalence", an engineering phenomenon concerning the mechanism that multiple error sources result in the identical variation pattern. This fact impacts almost every stage of variation control (e.g., process root cause diagnosis and error compensation). Therefore, to better predict the process performance, error equivalence has to be quantitatively modeled and analyzed.
- *Control of a varying process.* Variation control strategies must be incorporated in the early stage of manufacturing process design. The control strategy involves statistical quality control (SQC), root cause identification and automatic process error compensation to reduce potential large variations. The dual effects of error equivalence on process control have not been well studied. For instance, the phenomenon of error equivalence could conceal the information of multiple errors

and thus significantly increase the complexity of root cause identification (diagnosis). It may provide an opportunity to purposely use one error source to counteract the others and thereby reduce overall process variations. Hence, the inclusion of error equivalence mechanism into quality control may create a new control paradigm of manufacturing process, i.e., information collection in support of process diagnosis, root cause identification, and SPC (statistical process control) integrated process error compensation.

Therefore, the aforementioned issues entail an essential analysis of error equivalence for process improvement. The goal of this work is to model the error equivalence in traditional discrete manufacturing to achieve an insightful understanding of process variation and a better process control.

1.1 Phenomena of Error Equivalence in Manufacturing Processes

In a manufacturing process, product quality can be affected by multiple error sources. For example, the dominant root cause of quality problems in a machining process includes fixture, datum, and machine tool errors. A fixture is a device used to locate, clamp, and support a workpiece during machining, assembly, or inspection. Fixture error is considered to be a significant fixture deviation of a locator from its specified position. Machining datum surfaces are those part features that are in direct contact with the fixture locators. Datum error is deemed to be the significant deviation of datum surfaces and is mainly induced by imperfections in raw workpieces or faulty operations in the previous stages. Together the fixture and datum surfaces provide a reference system for accurate cutting operations using machine tools. Machine tool error

is modeled in terms of significant tool path deviations from its intended route. This dissertation mainly focuses on kinematic aspects of these three error types.

A widely observed engineering phenomenon is that the individual error sources can result in the identical variation patterns on product features in manufacturing process. For instance, in a machining process, all aforementioned process deviations can generate the same amount of feature deviation **x** as shown in Fig. 1.1 (Wang, Huang, and Katz, 2005; and Wang and Huang, 2006). This error equivalence phenomenon is also observed in many other manufacturing processes, e.g., the automotive body assembly process (Fig. 1.2, Ding, *et al.*, 2005).

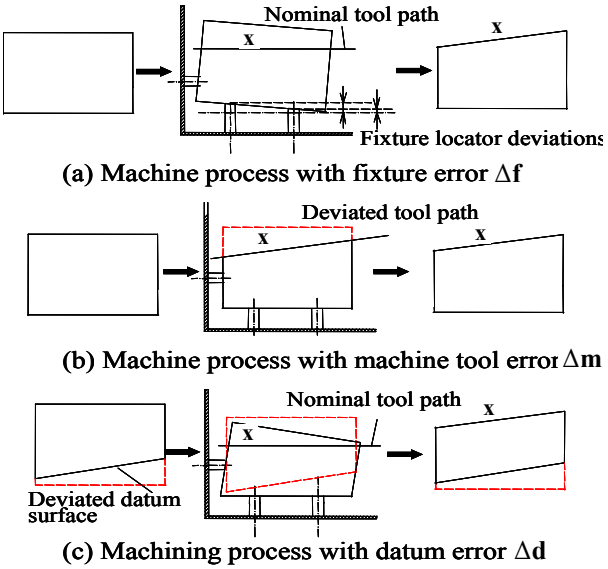

Figure 1.1 Error Equivalence in Machining

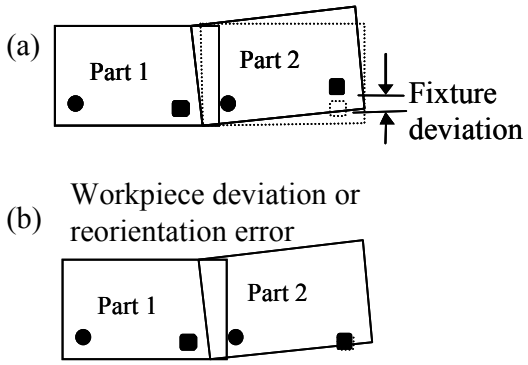

Figure 1.2 Error Equivalence in Assembly

The impact of such an error equivalence phenomenon on manufacturing process control is twofold. On the one hand, it significantly increases the complexity of variation control. As an example, identifying the root causes becomes extremely challenging when different error sources are able to produce the identical dimensional variations. On the other hand, the error equivalence phenomenon provides an opportunity to purposely use

one error source to counteract another in order to reduce process variation. In both cases, a fundamental understanding of this complex engineering phenomenon will assist to improve manufacturing process control.

1.2 Related Work and the State of the Arts

The study on error equivalence is, however, very limited. Most related research on process error modeling has been focused on the analysis of the individual error sources, e.g., the fixture errors and machine tool errors, how these errors impact the product quality, and thereby how to diagnose the errors and reduce variation by process control. This section reviews the related research on process errors modeling, diagnosis and control.

1.2.1 Research Review for Modeling Process Errors

Fixture error. Fixture error has been considered as one of crucial factors in the optimal fixture design and analysis. Shawki and Abdel-Aal (1965) experimentally studied the impact of fixture wear on the positional accuracy of the workpiece. Asada and By (1985) proposed kinematic modeling, analysis, and characterization of adaptable fixturing. Screw theory has been developed to estimate the locating accuracy under the rigid body assumption (Ohwovoriole, 1981). Weil, Darel, and Laloum (1991) then developed several optimization approaches to minimize the workpiece positioning errors. A robust fixture design was proposed by Cai, Hu, and Yuan (1997) to minimize the positional error. Marin and Ferreira (2003) analyzed the influence of dimensional locator errors on tolerance allocation problem. Researchers also considered the geometry of datum surface for the fixture design. Optimization of locating setup proposed by Weil, *et al.* (1991) was

based on the locally linearized part geometry. Choudhuri and De Meter (1999) considered the contact geometry between the locators and workpiece to investigate the impact of fixture locator tolerance scheme on geometric error of the feature.

Machine tool error. Machine tool error can be due to thermal effect, cutting force, and geometric error of machine tool. Various approaches have been proposed for the machine tool error modeling and compensation. The cutting process modeling has been focused on the understanding of cutting forces, dynamics of machine tool structure, and surface profile generation (Smith and Tlusty, 1991; Ehmann, *et al.*, 1991; Kline, Devor, and Shareef, 1982; Wu and Liu, 1985; Sutherland and DeVor, 1986; Altintas and Lee, 1998; Kapoor, *et al.*, 1998; Huang and Liang, 2005; Mann, *et al.*, 2005; Li and Shin, 2006; and Liu, *et al.*, 2006). Machine volumetric error modeling studies the error of the relative movement between the cutting tool and the ideal workpiece for error compensation or machine design (Schultschik, 1977; Ferreira and Liu, 1986; Donmez, *et al.*, 1986; Anjanappa, *et al.*, 1988; Bryan, 1990; Kurtoglu, 1990; Soons, Theuws, and Schellekens, 1992; Chen, *et al.*, 1993; and Frey, Otto, and Pflager, 1997). A volumetric error model of a 3-axis jig boring machine is developed by Schultschik (1977) using a vector chain expression. Ferreira and Liu (1986) developed a model studying the geometric error of a 3-axis machine using homogeneous coordinate transformation. A general methodology for modeling the multi-axis machine was developed by Soons, Theuws, and Schellekens (1992). The volumetric error model combining geometric and thermal errors was proposed to compensate for time varying error in real time (Chen, *et al.*, 1993). Other approaches, including empirical, trigonometric, and error matrix methods were summarized by Ferreira and Liu (1986).

Machine tool thermal error. With the increasing demand for improved machining accuracy in recent years, the problem of thermal deformation of machine tool structures is becoming more critical than ever. In order to maintain part quality under various thermal conditions, two approaches have been studied extensively over the past decades: error avoidance approach and error compensation approach (Bryan, 1990). Thermal errors could be reduced with structural improvement of machine tools through careful design and manufacturing technology. This is known as the error avoidance approach. However, there are, in many cases, cost or physical limitations to accuracy improvement that cannot be overcome solely by production and design techniques. Recently, due to the development of sensing, modeling, and computer techniques, the thermal error reduction through real time machine tool error compensation has been increasingly considered, in which the thermal error is modeled as a function of machine temperatures collected by thermal sensors (Chen, *et al.*, 1993).

For most thermal error compensation systems, the thermal errors are predicted with temperature-error models. The effectiveness of thermal error compensation largely relies on the accuracy of prediction of time varying thermal errors during machining. Various thermal error modeling schemes have been reported in literature, which can be classified into two categories: time independent static modeling and time dependent dynamic modeling. The first category of studies, time independent static modeling, assumes that thermal errors can be uniquely described by current machine tool temperature measurements (Chen, *et al.*, 1993; and Kurtoglu, 1990). It only considers the statistical relationship between temperature measurements and thermal deformations, while neglects the dynamic characteristics of machine thermoelastic systems.

Nevertheless, the information contained in the discrete temperature measurements, which only catches a subset of the whole machine tool temperature field (Venugopal and Barash, 1986), is incomplete and therefore the problem is not uniquely defined. This motivates the second category of studies for modeling the dynamic effects of thermal errors (Moriwaki, *et al.*, 1998) and the recent progress is to apply system identification (SI) theory to thermal error modeling (Yang and Ni, 2003). Both these two categories of studies reveal that the number of sensors, sensor location, temperature history, and lagged variable selection are critical to achieve high model prediction accuracy and model robustness to different working conditions.

As a summary, the studies of process errors have been focused on the modeling of individual error sources, process variation monitoring, and variation reduction. Equivalence relationship between multiple errors has not been sufficiently addressed.

Causality modeling. Models of predicting surface quality are often deterministic and used for a single machining station (Li and Shin, 2006). In the recent decade, more research can be found to investigate the causal relationship between part features and errors, especially in a complex manufacturing system. The available model formulation includes time series model (Lawless, Mackay, and Robinson, 1999), state space models (Jin and Shi, 1999; Ding, Ceglarek, and Shi, 2000; Huang, Shi, and Yuan, 2003; Djurdjanovic and Ni, 2001; Zhou, Huang, and Shi, 2003; and Huang and Shi, 2004), and state transition model (Mantripragada and Whitney, 1999). The results of the process error model can be summarized as follows. Denote by x the dimensional deviation of a workpiece of N operations and by $\mathbf{u}=(u_1, u_2, \ldots, u_p)^T$ the multiple error sources from all operations. The relationship between **x** and **u** can be represented by

$$\mathbf{x} = \sum_{i=1}^{p} \mathbf{\Gamma}_i \mathbf{u}_i + \boldsymbol{\varepsilon} = \mathbf{\Gamma}\mathbf{u} + \boldsymbol{\varepsilon}, \quad (1.1)$$

where $\mathbf{\Gamma}_i$'s are sensitivity matrices determined by process and product design and $\mathbf{\Gamma}=\left[\mathbf{\Gamma}_1 \mid \mathbf{\Gamma}_2 \mid \cdots \mid \mathbf{\Gamma}_p\right]$. $\boldsymbol{\varepsilon}$ is the noise term. This line of research (Hu, 1997; Jin and Shi, 1999; Mantripragada and Whitney, 1999; Djurdjanovic and Ni, 2001; Camelio, Hu, and Ceglarek, 2003; Agapiou, *et al.*, 2003; Agapiou, *et al.*, 2005; Zhou, *et al.*, 2003; Huang, Zhou, and Shi, 2002; Zhou, Huang, and Shi, 2003; Huang, Shi, and Yuan, 2003; and Huang and Shi, 2004) provides a solid foundation for conducting further analysis of the error equivalence.

1.2.2 Research Review for Process Root Cause Diagnosis

The approaches developed for root cause diagnosis include variation pattern mapping (Ceglarek and Shi, 1996), variation estimation based on physical models (Apley and Shi, 1998; Chang and Gossard, 1998; Ding, Ceglarek, and Shi, 2002; Zhou, *et al.*, 2003; Camelio and Hu, 2004; Carlson and Söderberg, 2003; Huang, Zhou, and Shi, 2002; Huang and Shi, 2004; and Li and Zhou, 2006), and variation pattern extraction from measurement data.

Ceglarek, Shi, and Wu (1994) developed root cause diagnostic algorithm for autobody assembly line where fixture errors are dominant process faults. Principal component analysis (PCA) has been applied to fixture error diagnosis by Hu and Wu (1992), who make a physical interpretation of the principal components and thereby get insightful understanding of root causes of process variation. Ceglarek and Shi (1996) integrated PCA, fixture design, and pattern recognition and have achieved considerable success in identifying problems resulting from worn, loose, or broken fixture elements in

the assembly process. However, this method cannot detect multiple fixture errors. A PCA based diagnostic algorithm has also been proposed by Rong, Ceglarek, and Shi (2000). Apley and Shi (1998) developed a diagnostic algorithm that is able to detect multiple fixture faults occurring simultaneously. Their continuing work in 2001 presented a statistical technique to diagnose root causes of process variability by using a causality model. Ding, Ceglarek, and Shi (2002) derived a PCA based diagnostics from the state space model.

However, the number of the simultaneous error patterns may grow significantly as more manufacturing operations are involved. The multiple error patterns are rarely orthogonal and they are difficult to distinguish from each other. Therefore, the manufacturing process may not be diagnosable. Ding, Shi, and Ceglarek (2002) analyzed the diagnosability of multistage manufacturing processes and applied the results to the evaluation of sensor distribution strategy. Zhou, *et al.* (2003) developed a more general framework for diagnosability analysis by considering aliasing faulty structures for coupled errors in a partially diagnosable process. Further studies are needed on the fault diagnosis for a general machining process where multiple types of errors occur.

1.2.3 Research Review for Process Control

The objective of process control is to keep the output as close as possible to the target all the time. Other than the traditional SPC where Shewhart, EWMA, and CUSUM control charts are the common techniques, automatic process control (APC) and its integration with SPC have gained more attention in recent decades.

Automatic process control. APC uses feedback or feedforward control to counteract the effects of root causes and reduce the process variation. Although SPC achieved great success in discrete manufacturing, APC is more likely to be used in continuous process industries where the process output has a tendency to drift away. The early research on APC can be tracked back to Box's early research (Box, 1957; Box and Jenkins 1963, 1970; Box and Draper, 1969; 1970; and Box and Kramer, 1992). In APC, the most theoretically discussed control rule is the minimum mean squared error (MMSE) control. It is based on the stochastic control theory (Åström, 1970) to find out the optimal control rule to minimize the mean square error of the process output. However, since MMSE control has unstable modes (Åström and Wittenmark, 1990; and Tsung, 2000), in some occasions, it causes the process to adapt to the disturbance changes and causes larger output response. In industries, proportional-integral-derivative (PID) control tuning is the most common control technique (Åström, 1988). Its purpose is to reduce the output variance as much as possible based on the PID controller. Compared with many MMSE controllers, PID controller is more robust in varying environments.

Integration of APC and SPC. More recently, more research efforts are directed towards the approach combining SPC and APC to secure both the process optimization and quality improvement. MacGregor (1988) was among the first to suggest SPC charts to monitor the controlled process. The similarities and overlap between SPC and APC were described. The integration of APC and SPC has been reviewed by Box and Kramer (1992). In these early dissertations, a minimum cost strategy is suggested to adjust the process and SPC chart is used as dead bands or filtering device (English and Case, 1990) for feedback controlled process. This dead band concept was extended for multivariate

problems by Del Castillo (1996). Vander Wiel, *et al.* (1992) proposed an algorithmic statistical process control (ASPC), which reduces the process variation by APC and then monitors the process to detect and remove root cause of variation using SPC. Tucker, *et al.* (1993) elaborated on the ASPC by giving an overall philosophy, guidelines, justification, and indicating related research issues.

Parallel to the integration work, research (MacGregor and Harris, 1997; Harris and Ross, 1991) has been implemented for correcting SPC procedures due to the effect of correlation and applying these procedures for monitoring a controlled process. Tsung (2000) proposed an integrated approach to simultaneously monitor and diagnose controlled process using dynamic principal component analysis and minimax distance classifier.

In the early research of integrating APC and SPC, the only monitored variable is the controlled output. Output monitoring alone cannot provide sufficient information on the process change because it has been compensated for by controllers. MacGregor (1991) suggested monitoring the output of the controller. Messina, *et al.* (1996) then considered the monitoring controller output under an autoregressive moving average disturbance process and proposed jointly monitoring for process output and controlled signal. Tsung, *et al.* (1999) proposed a procedure for jointly monitoring the PID controlled output and controlled signal using bivariate SPC. The SPC robustness was also investigated. In addition, researchers also applied APC and SPC to run-to-run (RTR) process control, which refers to performing control action between runs instead of during a run (Del Castillo, 1996; Butler and Stefani, 1994; Mozumder, *et al.*, 1994; Sachs, *et al.*, 1995; and

Tsung and Shi, 1999). Del Castillo and Hurwitz (1997) reviewed research work on RTR control.

Most of SPC integrated APC approaches have been mainly applied to continuous process. The adjustment in discrete process relies on the control of servo motor, interpolator and adaptive loop in the machine tools (Åström, 1970, 1990) or compensation of individual error sources. Little work discussed the potential application of APC in a discrete manufacturing process where the dominant control strategy is to construct control chart to identify the assignable cause. There is a lack of methodology that can compensate for the joint effect of multiple error sources.

1.2.4 Summary of Literature Review

- *Process modeling*. Previous research has been focused on the analyses of individual errors and causality modeling in manufacturing processes. The research on the variation reduction and process control has not studied the error equivalence phenomenon in manufacturing processes. There is a lack of physical model to describe the error equivalence so as to study its impact on process control.
- *Model based root cause diagnosis*. Previous research has extensively studied the process sensing strategy, statistical process monitoring, diagnosability analysis, and diagnostic algorithms. Those studies did not address the challenges the error equivalence brings to the root cause diagnosis of manufacturing process with multiple error sources.
- *Error compensation*. Previous research widely studied the SPC integrated automatic process adjustment in continuous manufacturing processes. The traditional error

compensation strategy for a discrete manufacturing process is to offset the process errors individually and may not be cost effective. Hence it is desirable to study the impact of the error equivalence mechanism on the error compensation.

1.3 Dissertation Outline

The insightful understanding and full utilization of the error equivalence require advances in: mathematical modeling of the error equivalence phenomenon in manufacturing, error equivalence analysis for root cause identification, and error equivalence analysis for automatic process error compensation with integration of SPC. These research aspects constitute the error equivalence theory.

The challenge for these research advances is the fusion of engineering science and statistics into the modeling of error equivalence and the life cycle of controlling process variations. The overall framework of error equivalence theory is shown in Fig 1.1.

Chapter 1 describes phenomenon of error equivalence and reviews the related work for process modeling, diagnosis, and process control.

Chapter 2 presents a tentative mathematical definition of error equivalence and models the error equivalence phenomenon through a kinematic analysis of workpiece and errors. The error equivalence model has been verified by a real milling process. In addition, a state space model based on error equivalence is derived to study the variation stackup in the multistage manufacturing process. The procedure of variation propagation model based on error equivalence has been demonstrated via a case study.

Chapter 3 intends to further explore the error equivalence mechanism and discusses its theoretical implication in root cause identification as well as automatic

process adjustment for time invariant errors. A sequential root cause identification procedure has been proposed to distinguish multiple types of errors in the machining processes. The diagnostic algorithm is experimentally validated by a milling process. The process adjustment based on error equivalence is illustrated with a simulation.

Chapter 4 builds a dynamic model of process errors to study the dynamic error equivalence. In addition, statistical process control is introduced to monitor the dynamic equivalent errors.

Based on the conclusion of Chapter 4, an automatic process adjustment algorithm using error equivalence is derived to compensate for dynamic errors in a discrete manufacturing process in Chapter 5. The performance of the adjustment rule, including stability and sensitivity has been evaluated. Furthermore, the adjustment algorithm is integrated with SPC so that changes in both adjustment algorithm and manufacturing can be detected.

Chapter 6 concludes the dissertation. Prospects of future research are also discussed.

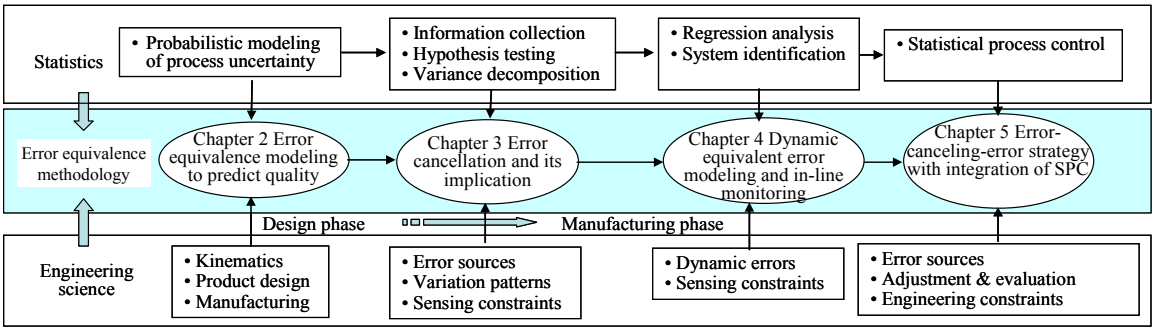

Figure 1.3 The Framework of Error Equivalence Theory

Chapter 2

Error Equivalence Modeling and Variation Propagation Modeling Based on Error Equivalence*

This chapter models the phenomenon of the error equivalence in the machining processes by considering how multiple errors (including fixture, and datum, and machine tool) generate the same pattern on part features. The equivalent transformations between multiple errors are derived through a kinematic analysis of process errors. As a result, error sources can be grouped so that root cause identification can be conducted in a sequential manner, which generally requires fewer feature measurements than the previous approaches. The case study demonstrates the model validity through a real cutting experiment.

The chapter is organized as follows. Section 2.1 introduces some preliminaries and notations. Section 2.2 defines the error equivalence and overviews the methodology. Error equivalence model in machining processes is derived in Section 2.3. As an example of applying the error equivalence model, Section 2.4 presents a new variation propagation model for multi-operational machining processes. The case studies have been conducted in Section 2.5. Conclusions and future research work are discussed in Section 2.6.

*The work in this chapter has appeared in Wang, H., Huang, Q., and Katz, R., 2005, "Multi-Operational Machining Processes Modeling for Sequential Root Cause Identification and Measurement Reduction," *ASME Transactions, Journal of Manufacturing Science and Engineering*, 127, pp. 512-52.

2.1 Preliminaries and Notations

This section introduces kinematic analysis of machining process, including representations of surface and its spatial transformation caused by process errors in a manufacturing process. The results will be used to derive error equivalence transformation.

By vectorial surface model (Martinsen, 1993; and Huang, Shi, and Yuan, 2003), an *M*-surface part **X** is represented as a vector in the part coordinate system (PCS)

$$\mathbf{X} = \left(\mathbf{X}_1^T \ldots \mathbf{X}_j^T \ldots \mathbf{X}_M^T\right)^T,\ j=1, \ldots, M, \tag{2.1}$$

where $\mathbf{X}_j$ denotes the *j*th surface and it is represented as

$$\mathbf{X}_j = \left(\mathbf{v}_j^T \quad \mathbf{p}_j^T \quad r_j\right)^T = (v_{jx}\ \ v_{jy}\ v_{jz}\ p_{jx}\ p_{jy}\ \ p_{jz}\ \ r_j)^T, \tag{2.2}$$

where $\mathbf{v}_j=(v_{jx}\ \ v_{jy}\ v_{jz})^T$, $\mathbf{p}_j=(p_{jx}\ p_{jy}\ \ p_{jz})^T$, and r_j are orientation, location and size of surface *j*, respectively. Subscripts *x*, *y*, and *z* denote orthogonal directions in the coordinate system. *M* is determined by product design and process planning. The size of cylindrical hole can be represented by the radius of the hole and size of plane is zero.

The nominal surface *j* and part are denoted as $\mathbf{X}_j^0$ and $\mathbf{X}^0$, respectively. The deviation of $\mathbf{X}_j$ is denoted as $\mathbf{x}_j=\mathbf{X}_j-\mathbf{X}_j^0=\left(\Delta\mathbf{v}_j^T \quad \Delta\mathbf{p}_j^T \quad \Delta r_j\right)^T$ as shown in Fig. 2.1, where Euler parameters and matrix **H** will be described in Eq. (2.4). Accordingly, the part deviation is denoted as $\mathbf{x}= \left(\mathbf{x}_1^T \ldots \mathbf{x}_j^T \ldots \mathbf{x}_M^T\right)^T$. The feature deviation **x** of a workpiece can be represented as a function of multiple errors sources $(\mathbf{u}_1, \mathbf{u}_2, \ldots, \mathbf{u}_p)^T$,

$$\mathbf{x} = \Sigma_{i=1}^{p}\mathbf{f}_i(\mathbf{u}_i) + \boldsymbol{\varepsilon}, \tag{2.3}$$

where $\mathbf{f}_i(.)$'s are functions determined by process and product design. $\boldsymbol{\varepsilon}$ is the noise term. Process errors $\{\mathbf{u}_i\}$ involved in machining mainly include those during setup and cutting

operations. Since the part is modeled as a vector, operations and their errors can be viewed as vector transformations. Therefore, homogeneous transformation matrix (HTM) is generally applied to model both operations and operational errors. For instance, HTM ${}^{F}\mathbf{H}_{P}$ is used to model the nominal setup at operation k. It transforms $\mathbf{X}_j^0$ from the nominal PCS (denoted as PCS^0) to the nominal fixture coordinate system (FCS^0). Since setup error could be induced by fixture error and datum error, we use HTMs $\mathbf{H}_f$ and $\mathbf{H}_d$ to denote the additional transformation of $\mathbf{X}_j^0$ in the FCS^0 caused by fixture error and datum error, respectively.

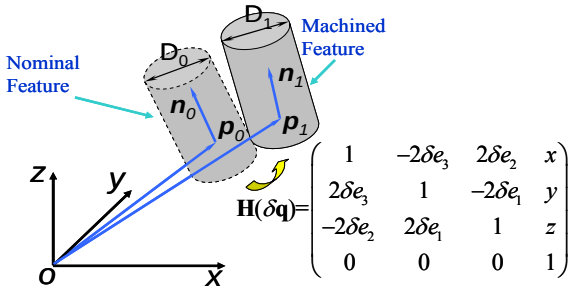

Figure 2.1 Modeling of Part Feature Deviation

To describe fixture error, the common 3-2-1 fixture locating scheme is adopted (Fig. 2.2). The fixture is represented by the positions of 6 locators in the FCS, i.e., $(f_{ix}\ f_{iy}\ f_{iz})^T$, i=1,…, 6. Not losing generality, the FCS^0 is established with f_{1z}=f_{2z}=f_{3z} =f_{4y}=f_{5y}=f_{6x}= 0. The fixture error is denoted as deviations of locators, i.e., $\Delta\mathbf{f}$=$(\Delta f_{1z}\ \Delta f_{2z}\ \Delta f_{3z}\ \Delta f_{4y}\ \Delta f_{5y}\ \Delta f_{6x})^T$. Cai, Hu, and Yuan (1997) nicely presented the relationship between $\Delta\mathbf{f}$ and $\mathbf{H}_f$. Their key results are summarized in Appendix A.

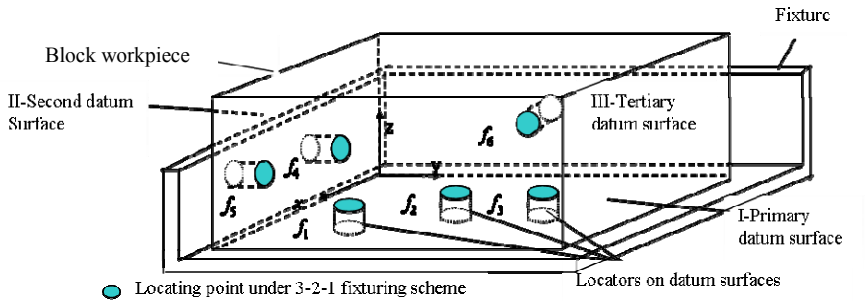

Figure 2.2 General 3-2-1 Locating Scheme and FCS^0

The datum error is included in the incoming workpiece **x**. For the surfaces used as the primary, secondary, and tertiary datum, their errors are denoted as $\mathbf{x}_{\mathrm{I}}$, $\mathbf{x}_{\mathrm{II}}$, and $\mathbf{x}_{\mathrm{III}}$, respectively. Datum error is then $\mathbf{x}_{\mathrm{D}} = (\mathbf{x}_{\mathrm{I}}^T \quad \mathbf{x}_{\mathrm{II}}^T \quad \mathbf{x}_{\mathrm{III}}^T)^T$. The relationship between datum error and $\mathbf{H}_d$ will be derived in Section 2.2 using the concept of equivalent fixture error. The datum error is first converted to the equivalent amount of fixture locator errors (denoted as $\Delta\mathbf{d}$). Then the results in Cai , Hu, and Yuan (1997) can be directly applied to find $\mathbf{H}_d$ through $\Delta\mathbf{d}$.

The nominal cutting operation or the tool path can be modeled as ${}^{M}\mathbf{H}_F {}^{F}\mathbf{H}_P \mathbf{X}_j^0$, where ${}^{M}\mathbf{H}_F$ transforms a part surface from the FCS^0 to the nominal machine tool coordinate system (MCS^0). (When deriving the results, we choose the MCS^0 to be the same as the FCS^0, i.e., ${}^{M}\mathbf{H}_F = \mathbf{I}_{8\times 8}$. Discussion is given in Section 2.4.3 when ${}^{M}\mathbf{H}_F$ is not identity matrix.) We use $\mathbf{H}_m$ to represent the transformation of tool path (from nominal to the real one) caused by machine tool error. Only geometric errors of machine tool are considered in this work. Fig. 2.3 shows the transformation due to process errors. As an example to show the form of HTM, $\mathbf{H}_m$ is given as

$$\mathbf{H}_m = \left(\begin{array}{c|c|c|c} \mathbf{Rot}_m & \mathbf{0} & \mathbf{0} & \mathbf{0} \\ \hline \mathbf{0} & \mathbf{Rot}_m & \mathbf{0} & \begin{matrix} x_m \\ y_m \\ z_m \end{matrix} \\ \hline \mathbf{0} & \mathbf{0} & \gamma_m & 0 \\ \hline \mathbf{0} & \mathbf{0} & 0 & 1 \end{array}\right), \tag{2.4}$$

where rotation matrix $\mathbf{Rot}_m$ has the following form under small deviation assumption (Huang and Shi, 2003),

$$\mathbf{Rot}_m = \begin{pmatrix} 1 & -2\delta e_{3m} & 2\delta e_{2m} \\ 2\delta e_{3m} & 1 & -2\delta e_{1m} \\ -2\delta e_{2m} & 2\delta e_{1m} & 1 \end{pmatrix}$$

and $(\delta e_{1m} \;\; \delta e_{2m} \;\; \delta e_{3m})^T$ are deviations of Euler parameters, representing deviation of tool path orientation. $\mathbf{Rot}_m$ on the upper left corner of Eq. (2.4) transforms the orientation of surface, while the second $\mathbf{Rot}_m$ transforms the surface position. $(x_m \;\; y_m \;\; z_m)^T$ represents deviation of tool path in position. γ_m is the ratio of actual and ideal surface size. When γ_m=1, there is no size deviation due to the machine tool error. Accordingly, we define the machine tool error as $(\delta\mathbf{q}_m^T \;\; \gamma_m\text{-}1)^T$, where $\delta\mathbf{q}_m$=$(x_m \;\; y_m \;\; z_m \;\; \delta e_{1m} \;\; \delta e_{2m} \;\; \delta e_{3m})^T$. The equivalent fixture error due to machine tool is denoted as $\Delta\mathbf{m}$.

Notations $\delta\mathbf{q}_d$ and $\delta\mathbf{q}_f$ can also be introduced for the parameters in $\mathbf{H}_d$ and $\mathbf{H}_f$ in a similar way. Since datum and fixture errors have no impact on the surface size, we have γ_d= γ_f=1.

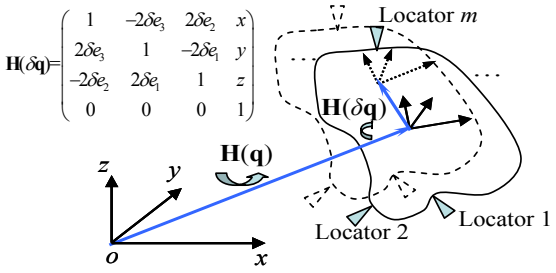

Figure 2.3 Modeling of Workpiece Positioning Error

2.2 Mathematical Modeling of the Error Equivalence Phenomenon in Manufacturing

Suppose p random error sources $\mathbf{u}_i$'s lead to dimensional deviation $\mathbf{x}$ as $\mathbf{x} = \mathbf{f}_i(\mathbf{u}_i)+\boldsymbol{\varepsilon}_i$, i=1,2,…,p. $\mathbf{u}_i$'s are assumed to be independent from one another and the noise term has mean $E(\boldsymbol{\varepsilon}_i)=\mathbf{0}$, and covariance $Cov(\boldsymbol{\varepsilon}_i)=\sigma_{\varepsilon_i}^2\ \mathbf{I}$, where $\mathbf{I}$ is an identity matrix. A tentative definition of error equivalence is given as follows.

Definition: Two error sources $\mathbf{u}_i$ and $\mathbf{u}_j$ are equivalent if expectation $E[\mathbf{f}_i(\mathbf{u}_i)]= E[\mathbf{f}_j(\mathbf{u}_j)]$. That is, the equivalence among random errors is evaluated by the resultant mean shift patterns in product features.

It should be noted that errors might not be equivalent under all situations. For instance, the surface profile deviation caused by a machine tool might not be reproduced by a fixture. This study only focuses on the situations that error equivalence holds.

If error sources $\mathbf{u}_i$ and $\mathbf{u}_j$ are equivalent, it is feasible to transform $\mathbf{u}_i$ into equivalent amount of error in terms of $\mathbf{u}_j$ without affecting the analysis of feature deviation $\mathbf{x}$. This fact prompts error equivalence transformation to derive the error equivalence model.

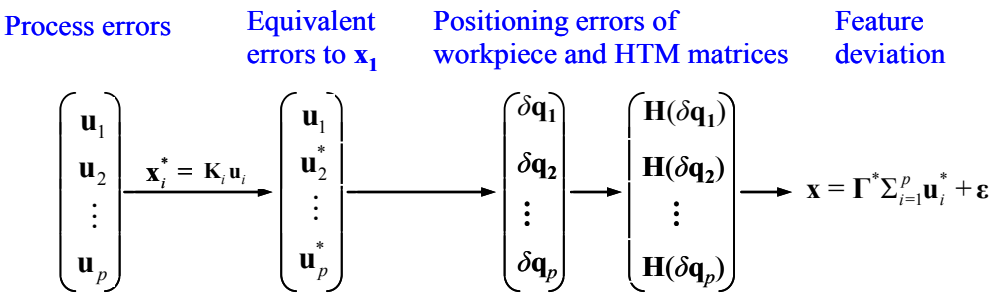

Figure 2.4 Mathematical Modeling of Error Equivalence

Fig. 2.4 outlines the basic idea of mathematical modeling of the error equivalence phenomenon. If p process errors $\mathbf{u}_i$'s are equivalent, the first step of modeling is to transform $\mathbf{u}_i$'s into a base type error $\mathbf{u}_1$ through $\mathbf{u}_i^* = \mathbf{K}_i \mathbf{u}_i$. A significant advantage of this equivalent transformation is that the causal relationship between base error $\mathbf{u}_1$ and feature deviation, i.e., $\mathbf{x}=\mathbf{f}_1(\mathbf{u}_1)$, can be generally applied to other types of error sources. The manufacturing operation (e.g., cutting or setup operation) can be represented by a HTM matrix $\mathbf{H}(\delta\mathbf{q})$, where the deviation of Euler parameters ($\delta\mathbf{q}$) (see Fig. 2.3) are related to the operational error. The remaining modeling steps can therefore be focused on the causal model $\mathbf{x}=\mathbf{f}_1(\mathbf{u}_1)$ because the transformed errors $\mathbf{u}_i^*$'s are to be grouped together into $\Sigma_{i=1}^{p}\mathbf{u}_i^*$ with $\mathbf{u}_1^* = \mathbf{u}_1$. The process model presented by Eq. (2.3) can be rewritten as $\mathbf{x}= \Sigma_{i=1}^{p}\mathbf{f}_i(\mathbf{u}_i^*)$. Since $\mathbf{u}_i^*$'s are treated as base error $\mathbf{u}_1$, the process model based on error equivalence modeling thus becomes

$$\mathbf{x} = f(\mathbf{u}_1, \mathbf{u}_2, ..., \mathbf{u}_p) + \boldsymbol{\varepsilon} = \Sigma_{i=1}^{p}\mathbf{f}_1(\mathbf{u}_i^*) + \boldsymbol{\varepsilon}. \tag{2.5}$$

If function $\mathbf{f}_1$ could be approximated by a linear function $\mathbf{\Gamma}^*$, the model becomes

$$\mathbf{x}= \mathbf{\Gamma}^*\mathbf{u} + \boldsymbol{\varepsilon}, \text{ with } \mathbf{u}= \Sigma_{i=1}^{p}\mathbf{u}_i^*. \tag{2.6}$$

The definition also shows the way to check the error equivalence condition. We can first estimate E($\mathbf{u}_i^*$) and Cov($\mathbf{u}_i^*$) from measurement data using maximum likelihood estimation (MLE) method. Then the definition of error equivalence can be directly applied.

Transforming error sources into a base error implies the transformation of manufacturing operations into a base operation, i.e., the operation with base error only. Operations with other types of errors become flawless because all the process errors have been transferred to the base operation.

The derivation of this dissertation is under the linearity assumption, under which equivalence transformation and quality prediction model assume linear form. The nonlinear deformation of products is not considered in this study.

2.3 Error Equivalence Modeling for Machining Processes

We first introduce the concept of equivalent fixture error, by which a variation propagation model is developed by grouping fixture, datum, and machine tool errors. Condition of error grouping is also discussed in this section.

2.3.1 Concept of Equivalent Fixture Error

In a general machining process, three major error sources are considered: fixture error $\Delta\mathbf{f}$, machine tool error $\delta\mathbf{q}_m$, and datum surface error $\mathbf{x}_D$. The fixture error is chosen as the base error because of the following reasons:

- Fixture error is simply represented by the deviation of fixture locators, while machine tool error is relatively complicated. The datum error is usually caused by fixture or machine tool errors.

- Fixture error has been well studied. Methods are readily available for the analysis of workpiece positioning error (Weill, Darel, and Laloum, 1991; Rong and Bai, 1996; Cai, Hu, and Yuan, 1997; Wang, 2000; and Marin and Ferreira, 2003), the resultant feature deviation, and fixture error diagnosis (Hu and Wu, 1992; Apley and Shi, 1998, 2001; and Ceglarek and Shi, 1996).
- Flexible fixtures have been available whose locators are adjustable for accommodating a product family. It is possible to adjust the locator lengths for the purpose of error compensation.

The base error in terms of fixture error is called equivalent fixture error (EFE), which can be illustrated with a 2-D block workpiece (Fig. 2.5).

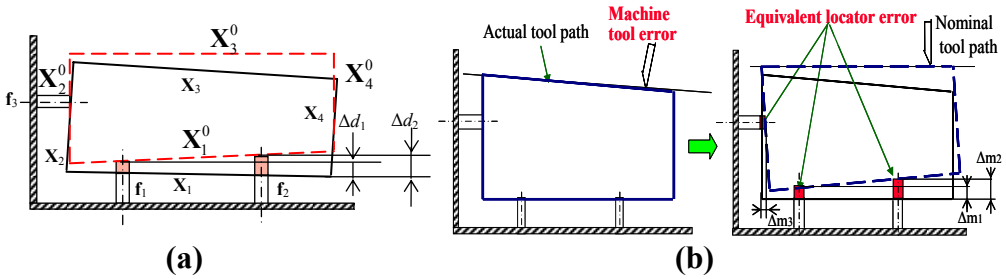

Figure 2.5 Equivalent Fixture Error

In Fig. 2.5(a), the dash line block with surfaces ($\mathbf{X}_1^0$ $\mathbf{X}_2^0$ $\mathbf{X}_3^0$ $\mathbf{X}_4^0$) is in its nominal setup position. Due to datum error occurring on surface $\mathbf{X}_1$, the block has to be transformed to position ($\mathbf{X}_1$ $\mathbf{X}_2$ $\mathbf{X}_3$ $\mathbf{X}_4$) (the solid line block) around the locating point $\mathbf{f}_3$. The workpiece position transformation is described by HTM $\mathbf{H}_d$. The EFE due to datum error, denoted by $\Delta\mathbf{d}=(\Delta d_{1z}\ \Delta d_{2z}\ \Delta d_{3z}\ \Delta d_{4y}\ \Delta d_{5y}\ \Delta d_{6x})^T$, can be derived by finding the difference between actual ($\mathbf{H}_d\ {}^F\mathbf{H}_P\ (\mathbf{X}_j^{0T}\ \ 1)^T$) and nominal datum surfaces (${}^F\mathbf{H}_P\ (\mathbf{X}_j^{0T}\ \ 1)^T$), where $\{j\} \subset \{\text{I, II, III}\}$. In Fig. 2.5(a), the equivalent fixture deviation is Δd_1 and Δd_2. In Fig. 2.5(b), EFE due to machine tool error can be derived in a similar way. The left panel

shows that the machined surface $\mathbf{X}_3$ deviates from designed position $\mathbf{X}_3^0$ due to machine tool errors. The EFE transforms the workpiece from nominal position ($\mathbf{X}_1^0$ $\mathbf{X}_2^0$ $\mathbf{X}_3^0$ $\mathbf{X}_4^0$) to dash line position shown in right panel. A nominal cutting operation can yield the same surface deviation as machine tool error does in the left panel. Therefore, the inverse of $\mathbf{H}_m$ transforms $\mathbf{X}_3$ to its nominal position $\mathbf{X}_3^0$ in the FCS. The EFE due to machine tool error, denoted by $\Delta\mathbf{m}=(\Delta m_{1z}\ \Delta m_{2z}\ \Delta m_{3z}\ \Delta m_{4y}\ \Delta m_{5y}\ \Delta m_{6x})^T$, can be uniquely determined by the difference between $\mathbf{H}_m^{-1}{}^F\mathbf{H}_P\,(\mathbf{X}_j^{0T}\ \ 1)^T$ and ${}^F\mathbf{H}_P\,(\mathbf{X}_j^{0T}\ \ 1)^T$ at the locating point, where $\{j\} \subset \{\text{I, II, III}\}$. In this example, the equivalent fixture locator deviation Δm_1 and Δm_2 is determined by difference between surfaces $\mathbf{X}_1^0$ and $\mathbf{X}_1$ at locating point 1 and 2. Δm_3 can be computed by the difference between surfaces $\mathbf{X}_2^0$ and $\mathbf{X}_2$ at locating point 3.

2.3.2 Derivation of EFE Model

The equivalent locator deviation caused by either datum error or machine tool error can be computed by the distance between two points where locators intersect the nominal datum $\mathbf{X}_j^0=(v_{jx}^0\ \ v_{jy}^0\ \ v_{jz}^0\ \ p_{jx}^0\ \ p_{jy}^0\ \ p_{jz}^0)^T$ and deviated datum surfaces $\mathbf{X}_j=(v_{jx}\ \ v_{jy}\ \ v_{jz}\ \ p_{jx}\ \ p_{jy}\ \ p_{jz})$ (Fig. 2.6), where j=I, II, III represents three datum surfaces. $\mathbf{n}_j$ is the normal vector of datum surface and it is equal to orientation vector $\mathbf{v}_j$ when datum surface is planar.

Let $\Delta\mathbf{d}=(\Delta d_{1z}\ \Delta d_{2z}\ \Delta d_{3z}\ \Delta d_{4y}\ \Delta d_{5y}\ \Delta d_{6x})^T$ and $\Delta\mathbf{m}=(\Delta m_{1z}\ \Delta m_{2z}\ \Delta m_{3z}\ \Delta m_{4y}\ \Delta m_{5y}\ \Delta m_{6x})^T$ represent EFEs caused by datum and machine tool errors, respectively. Using analytical geometry, EFEs can be derived as

$$\begin{aligned}
\Delta d_{iz}(or\ \ \Delta m_{iz}) &= -[n_{\mathrm{Ix}}(f_{ix} - p_{\mathrm{Ix}}) + n_{\mathrm{Iy}}(f_{iy} - p_{\mathrm{Iy}})]/n_{\mathrm{Iz}} + p_{\mathrm{Iz}} - f_{iz}, i = 1,2,3,\\
\Delta d_{iy}(or\ \ \Delta m_{iy}) &= -[n_{\mathrm{IIx}}(f_{ix} - p_{\mathrm{IIx}}) + n_{\mathrm{IIz}}(f_{iz} - p_{\mathrm{IIz}})]/n_{\mathrm{IIy}} + p_{\mathrm{IIy}} - f_{iy}, i = 4,5,\\
\Delta d_{ix}(or\ \ \Delta m_{ix}) &= -[n_{\mathrm{IIIy}}(f_{iy} - p_{\mathrm{IIIy}}) + n_{\mathrm{IIIz}}(f_{iz} - p_{\mathrm{IIIz}})]/n_{\mathrm{IIIx}} + p_{\mathrm{IIIx}} - f_{ix}, i = 6.
\end{aligned} \tag{2.7}$$

The orientation vector $\mathbf{n}_j$ and position $\mathbf{p}_j$ of the plane $\mathbf{X}_j$ can be further expanded by datum error $\mathbf{x}_j$ or machine tool error $\delta\mathbf{q}_m$.

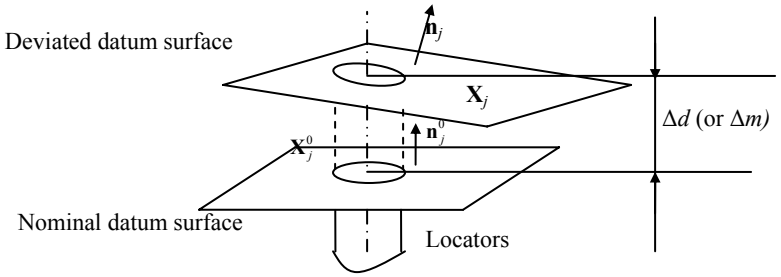

Figure 2.6 EFE Derivation

When computing $\Delta\mathbf{d}$, deviated surface $\mathbf{X}_j$ can be determined by datum error plus the nominal, i.e., $\mathbf{X}_j = \mathbf{X}_j^0 + \mathbf{x}_j$. Eq. (2.7) is then linearized as:

$$\begin{aligned}
\Delta d_{iz} &= -f_{ix}\Delta v_{\mathrm{Ix}} - f_{iy}\Delta v_{\mathrm{Iy}} - \Delta p_{\mathrm{Iz}},\ \ i = 1,2,3,\\
\Delta d_{iy} &= -f_{ix}\Delta v_{\mathrm{IIx}} - f_{iz}\Delta v_{\mathrm{IIz}} - \Delta p_{\mathrm{IIy}},\ \ i = 4,5,\ \text{or}\ \ \Delta\mathbf{d} = \mathbf{K}_2\begin{pmatrix}\mathbf{x}_{\mathrm{I}}\\ \mathbf{x}_{\mathrm{II}}\\ \mathbf{x}_{\mathrm{III}}\end{pmatrix}.\\
\Delta d_{ix} &= -f_{iy}\Delta v_{\mathrm{IIIy}} - f_{iz}\Delta v_{\mathrm{IIIz}} - \Delta p_{\mathrm{IIIx}},\ \ i = 6.
\end{aligned} \tag{2.8}$$

The mapping matrix relating datum error to $\Delta\mathbf{d}$ is $\mathbf{K}_2 = \left(\begin{array}{c|c|c}\mathbf{G}_1 & \mathbf{0} & \mathbf{0}\\ \hline \mathbf{0} & \mathbf{G}_2 & \mathbf{0}\\ \hline \mathbf{0} & \mathbf{0} & \mathbf{G}_3\end{array}\right)$ where

$$\mathbf{G}_1 = -\begin{pmatrix} f_{1x} & f_{1y} & 0 & 0 & 0 & 1\\ f_{2x} & f_{2x} & 0 & 0 & 0 & 1\\ f_{3x} & f_{3x} & 0 & 0 & 0 & 1\end{pmatrix},\ \mathbf{G}_2 = -\begin{pmatrix} f_{4x} & 0 & f_{4z} & 0 & 1 & 0\\ f_{5x} & 0 & f_{5z} & 0 & 1 & 0\end{pmatrix},\ \text{and}$$

$$\mathbf{G}_3 = -\begin{pmatrix}0 & f_{6y} & f_{6z} & 1 & 0 & 0\end{pmatrix}.$$

When deriving $\Delta\mathbf{m}$, we use the relationship between $\mathbf{X}_j$ and machine tool error $\delta\mathbf{q}_m$. Linearization of Eq. (2.7) using the first order of Tayler expansion then yields

$$\Delta\mathbf{m} = \mathbf{K}_3\,\delta\mathbf{q}_m, \text{ and}$$

$$\mathbf{K}_3 = \begin{pmatrix} 0 & 0 & -1 & -2f_{1y} & 2f_{1x} & 0 \\ 0 & 0 & -1 & -2f_{2y} & 2f_{2x} & 0 \\ 0 & 0 & -1 & -2f_{3y} & 2f_{3x} & 0 \\ 0 & -1 & 0 & 2f_{4z} & 0 & -2f_{4x} \\ 0 & -1 & 0 & 2f_{5z} & 0 & -2f_{5x} \\ -1 & 0 & 0 & 0 & -2f_{6z} & 2f_{6y} \end{pmatrix}. \tag{2.9}$$

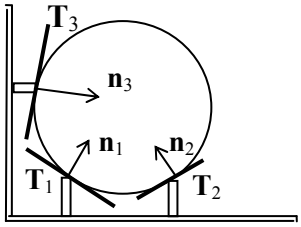

Figure 2.7 Non-Planar Datum Surfaces

This modeling is applicable for the case where datum surfaces are all planes. When the surface is not planar, we should use tangential plane of surface at each locating point as datum surface. Fig. 2.7 shows the setup of a 2-D part with non-planar datum surfaces. The datum surfaces are tangential planes $\mathbf{T}_1$, $\mathbf{T}_2$, and $\mathbf{T}_3$. The corresponding normal vectors are $\mathbf{n}_1$, $\mathbf{n}_2$, and $\mathbf{n}_3$, respectively. If the implicit form surface equation is represented by $f_j(x_j, y_j, z_j)=0$, $\mathbf{n}_j$ and $\mathbf{p}_j$ are determined by

$$\mathbf{n}_j = \left(\frac{\partial f_j}{\partial x_j} \quad \frac{\partial f_j}{\partial y_j} \quad \frac{\partial f_j}{\partial z_j} \right)^T, \quad f_j(p_{jx}, p_{jy}, p_{jz}) = 0, j=\text{I,II,…,VI.} \tag{2.10}$$

The following is for a brief derivation on orientation $\mathbf{v}$ and position vector $\mathbf{p}$ of three datum surfaces. If the features j_1, j_2 and j_3 that are selected as the first, second and tertiary datum surface are planar, orientation vector of three datum surfaces can be $\mathbf{v}_{\text{I}}=\mathbf{v}_{j1}$, $\mathbf{v}_{\text{II}}=\mathbf{v}_{j2}$, and $\mathbf{v}_{\text{III}}=\mathbf{v}_{j3}$. However, if j_2 and j_3 are cylindrical holes where round pin and diamond pin reside respectively, such locating scheme is equivalent to a simplified 3-2-1

fixture locating scheme as shown in Fig. 2.8. We can set the origin of fixture coordinate system at the point of $\mathbf{p}_{j2}$, and $f_{1z}=f_{2z}=f_{3z}=f_{4x}=f_{4y}=f_{4z}=f_{5y}=f_{5z}=f_{6x}=f_{6y}=f_{6z}=0$.

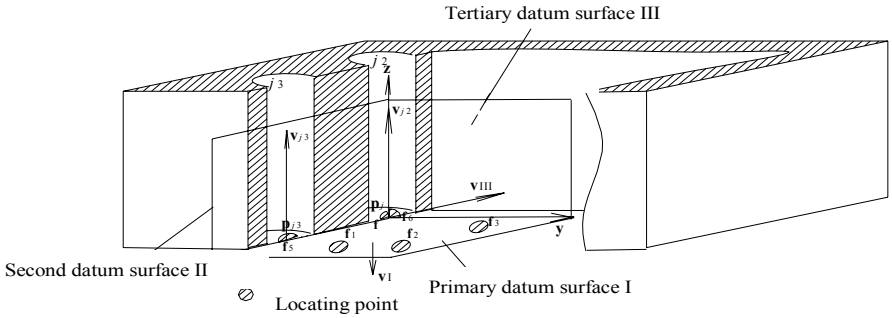

Figure 2.8 Pin-Hole Locating Scheme

The orientation vector for second datum surface is defined to be

$$\begin{aligned}\mathbf{v}_{\mathrm{II}} &= \mathbf{v}_{j_2}\times(\mathbf{p}_{j_2}-\mathbf{p}_{j_3})\\ &=\left(-v_{j_3y}p_{j_2z}+v_{j_3y}p_{j_2z}+v_{j_3z}p_{j_3y}-v_{j_3z}p_{j_2y}\quad -v_{j_3z}p_{j_3x}+v_{j_3z}p_{j_2x}+v_{j_3x}p_{j_3z}-v_{j_3x}p_{j_2z}\quad -v_{j_3x}p_{j_3y}+v_{j_3x}p_{j_2y}+v_{j_3y}p_{j_3x}-v_{j_3y}p_{j_2x}\right),\end{aligned} \tag{2.11}$$

where orientation $\mathbf{v}_j$ and position $\mathbf{p}_j$ of holes are parameters that vary within infinitesimal range. The normal vector for the tertiary datum surface is

$$\mathbf{n}_{\mathrm{III}}=\mathbf{p}_{j_2}-\mathbf{p}_{j_3}=\left(p_{j_2x}-p_{j_3x}\quad p_{j_2y}-p_{j_3y}\quad p_{j_2z}-p_{j_3z}\right). \tag{2.12}$$

Deviation of normal vector is determined by differentiation and linearization of $\mathbf{v}_{\mathrm{I}}$, $\mathbf{v}_{\mathrm{II}}$, and $\mathbf{v}_{\mathrm{III}}$. The results are given as follows:

If three datum surfaces are planar:

$$\Delta\mathbf{n}_{\mathrm{I}}=\Delta\mathbf{v}_{j1},\ \Delta\mathbf{n}_{\mathrm{II}}=\Delta\mathbf{v}_{j2},\ \Delta\mathbf{n}_{\mathrm{III}}=\Delta\mathbf{v}_{j3}\ ,\ \text{and} \tag{2.13}$$

$$\Delta\mathbf{p}_{\mathrm{I}}=\Delta\mathbf{p}_{j1},\ \Delta\mathbf{p}_{\mathrm{II}}=\Delta\mathbf{p}_{j2},\ \Delta\mathbf{p}_{\mathrm{III}}=\Delta\mathbf{p}_{j3}.$$

If j_1 is plane, j_2 and j_3 are cylindrical hole:

$$\Delta \mathbf{n}_1=\Delta \mathbf{v}_{j1},$$

$$\begin{aligned}
\Delta n_{\mathrm{II}x} &= (p_{j_2y} - p_{j_3y})\Delta v_{j_3z} - \Delta p_{j_3y} + \Delta p_{j_2y} = -\Delta p_{j_3y} + \Delta p_{j_2y}, \\
\Delta n_{\mathrm{II}y} &= (p_{j_3x} - p_{j_2x})\Delta v_{j_3z} + \Delta p_{j_3x} - \Delta p_{j_2x}, \\
\Delta n_{\mathrm{II}z} &= (p_{j_3y} - p_{j_2y})\Delta v_{j_3x} + (p_{j_2x} - p_{j_3x})\Delta v_{j_3z} = (p_{j_2x} - p_{j_3x})\Delta v_{j_3z}, \\
\Delta n_{3x} &= \Delta p_{j_2x} - \Delta p_{j_3x}, \\
\Delta n_{3y} &= \Delta p_{j_2y} - \Delta p_{j_3y}, \\
\Delta n_{3z} &= \Delta p_{j_2z} - \Delta p_{j_3z}.
\end{aligned} \tag{2.14}$$

2.4 Variation Propagation Modeling Based on Error Equivalence for Multi-Operation Machining Process

2.4.1 Background Review for Multi-Operational Manufacturing Process

Due to the increasing complexity of products and the requirements of quick response and flexibility, manufacturing process has evolved into complex systems consisting of many stages, where the variation can be accumulated through multiple stages onto the final product. Such variation transmission has been widely investigated.

Variation propagation modeling has been proved to be an effective way for variation reduction and design synthesis in multi-operational manufacturing processes. A brief review is given to the previously developed state space model.

For an N-operation manufacturing process, the state of the kth operation $\mathbf{x}(k)$ is described as a linear combination of the previous state $\mathbf{x}(k\text{-}1)$, process input $\mathbf{u}(k)$, and natural process variation $\boldsymbol{\zeta}(k)$. Quality characteristic $\mathbf{y}(k)$ is a linear transformation of state $\mathbf{x}(k)$ plus measurement noise $\boldsymbol{\eta}(k)$. Under small deviation assumption, the model has the following form

$$\mathbf{x}(k)=\mathbf{A}(k\text{-}1)\mathbf{x}(k\text{-}1)+\mathbf{B}(k)\mathbf{u}(k)+\boldsymbol{\zeta}(k), \quad k=1, 2, \ldots, N, \tag{2.15}$$

$$\mathbf{y}(k)=\mathbf{C}(k)\mathbf{x}(k)+\boldsymbol{\eta}(k), \quad \{k\} \subset \{1, 2, \ldots, N\}.$$

For machining processes, state vector $\mathbf{x}(k)$ represents the deviations of part features. The process deviation $\mathbf{u}(k)$ includes fixture and machine tool deviations, while the datum deviation is contained in $\mathbf{x}(k\text{-}1)$. State transition matrix $\mathbf{A}(k\text{-}1)$ and input coefficient matrix $\mathbf{B}(k)$ are constant matrices determined by product and process design. The matrix $\mathbf{C}(k)$ is determined by measurement design. Denote by $\mathbf{y}$ the quality characteristics of N operations and by $\mathbf{u}$ the process deviations from all operations. The relationship between $\mathbf{y}$ and $\mathbf{u}$ can be obtained by solving Eq. (2.15), which ends up with a linear model in the form $\mathbf{y}=\boldsymbol{\Gamma}\mathbf{u}+\boldsymbol{\varepsilon}$ or $\mathbf{x}=\boldsymbol{\Gamma}\mathbf{u}+\boldsymbol{\varepsilon}$. Diagnosis and measurement synthesis can be performed by analyzing the rank of matrix $\boldsymbol{\Gamma}$ (Ding, *et al.*, 2003; and Zhou, Huang, and Shi, 2003). The problem encountered, however, is that $\boldsymbol{\Gamma}$ is often not full rank for machining processes. One natural thought is to increase the dimension of quality characteristics $\mathbf{y}$ to increase the rank of $\boldsymbol{\Gamma}$ matrix. Nevertheless, this strategy cannot guarantee the full rank of $\boldsymbol{\Gamma}$ because datum, fixture, and machine tool errors could generate the same error patterns on part features. Previously developed approaches for machining processes (Huang, Shi, and Yuan, 2003; Djurdjanovic and Ni, 2001; and Zhou, Huang, and Shi, 2003), however, did not model the error equivalence. Consequently, it is difficult to distinguish error sources at each operation (Huang and Shi, 2004).

The strategy proposed in this chapter is to formulate the variation propagation model using the proposed EFE concept. With this concept, datum error and machine tool error are transformed to equivalent fixture locator errors at each operation. As a result, the dimension of $\mathbf{u}$ can be reduced by properly grouping three types of errors together.

The rationale of the proposed methodology is to conduct measurement in a sequential manner for root cause identification. First, only necessary information is provided to identify whether there is any error in the process. If not, additional measurement is deemed as waste of resources. Second, if any error is identified, further measurement will be conducted to distinguish three types of errors. This methodology generally requires less feature measurements than the previous approaches. A detailed diagnostic algorithm will be presented in Chapter 3.

2.4.2 Variation Propagation Model Derivation

This section shows the derivation procedure for the surface deviation $\mathbf{x}_j(k)$ (Fig. 2.9). It can be easily extended for part deviation $\mathbf{x}(k)$ and establishing state space model.

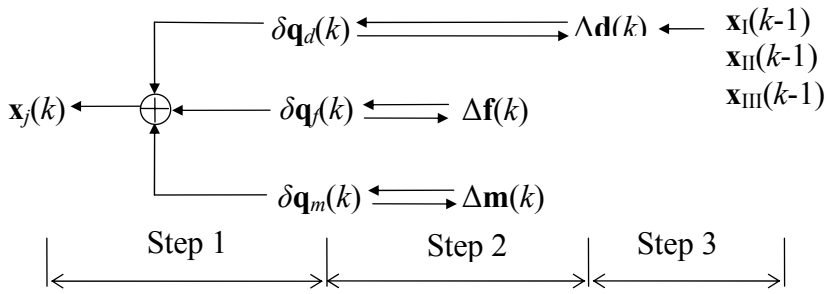

Figure 2.9 Model Derivation

Step 1 models how feature quality is affected by faulty setup and cutting operation at the kth stage. Parameters $\delta\mathbf{q}_d(k)$, $\delta\mathbf{q}_f(k)$, and $\delta\mathbf{q}_m(k)$ in HTMs are intermediate variables linking $\Delta\mathbf{f}(k)$, $\Delta\mathbf{d}(k)$, and $\Delta\mathbf{m}(k)$ with feature deviation $\mathbf{x}_j(k)$. Step 2 derives how fixture error $\Delta\mathbf{f}(k)$, EFE $\Delta\mathbf{d}(k)$ and $\Delta\mathbf{m}(k)$ affect $\delta\mathbf{q}_d(k)$, $\delta\mathbf{q}_f(k)$, and $\delta\mathbf{q}_m(k)$, respectively. Step 3 describes how errors from previous operation (datum error) affect $\Delta\mathbf{d}(k)$.

Step 1. After setup operation, the part surface can be represented by ${}^{F}\mathbf{H}_{P}(k)(\mathbf{X}_{j}^{0T}(k)\ \ 1)^{T}$. The machined surface j is represented as $\mathbf{H}_{m}(k){}^{F}\mathbf{H}_{P}(k)(\mathbf{X}_{j}^{0T}(k)\ \ 1)^{T}$ in the FCS^0. After transforming the surface to the PCS^0 (Huang and Shi, 2003), the actual surface $\mathbf{X}_j(k)$ is:

$$\left(\mathbf{X}_{j}^{T}(k)\ \ 1\right)^{T} = {}^{F}\mathbf{H}_{P}^{-1}(k)\mathbf{H}_{d}^{-1}(k)\mathbf{H}_{f}^{-1}(k)\mathbf{H}_{m}(k){}^{F}\mathbf{H}_{P}(k)\left(\mathbf{X}_{j}^{0T}(k)\ \ 1\right)^{T}, \tag{2.16}$$

where $\mathbf{X}_{j}^{0}(k)=(v_{jx}^{0}(k)\ \ v_{jy}^{0}(k)\ \ v_{jz}^{0}(k)\ \ p_{jx}^{0}(k)\ \ p_{jy}^{0}(k)\ \ p_{jz}^{0}(k))^{T}$. By substituting Eq. (2.4) into Eq. (2.16), we can compute the actual machined surface $\mathbf{X}_j(k)$. After ignoring higher order error terms, Eq. (2.16) can be rewritten as:

$$\mathbf{x}_{j}(k)=\left(\begin{array}{c|c|c|c}\mathbf{A}_{jd}(k) & \mathbf{A}_{jf}(k) & -\mathbf{A}_{jm}(k) & \mathbf{0}_{6\times1}\\ \hline \multicolumn{3}{c|}{\mathbf{0}_{1\times18}} & r_{j}^{0}(k)\end{array}\right)\delta\mathbf{q}(k)+\boldsymbol{\zeta}_{j}(k), \text{ and}$$

$$\mathbf{A}_{jd}(k)=\mathbf{A}_{jf}(k)=-\mathbf{A}_{jm}(k)=\begin{pmatrix}0&0&0&0&-2v_{jz}^{0}&2v_{jy}^{0}\\0&0&0&2v_{jz}^{0}&0&-2v_{jx}^{0}\\0&0&0&-2v_{jy}^{0}&2v_{jx}^{0}&0\\-1&0&0&0&-2p_{jz}^{0}&2p_{jy}^{0}\\0&-1&0&2p_{jz}^{0}&0&-2p_{jx}^{0}\\0&0&-1&-2p_{jy}^{0}&2p_{jx}^{0}&0\end{pmatrix} \text{ if } {}^{F}\mathbf{H}_{P}(k)=\mathbf{I}, \tag{2.17}$$

where rank($\mathbf{A}_{jd}$)≤5 and $\delta\mathbf{q}(k)=\left(\delta\mathbf{q}_{d}^{T}(k)\mid\delta\mathbf{q}_{f}^{T}(k)\mid-\delta\mathbf{q}_{m}^{T}(k)\mid\gamma_{m}(k)-1\right)^{T}$. $\boldsymbol{\zeta}(k)$ is the modeling error for operation k. Index k is omitted within matrices $\mathbf{A}_{jd}(k)$, $\mathbf{A}_{jf}(k)$ and $\mathbf{A}_{jm}(k)$.

The $\delta\mathbf{q}(k)$ can be grouped because of $\mathbf{A}_{jd}(k)=\mathbf{A}_{jf}(k)=-\mathbf{A}_{jm}(k)$. Eq. (2.17) is

$$\mathbf{x}_{j}(k)=\left(\begin{array}{c|c}\mathbf{A}_{jd}(k) & \mathbf{0}_{6\times1}\\ \hline \mathbf{0}_{1\times6} & r_{j}^{0}(k)\end{array}\right)\left((\delta\mathbf{q}_{d}^{T}(k)\quad0)^{T}+\left((\delta\mathbf{q}_{f}(k)-\delta\mathbf{q}_{m}(k))^{\mathrm{T}}\quad\gamma_{m}(k)\text{-}1\right)^{T}\right)+\boldsymbol{\zeta}(k), \tag{2.18}$$

where the dimension of $\delta\mathbf{q}(k)$ is reduced from 19 to 7.

The expression for $\mathbf{A}_{jd}(k)$, $\mathbf{A}_{jf}(k)$ and $-\mathbf{A}_{jm}(k)$ in Eq. (2.17) is only given under the condition of ${}^{F}\mathbf{H}_{P}(k)=\mathbf{I}$. In Section 2.4.3, we will show that $\mathbf{A}_{jd}(k)=\mathbf{A}_{jf}(k)=-\mathbf{A}_{jm}(k)$ and error grouping still hold if ${}^{F}\mathbf{H}_{P}(k)\neq\mathbf{I}$.

Step 2. Relationship between $\delta\mathbf{q}_f(k)$ and $\Delta\mathbf{f}$ has been given as $\delta\mathbf{q}_f = \text{-}\mathbf{J}^{-1}\mathbf{\Phi}\mathbf{E}\Delta\mathbf{f}$ by Cai, *et al.*, (1997) (refer to Appendix A for a brief summary of the result). By the concept of EFE, $\Delta\mathbf{d}$ and $\Delta\mathbf{m}$ are equivalent to $\Delta\mathbf{f}$. Therefore, $\delta\mathbf{q}_d(k)$ and $\delta\mathbf{q}_m(k)$ can be determined accordingly by the same approach, i.e.,

$$\delta\mathbf{q}_d = \text{-}\mathbf{J}^{-1}\mathbf{\Phi}\mathbf{E}\Delta\mathbf{d} \text{ and} \tag{2.19}$$

$$\delta\mathbf{q}_m = -(-\mathbf{J}^{-1}\mathbf{\Phi}\mathbf{E}\Delta\mathbf{m}) = \mathbf{J}^{-1}\mathbf{\Phi}\mathbf{E}\Delta\mathbf{m}, \tag{2.20}$$

where matrix $\mathbf{E}$ is an 18×6 matrix (see Appendix A). Since $\mathbf{H}_m^{-1}$ (not $\mathbf{H}_m$) transforms the workpiece from nominal position to its real position in the FCS (refer to Fig. 2.5(b)), we add minus sign before $-\mathbf{J}^{-1}\mathbf{\Phi}\mathbf{E}\Delta\mathbf{m}$ in Eq. (2.20). It turns out that Jacobian matrix $\mathbf{J}$ and orientation matrix $\mathbf{\Phi}$ in Eqs. (2.19) and (2.20) are the same as those in Eq. (A.1). Therefore, we still can group errors after substituting Eqs. (A.1), (2.19), and (2.20) into Eq. (2.18),

$$\mathbf{x}_j(k) = \mathbf{B}_j(k)\begin{pmatrix}\Delta\mathbf{d}^T(k) & 0\end{pmatrix}^T + \mathbf{B}_j(k)\mathbf{u}(k) + \boldsymbol{\zeta}_j(k), \tag{2.21}$$

where $\mathbf{B}_j(k) = \left(\begin{array}{c|c} \text{-}\mathbf{A}_{jd}(k)\mathbf{J}^{-1}(k)\mathbf{\Phi}(k)\mathbf{E} & \mathbf{0}_{6\times 1} \\ \hline \mathbf{0}_{1\times 6} & r_j^0(k) \end{array}\right)$ is the input coefficient matrix linking errors at the current operation with feature deviation, rank $(\text{-}\mathbf{A}_{jd}(k)\mathbf{J}^{-1}(k)\mathbf{\Phi}(k)\mathbf{E}) \leq 5$, and $\mathbf{u}(k)=((\Delta\mathbf{f}(k)+\Delta\mathbf{m}(k))^T, \gamma_m(k)\text{-}1)^T$.

Step 3. EFE $\Delta\mathbf{d}(k)$ in Eq. (2.18) becomes

$$\begin{pmatrix}\Delta\mathbf{d}(k)\\ 1\end{pmatrix} = \begin{pmatrix}\mathbf{\Psi} & \mathbf{0}\\ \mathbf{0} & 1\end{pmatrix}_{7\times 22} \mathbf{H}_{22\times 22} \begin{pmatrix}\mathbf{G} & \mathbf{0}\\ \mathbf{0} & 1\end{pmatrix}_{22\times 22} \begin{pmatrix}\mathbf{x}_{\mathrm{I}}(k-1)\\ \hline \mathbf{x}_{\mathrm{II}}(k-1)\\ \hline \mathbf{x}_{\mathrm{III}}(k-1)\\ 1\end{pmatrix}_{22\times 1}, \tag{2.22}$$

where matrix **H** transforms deviations of three datum surfaces from PCS^0 to FCS^0. It is defined as $\left(\begin{array}{c|c} {}^F\mathbf{R}_P & \begin{matrix}(\mathbf{0}_{1\times3}\ {}^Fx_P\ {}^Fy_P\ {}^Fz_P\ 0)^T \\ (\mathbf{0}_{1\times3}\ {}^Fx_P\ {}^Fy_P\ {}^Fz_P\ 0)^T \\ (\mathbf{0}_{1\times3}\ {}^Fx_P\ {}^Fy_P\ {}^Fz_P\ 0)^T\end{matrix} \\ \hline \mathbf{0}_{1\times21} & 1 \end{array}\right)$; where ${}^F\mathbf{R}_P$= diag(${}^F\mathbf{Rot}_P$ ${}^F\mathbf{Rot}_P$ γ_m ${}^F\mathbf{Rot}_P$ ${}^F\mathbf{Rot}_P$ γ_m ${}^F\mathbf{Rot}_P$ ${}^F\mathbf{Rot}_P$ γ_m). ${}^F\mathbf{Rot}_P$ is the rotational block matrix in ${}^F\mathbf{H}_P$. $({}^Fx_P\ {}^Fy_P\ {}^Fz_P)^T$ are translation parameters. Matrix $\mathbf{\Psi}=\begin{pmatrix}\mathbf{\Psi}_1 & \mathbf{0} & \mathbf{0} \\ \mathbf{0} & \mathbf{\Psi}_2 & \mathbf{0} \\ \mathbf{0} & \mathbf{0} & \mathbf{\Psi}_3\end{pmatrix}$ maps the deviation of workpiece to the EFE with $\mathbf{\Psi}_1=-\begin{pmatrix} f_{1x} & f_{1y} & 0 & 0 & 0 & 1 & 0 \\ f_{2x} & f_{2y} & 0 & 0 & 0 & 1 & 0 \\ f_{3x} & f_{3y} & 0 & 0 & 0 & 1 & 0\end{pmatrix}$, $\mathbf{\Psi}_2=-\begin{pmatrix} f_{4x} & 0 & f_{4z} & 0 & 1 & 0 & 0 \\ f_{5x} & 0 & f_{5z} & 0 & 1 & 0 & 0\end{pmatrix}$, and $\mathbf{\Psi}_3=-\begin{pmatrix}0 & f_{6y} & f_{6z} & 1 & 0 & 0 & 0\end{pmatrix}$. Matrix **G** is introduced for computing deviation of orientation vector of datum surface under two conditions:

- If all datum surfaces are planar: **G**=**I**;
- If $\mathbf{X}_\mathrm{I}$ is plane, $\mathbf{X}_\mathrm{II}$ and $\mathbf{X}_\mathrm{III}$ are cylindrical holes, **G** can be obtained by differentiating $\mathbf{v}_\mathrm{II}\times(\mathbf{p}_\mathrm{II}-\mathbf{p}_\mathrm{III})$ and $\mathbf{p}_\mathrm{II}$-$\mathbf{p}_\mathrm{III}$. Considering the results in Eq. (2.14), we have

$$\mathbf{G}=\left(\begin{array}{c|c|c} \mathbf{I}_{7\times7} & \mathbf{0} & \mathbf{0} \\ \hline \mathbf{0} & \begin{matrix}\mathbf{G}_{11} \\ \mathbf{0}_{4\times3}\ \mathbf{I}_{4\times4}\end{matrix} & \begin{matrix}\mathbf{G}_{12} \\ \mathbf{0}_{4\times7}\end{matrix} \\ \hline \mathbf{0} & \begin{matrix}\mathbf{G}_{21} \\ \mathbf{0}_{4\times3}\ \mathbf{I}_{4\times4}\end{matrix} & \begin{matrix}\mathbf{G}_{22} \\ \mathbf{0}_{4\times7}\end{matrix} \end{array}\right),\ \text{where}\ \mathbf{G}_{11}=\begin{pmatrix}0 & 0 & 0 & 0 & -1 & 0 & 0 \\ 0 & 0 & p_{j_2x}\text{-}p_{j_3x} & 1 & 0 & 0 & 0 \\ 0 & p_{j_3x}\text{-}p_{j_2x} & 0 & 0 & 0 & 0 & 0\end{pmatrix},$$

$$\mathbf{G}_{12}=\begin{pmatrix}0 & 0 & 0 & 0 & 1 & 0 & 0 \\ 0 & 0 & 0 & -1 & 0 & 0 & 0 \\ 0 & 0 & 0 & 0 & 0 & 0 & 0\end{pmatrix},\ \mathbf{G}_{21}=\begin{pmatrix}0 & 0 & 0 & 1 & 0 & 0 & 0 \\ 0 & 0 & 0 & 0 & 1 & 0 & 0 \\ 0 & 0 & 0 & 0 & 0 & 1 & 0\end{pmatrix},\ \mathbf{G}_{22}=\begin{pmatrix}0 & 0 & 0 & -1 & 0 & 0 & 0 \\ 0 & 0 & 0 & 0 & -1 & 0 & 0 \\ 0 & 0 & 0 & 0 & 0 & -1 & 0\end{pmatrix}.$$

Substituting Eq. (2.22) into Eq. (2.21), state transition matrix $\mathbf{A}_j(k\text{-}1)$ can be obtained and we derive the variation propagation model for the surface j at operation k. If we assemble the model for all the features and datum surfaces, the equation in the form of the state space model can be obtained. The dimension of input vector $\mathbf{u}(k)$ is reduced from 13 to 7 because of error grouping. Thus the order of matrix $\mathbf{\Gamma}^{*T}\mathbf{\Gamma}^{*}$ is greatly reduced. The dimension of output vector $\mathbf{x}(k)$ required to make $\mathbf{\Gamma}^{*T}\mathbf{\Gamma}^{*}$ full rank is reduced as well. When FCS, PCS, and MCS coincide, and the orientation vectors of datum surfaces are $(0\ 0\ \text{-}1\ 0\ 0\ 0\ 0)^T$, $(0\ \text{-}1\ 0\ 0\ 0\ 0\ 0)^T$, and $(\text{-}1\ 0\ 0\ 0\ 0\ 0\ 0)^T$ in the FCS, we get input matrix $\mathbf{\Gamma}_j^*$ corresponding to the machined surface j $\begin{pmatrix} v_{x0} & v_{y0} & v_{z0} & p_{x0} & p_{y0} & p_{z0} & 0 \end{pmatrix}^T$ as

$$\mathbf{\Gamma}_j^* = -\mathbf{A}_{jd}\mathbf{J}^{-1}\mathbf{\Phi}\mathbf{E}, \tag{2.23}$$

which yields $\mathbf{\Gamma}_j^*$ matrix, i.e.,

$$\Gamma_j^* = \begin{pmatrix} \frac{f_{3x}(f_{4z}-f_{5z})v_{y0}+f_{2x}(-f_{4z}+f_{5z})v_{y0}+(f_{4x}-f_{5x})(f_{2y}-f_{3y})v_{z0}}{(f_{4x}-f_{5x})(f_{3x}(f_{1y}-f_{2y})+f_{2x}(-f_{1y}+f_{3y})+f_x(f_{2y}-f_{3y}))} & \frac{f_{3x}(f_{4z}-f_{5z})v_{y0}+f_{1x}(-f_{4z}+f_{5z})v_{y0}+(f_{4x}-f_{5x})(f_{1y}-f_{3y})v_{z0}}{(f_{4x}-f_{5x})(f_{3x}(-f_{1y}+f_{2y})+f_{2x}(f_{1y}-f_{3y})+f_{1x}(-f_{2y}+f_{3y}))} \\ \frac{(f_{2x}-f_{3x})(f_{4z}v_{x0}-f_{5z}v_{x0}+(-f_{4x}+f_{5x})v_{z0})}{(f_{4x}-f_{5x})(f_{3x}(-f_{1y}+f_{2y})+f_{2x}(f_{1y}-f_{3y})+f_x(-f_{2y}+f_{3y}))} & \frac{(f_x-f_{3x})(f_{4z}v_{x0}-f_{5z}v_{x0}+(-f_{4x}+f_{5x})v_{z0})}{(f_{4x}-f_{5x})(f_{3x}(-f_{1y}+f_{2y})+f_{1x}(-f_{2y}+f_{3y})+f_{2x}(f_{1y}-f_{3y}))} \\ \frac{-f_{2y}v_{x0}+f_{3y}v_{x0}+(f_{2x}-f_{3x})v_{y0}}{f_{3x}(f_{1y}-f_{2y})+f_{1x}(f_{2y}-f_{3y})+f_{2x}(-f_{1y}+f_{3y})} & \frac{f_{1y}v_{1x0}-f_{3y}v_{x0}+(-f_{1x}+f_{3x})v_{y0}}{f_{3x}(f_{1y}-f_{2y})+f_{1x}(f_{2y}-f_{3y})+f_{2x}(-f_{1y}+f_{3y})} \\ \frac{-f_{2x}(f_{4z}-f_{5z})(f_{6y}-p_{y0})+f_{3x}(f_{4z}-f_{5z})(f_{6y}+p_{y0})+(f_{4x}-f_{5x})(f_{2y}-f_{3y})(f_{6z}-p_{z0})}{(f_{4x}-f_{5x})(f_{3x}(-f_{1y}+f_{2y})+f_{2x}(f_{1y}-f_{3y})+f_{1x}(-f_{2y}+f_{3y}))} & \frac{-f_{1x}(f_{4z}-f_{5z})(f_{6y}-p_{y0})+f_{3x}(f_{4z}-f_{5z})(f_{6y}-p_{y0})+(f_{4x}-f_{5x})(f_{1y}-f_{3y})(f_{6z}-p_{z0})}{(f_{4x}-f_{5x})(f_{3x}(f_{1y}-f_{2y})+f_{1x}(f_{2y}-f_{3y})+f_{2x}(-f_{1y}+f_{3y}))} \\ \frac{(f_{2x}-f_{3x})((-f_{4z}+f_{5z})p_{x0}+f_{5x}(f_{4z}-p_{z0})+f_{4x}(-f_{5z}+p_{z0}))}{(f_{4x}-f_{5x})(f_{3x}(-f_{1y}+f_{2y})+f_{2x}(f_{1y}-f_{3y})+f_{1x}(-f_{2y}+f_{3y}))} & \frac{(f_{1x}-f_{3x})((-f_{4z}+f_{5z})p_{x0}+f_{5x}(f_{4z}+p_{z0})-f_{4x}(f_{5z}-p_{z0}))}{(f_{4x}-f_{5x})(f_{3x}(f_{1y}-f_{2y})+f_{1x}(f_{2y}-f_{3y})+f_{2x}(-f_{1y}+f_{3y}))} \\ \frac{(-f_{2y}+f_{3y})p_{x0}+f_{3x}(f_{2y}-p_{y0})-f_{2x}(f_{3y}-p_{y0})}{f_{3x}(f_{1y}-f_{2y})+f_{1x}(f_{2y}-f_{3y})+f_{2x}(-f_{1y}+f_{3y})} & \frac{(f_{1y}-f_{3y})p_{x0}-f_{3x}(f_{1y}-p_{y0})+f_{1x}(f_{3y}-p_{y0})}{f_{3x}(f_{1y}-f_{2y})+f_x(f_{2y}-f_{3y})+f_{2x}(-f_{1y}+f_{3y})} \end{pmatrix}$$

$$\begin{pmatrix} \frac{f_{2x}(f_{4z}-f_{5z})v_{y0}+f_{1x}(-f_{4z}+f_{5z})v_{y0}+(f_{4x}-f_{5x})(f_{1y}-f_{2y})v_{z0}}{(f_{4x}-f_{5x})(f_{3x}(f_{1y}-f_{2y})+f_{2x}(-f_{1y}+f_{3y})+f_x(f_{2y}-f_{3y}))} & \frac{v_{y0}}{f_{4x}-f_{5x}} & \frac{v_{y0}}{-f_{4x}+f_{5x}} & 0 \\ \frac{(f_x-f_{2x})(f_{4z}v_{x0}-f_{5z}v_{x0}+(-f_{4x}+f_{5x})v_{z0})}{(f_{4x}-f_{5x})(f_{3x}(f_{1y}-f_{2y})+f_{2x}(-f_{1y}+f_{3y})+f_{1x}(f_{2y}-f_{3y}))} & \frac{v_{x0}}{-f_{4x}+f_{5x}} & \frac{v_{x0}}{f_{4x}-f_{5x}} & 0 \\ \frac{-f_{1y}v_{x0}+f_{2y}v_{x0}+(f_{1x}-f_{2x})v_{y0}}{f_{3x}(f_{1y}-f_{2y})+f_{1x}(f_{2y}-f_{3y})+f_{2x}(-f_{1y}+f_{3y})} & 0 & 0 & 0 \\ \frac{-f_{1x}(f_{4z}-f_{5z})(f_{6y}-p_{y0})+f_{2x}(f_{4z}-f_{5z})(f_{6y}-p_{y0})+(f_{4x}-f_{5x})(f_{1y}-f_{2y})(f_{6z}-p_{z0})}{(f_{4x}-f_{5x})(f_{3x}(-f_{1y}+f_{2y})+f_{2x}(f_{1y}-f_{3y})+f_{1x}(-f_{2y}+f_{3y}))} & \frac{f_{6y}-p_{y0}}{-f_{4x}+f_{5x}} & \frac{f_{6y}-p_{y0}}{f_{4x}-f_{5x}} & -1 \\ \frac{(f_{1x}-f_{2x})((-f_{4z}+f_{5z})p_{x0}+f_{5x}(f_{4z}-p_{z0})-f_{4x}(f_{5z}-p_{z0}))}{(f_{4x}-f_{5x})(f_{3x}(-f_{1y}+f_{2y})+f_{2x}(f_{1y}-f_{3y})+f_{1x}(-f_{2y}+f_{3y}))} & \frac{f_{5x}-p_{x0}}{f_{4x}-f_{5x}} & \frac{f_{4x}-p_{x0}}{-f_{4x}+f_{5x}} & 0 \\ \frac{(-f_y+f_{2y})p_{x0}+f_{2x}(f_{1y}-p_{y0})-f_x(f_{2y}-p_{y0})}{f_{3x}(f_{1y}-f_{2y})+f_{1x}(f_{2y}-f_{3y})+f_{2x}(-f_{1y}+f_{3y})} & 0 & 0 & 0 \end{pmatrix},$$

where we can see that matrices $\mathbf{\Gamma}_j^*$ corresponding to three EFEs are the same.

The structure of Eq. (2.17) proves our previous claim that it is hard to conduct root cause identification using previously developed models. It also reveals that fixture and machine tool cannot be distinguished without in-process measurements on either fixture locators or the machine tool at each operation.

2.4.3 Discussion for Error Grouping in Machining Processes

In Section 2.4.2, the model derivation is based on the assumption that transformation matrix ${}^F\mathbf{H}_M(k)$ is identity. In addition, the expression of $\mathbf{A}_{jd}(k)$, $\mathbf{A}_{jf}(k)$ and $-\mathbf{A}_{jm}(k)$ are given under the condition of ${}^F\mathbf{H}_M(k)=\mathbf{I}$. In this section, a necessary and sufficient condition for error grouping is discussed.

Proposition 2.1 (Condition on grouping variables) The linear equation

$$\mathbf{x}=\begin{pmatrix} x_1 & x_2 & \dots & x_n \end{pmatrix}^T = \mathbf{\Gamma}\begin{pmatrix} u_1 & u_2 & \dots & u_m \end{pmatrix}^T, \tag{2.24}$$

where $\mathbf{\Gamma}=\{g_{ij}\}_{n\times m}$, i=1,2,…, n; j=1, 2,…, m; $x_1, x_{2,} ..., x_n$ and $u_1, u_{2,} ..., u_m$ are variables, can be grouped into the following form

$$\mathbf{x} = \begin{pmatrix} p_1 & p_2 & \cdots & p_n \end{pmatrix}^T u \text{ with } u = k_1u_1 + k_2u_2 + ... + k_mu_m . \tag{2.25}$$

where p_i and k_j are certain coefficients, if and only if the rank of matrix $\mathbf{\Gamma}$ is one or zero.

In our study, the coefficient matrices of $\Delta\mathbf{d}$, $\Delta\mathbf{f}$, and $\Delta\mathbf{m}$ are the same, (see Eqs. (A.1), (2.19), and (2.20)), which satisfies the sufficient condition for grouping.

In the above discussion, we assume the transformation matrix ${}^F\mathbf{H}_P$ and ${}^F\mathbf{H}_M$ to be identities. If three coordinate systems do not coincide with each other, the coefficient matrices for $\Delta\mathbf{d}$, $\Delta\mathbf{f}$, and $\Delta\mathbf{m}$ are still the same when ${}^F\mathbf{H}_P \neq \mathbf{I}_{8\times 8}$ and ${}^F\mathbf{H}_M = \mathbf{I}_{8\times 8}$. However, this is not true when ${}^F\mathbf{H}_M \neq \mathbf{I}_{8\times 8}$. We have the following conclusion.

Corollary. MCS^0 and FCS^0 must coincide to perform error grouping in the proposed model. However, this requirement can be easily satisfied in modeling stage. The proofs of the proposition and corollary are listed in Appendix B.

2.5 EFE Validation and Modeling Demonstration

This section validates the EFE with a milling process and demonstrates the modeling procedures for a multi-operational machining process.

2.5.1 Experimental Validation of EFE

We machine 6 blocks to validate EFE model. The first three parts are cut with only datum error, while the rest are cut with only machine tool error. The datum error and machine tool error are set in such a way that $\Delta\mathbf{d}=\Delta\mathbf{m}=(1.105\ 0\ 0\ 0\ 0\ 0)^T$, i.e., their EFEs are the same based on Eqs. (2.8) and (2.9). Then we can measure the machined surface and compare the surface orientation and position.

Fig. 2.10 shows the specification of raw workpiece and fixture layout. Only top surface **X** is machined and its specification is $\mathbf{X}^0=(0\ 0\ 1\ 0\ 0\ 20.32\ 0)^T$. Using Eq. (2.21), the deviated surface **X** is predicted as $(0\ -0.0175\ 0.9998\ 0\ 0\ 18.88)^T$.

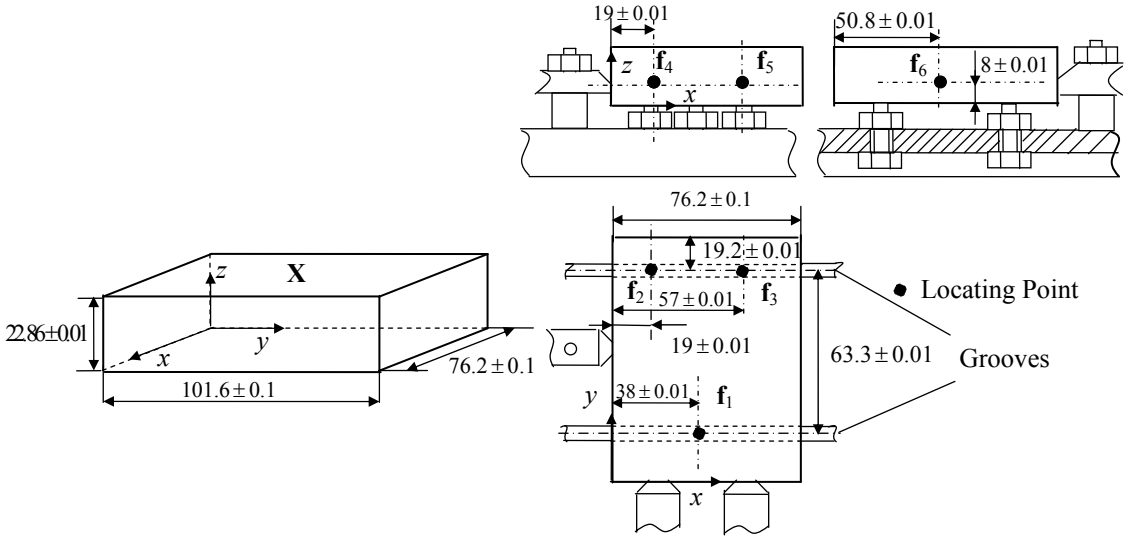

Figure 2.10 Raw Workpiece and Locating Scheme (Unit: mm)

Table 2.1 shows the measurement of the machined surface. As can be seen, the discrepancies between two samples are very small. The measurement data are also comparable with the predicted results. Therefore, the experiment supports EFE model.

Table 2.1 Measurement Results (Under PCS^0)

X	v_x	v_y	v_z	p_x	p_y	p_z
Sample 1 (Datum Error)	0	-0.0174	0.9998	0	0	18.880
	-0.0001	-0.0174	0.9998	0	0	18.882
	0	-0.0174	0.9998	0	0	18.881
Sample 2 (Machine Tool Error)	0	-0.0172	0.9999	0	0	18.880
	-0.0001	-0.0173	0.9999	0	0	18.884
	0	-0.0163	0.9999	0	0	18.887

2.5.2 Multi-Operational Variation Propagation Modeling With Grouped EFEs

A machining process for V-8 cylinder head is employed to illustrate modeling procedure and the advantage of the modeling approach. The drawing of workpiece and the locating points are shown in Fig. 2.11. The surfaces chosen are marked as $\mathbf{X}_1$- $\mathbf{X}_8$. $\mathbf{X}_1$ is the exhaust face, while $\mathbf{X}_2$ and $\mathbf{X}_3$ are two cup plug holes on the $\mathbf{X}_1$. $\mathbf{X}_4$ is spark plug tube hole and $\mathbf{X}_5$ is a hole for the exhaust lash adjuster. $\mathbf{X}_4$ and $\mathbf{X}_5$ are two angle holes and the specifications are given in section plots S_1-S_1 and S_2-S_2. Center of $\mathbf{X}_7$ is set to be the origin of nominal part coordinate system. Based on the dimensions shown in Fig. 2.11, the specification of each machined surface is listed in Table 2.2.

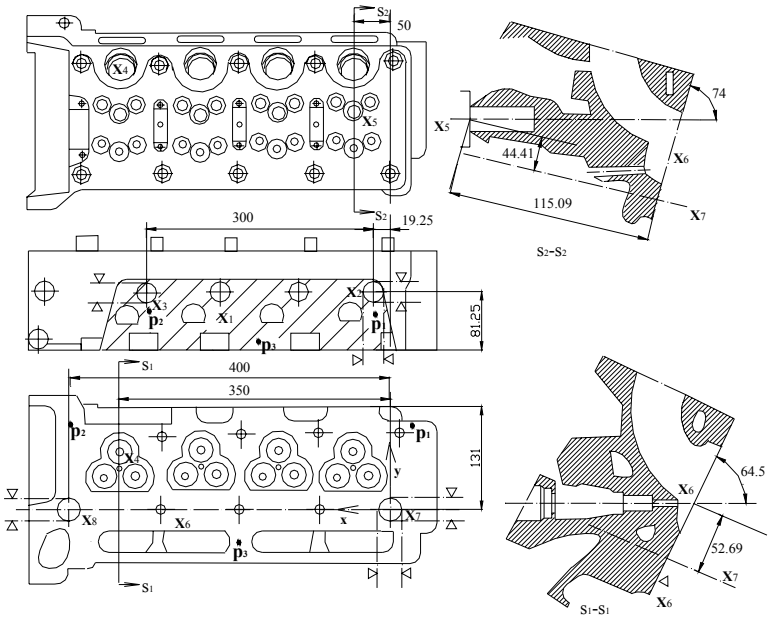

Figure 2.11 Workpiece and Locating

The workpiece goes through two operations (Fig. 2.12): the first operation mills $\mathbf{X}_1$ and drills $\mathbf{X}_2$ and $\mathbf{X}_3$ using datum surfaces $\mathbf{X}_6$, $\mathbf{X}_7$ and $\mathbf{X}_8$; and the second operation drills $\mathbf{X}_4$ and $\mathbf{X}_5$ using datum surface $\mathbf{X}_1$, $\mathbf{X}_2$ and $\mathbf{X}_3$. The locator positions on the primary datum planes are given in Table 2.3.

Table 2.2 Machined Features Specification

Feature Component	Part Features (In the PCS^0, Unit: mm)							
	$\mathbf{X}_1$	$\mathbf{X}_2$	$\mathbf{X}_3$	$\mathbf{X}_4$	$\mathbf{X}_5$	$\mathbf{X}_6$	$\mathbf{X}_7$	$\mathbf{X}_8$
$v_x(k)$	0	0	0	0	0	0	0	0
$v_y(k)$	1	1	1	0.43	0.28	0	0	0
$v_z(k)$	0	0	0	0.90	-0.96	-1	1	1
$p_x(k)$	0	19.25	319.25	350	50	0	0	400
$p_y(k)$	131	131	131	52.69	44.41	0	0	0
$p_z(k)$	0	81.25	81.25	0	115.09	0	0	0
$r(k)$	0	7.5	7.5	4.6	16.92	0	5	5

Table 2.3 Coordinates of Locating Points on the Primary Datum Surfaces (Unit: mm)

	p_1	p_2	p_3
Operation 1	(-7, 109, 0)	(407, 109, 0)	(200, -11, 0)
Operation 2	(19.25, 131, 61.25)	(319.25, 131, 61.25)	(169.25, 131, 11.25)

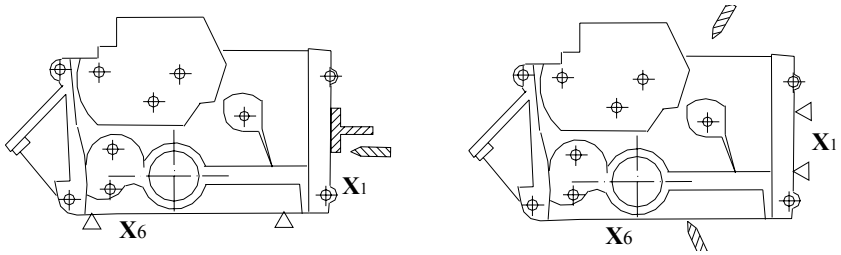

Operation 1 Operation 2

Figure 2.12 Two Cutting Operations

The state vector is $\mathbf{x}(k)=\left(\mathbf{x}_1^T(k) \quad \mathbf{x}_2^T(k) \quad \mathbf{x}_3^T(k) \quad \mathbf{x}_4^T(k) \quad \mathbf{x}_5^T(k)\right)^T$. Since diagnosis of feature size is relatively straightforward, we do not consider effect of size. In this case study, we also assume that the workpiece is perfect, i.e., $\mathbf{x}_j(0)=\mathbf{0}$, j=1,2,…,5.

As a comparison, before using the proposed methodology, we can check the number of necessary measurements for identifying errors via previously proposed model (Zhou, Huang, and Shi, 2003; Huang and Shi, 2004). It can be observed that there are 12 error components (6 fixture and 6 machine tool error components) as input to the model for each operation and therefore, total 24 inputs entails 24 components in quality characteristic for root cause identification. Since each feature contains 6 components, at least 12/6=2 features are required for each operation. However, we have shown in Eq. (2.21) that the rank of block matrix $-\mathbf{A}_{jd}\mathbf{J}^{-1}(k)\mathbf{\Phi}(k)\mathbf{E}$ in $\mathbf{B}_j(k)$ does not exceed 5. More features information is needed to identify all the errors. Therefore, the number of features identifying errors for each operation should be no less than 3. In this case study where only two operations are considered, total amount of measured features should not be less than $3\times2=6$ even if the purpose is to identify whether errors occur in the process. Using Eqs. (2.21) and (2.22), we calculate $\mathbf{A}_j(k)$ and $\mathbf{B}_j(k)$, based on which the model in the grouped form is formulated as follows.

Operation 1: Because the first operation only mills $\mathbf{X}_1$ and drills $\mathbf{X}_2$ and $\mathbf{X}_3$, input matrices for features 4 and 5 are zero. The results are:

$$\mathbf{B}_1(1)=\left(\begin{array}{cccccc|c} 0 & 0 & 0 & -0.0025 & 0.0025 & 0 & \\ 0 & 0 & 0 & 0 & 0 & 0 & \\ -0.0042 & -0.0042 & 0.0083 & 0 & 0 & 0 & \mathbf{0}_{6\times1} \\ 0 & 0 & 0 & -0.3275 & 0.3275 & -1 & \\ 0 & 0 & 0 & -1 & 0 & 0 & \\ -1.0748 & -0.1086 & 0.1833 & 0 & 0 & 0 & \\ \hline \multicolumn{6}{c|}{\mathbf{0}_{1\times6}} & 0 \end{array}\right), \mathbf{B}_2(1)=\left(\begin{array}{cccccc|c} 0 & 0 & 0 & -0.0025 & 0.0025 & 0 & \\ 0 & 0 & 0 & 0 & 0 & 0 & \\ -0.0042 & -0.0042 & 0.0083 & 0 & 0 & 0 & \mathbf{0}_{6\times1} \\ -0.1963 & 0.1963 & 0 & -0.3275 & 0.3275 & -1 & \\ 0.3385 & 0.3385 & -0.6771 & -0.9519 & -0.0481 & 0 & \\ -1.0283 & -0.1551 & 0.1833 & 0 & 0 & 0 & \\ \hline \multicolumn{6}{c|}{\mathbf{0}_{1\times6}} & 7.5 \end{array}\right),$$

$$\mathbf{B}_3(1)=\left(\begin{array}{cccccc|c} 0 & 0 & 0 & -0.0025 & 0.0025 & 0 & \\ 0 & 0 & 0 & 0 & 0 & 0 & \\ -0.0042 & -0.0042 & 0.0083 & 0 & 0 & 0 & \mathbf{0}_{6\times1} \\ -0.1963 & 0.1963 & 0 & -0.3275 & 0.3275 & -1 & \\ 0.3385 & 0.3385 & -0.6771 & -0.2019 & -0.7981 & 0 & \\ -0.3036 & -0.8797 & 0.1833 & 0 & 0 & 0 & \\ \hline \multicolumn{6}{c|}{\mathbf{0}_{1\times6}} & 7.5 \end{array}\right), \quad \mathbf{B}_4(1)=\begin{pmatrix}\mathbf{0}_{6\times6} & \\ & 4.6\end{pmatrix}, \text{ and } \quad \mathbf{B}_5(1)=\begin{pmatrix}\mathbf{0}_{6\times6} & \\ & 16.92\end{pmatrix}.$$

The state equation for operation k can be assembled as:

$$\underbrace{\begin{pmatrix}\mathbf{x}_1(1)\\ \mathbf{x}_2(1)\\ \mathbf{x}_3(1)\\ \mathbf{x}_4(1)\\ \mathbf{x}_5(1)\\ 1\end{pmatrix}}_{(\mathbf{x}(1)^T\ \ 1)^T} = \underbrace{\begin{pmatrix}\mathbf{I}_{7\times7} & \mathbf{0} & \mathbf{0} & \mathbf{0} & \mathbf{0} & \mathbf{0}\\ \mathbf{0} & \mathbf{I}_{7\times7} & \mathbf{0} & \mathbf{0} & \mathbf{0} & \mathbf{0}\\ \mathbf{0} & \mathbf{0} & \mathbf{I}_{7\times7} & \mathbf{0} & \mathbf{0} & \mathbf{0}\\ \mathbf{0} & \mathbf{0} & \mathbf{0} & \mathbf{I}_{7\times7} & \mathbf{0} & \mathbf{0}\\ \mathbf{0} & \mathbf{0} & \mathbf{0} & \mathbf{0} & \mathbf{I}_{7\times7} & \mathbf{0}\\ \mathbf{0} & \mathbf{0} & \mathbf{0} & \mathbf{0} & \mathbf{0} & 1\end{pmatrix}}_{diag(\mathbf{A}(0)\ 1)} \underbrace{\begin{pmatrix}\mathbf{0}\\ \mathbf{0}\\ \mathbf{0}\\ \mathbf{0}\\ \mathbf{0}\\ 1\end{pmatrix}}_{(\mathbf{x}(0)^T\ 1)^T} + \underbrace{\left(\begin{array}{c|c}\mathbf{B}_1(1) & \\ \mathbf{B}_2(1) & \\ \mathbf{B}_3(1) & \mathbf{0}_{35\times1}\\ \mathbf{B}_4(1) & \\ \mathbf{B}_5(1) & \\ \hline \mathbf{0}_{1\times35} & 0\end{array}\right)}_{diag(\mathbf{B}(1)\ \ 0)} \begin{pmatrix}\Delta f_{1z}(1)+\Delta m_{1z}(1)\\ \Delta f_{2z}(1)+\Delta m_{2z}(1)\\ \Delta f_{3z}(1)+\Delta m_{3z}(1)\\ \Delta f_{4y}(1)+\Delta m_{4y}(1)\\ \Delta f_{5y}(1)+\Delta m_{5y}(1)\\ \Delta f_{6x}(1)+\Delta m_{6x}(1)\\ \mathbf{0}_{2\times1}\end{pmatrix} + \begin{pmatrix}\zeta\ (1)\\ 0\end{pmatrix},$$

where identity block matrix in $\mathbf{A}(0)$ represents that the corresponding features have not been machined. Since HTM is used to derive $\Delta\mathbf{d}(k)$ as shown in Eq. (2.22), dimension of state vector has to be increased by using "1" as the last entry, i.e., $(\mathbf{x}^T(\mathrm{k})\ 1)^T$. $\boldsymbol{\zeta}(k)$ are the stackup of $\zeta_j(k)$, where j=1, 2,…,5. Zeros in the last row of the model are introduced to make the matrix dimension consistent.

Operation 2: Since ${}^F\mathbf{H}_P(2)\neq\mathbf{I}$, expression of $\mathbf{A}_{jd}(k)$ presented in Eq. (2.17) does not apply for the second operation. However, according to the corollary in Section 2.4.3, we

can still derive **A**(1) and **B**(2) by substituting non-identity matrix ${}^{F}\mathbf{H}_{P}$ in (2.16), followed by the same procedure for deriving Eqs. (2.17), (2.18), and (2.21).

$$\mathbf{B}_4(2)=\left(\begin{array}{cccccc|c} 0.001 & -0.001 & 0 & -0.0023 & 0.0023 & 0 & \\ 0.0038 & 0.0038 & -0.0075 & 0 & 0 & 0 & \\ -0.0018 & -0.0018 & 0.0036 & 0 & 0 & 0 & \\ -0.1892 & 0.1892 & 0 & 0.2025 & -0.2025 & -1 & \mathbf{0}_{6\times1} \\ -0.6081 & 0.0248 & 1.5833 & 0 & 0 & 0 & \\ 0.3263 & 0.3263 & -0.6526 & -0.1725 & -0.8275 & 0 & \\ \hline \multicolumn{6}{c|}{\mathbf{0}_{1\times6}} & 4.6 \end{array}\right), \mathbf{B}_5(2)=\left(\begin{array}{cccccc|c} 0.007 & -0.007 & 0 & 0.0024 & -0.0024 & 0 & \\ -0.004 & -0.004 & 0.008 & 0 & 0 & 0 & \\ -0.0011 & -0.0011 & -0.0023 & 0 & 0 & 0 & \\ -0.2092 & 0.2092 & 0 & -0.0852 & 0.0852 & -1 & \mathbf{0}_{6\times1} \\ 0.5961 & -0.2203 & 0.6242 & 0 & 0 & 0 & \\ 0.3608 & 0.3608 & -0.7216 & -0.9225 & -0.0775 & 0 & \\ \hline \multicolumn{6}{c|}{\mathbf{0}_{1\times6}} & 16.92 \end{array}\right),$$

$\mathbf{B}_1(2)= \mathbf{0}_{7\times7}$, and $\mathbf{B}_2(2)=\mathbf{B}_3(2)=\text{diag}(\mathbf{0}_{6\times6}, 7.5)$.

Since datum error is generated by the first operation, state transition matrix must be calculated. By Eqs. (2.21) and (2.22), rotational deviation of the surface caused by datum errors can be expressed by $-\mathbf{A}_{jd}(k)\mathbf{J}^{-1}(k)\mathbf{\Phi}(k)\mathbf{E}\mathbf{\Psi}\,{}^{F}\mathbf{R}_{P}\mathbf{G}\begin{pmatrix}\mathbf{x}_1(1)\\ \mathbf{x}_2(1)\\ \mathbf{x}_3(1)\end{pmatrix}$, where j=4, 5. For the convenience of displaying results, we can denote $\begin{pmatrix}\mathbf{\Lambda}_{j1} & \mathbf{\Lambda}_{j2} & \mathbf{\Lambda}_{j3}\end{pmatrix}=-\mathbf{A}_{jd}(k)\mathbf{J}^{-1}(k)\mathbf{\Phi}(k)\mathbf{E}\mathbf{\Psi}\;{}^{F}\mathbf{R}_{P}\mathbf{G}$. The results are

$$\mathbf{\Lambda}_{41}=\left(\begin{array}{ccccccc} 0.4305 & 0 & 0 & 0 & 0 & 0 & 0 \\ 0 & 0 & -0.9026 & 0 & 0 & 0 & 0 \\ 0 & 0 & 0.4305 & 0 & 0 & 0 & 0 \\ -78.31 & 0 & 0 & 0 & 0 & 0 & 0 \\ -331 & 0 & 81 & 0 & 1 & 0 & 0 \\ 0 & 0 & -78.31 & 0 & 0 & 0 & 0 \\ \hline \multicolumn{7}{c}{\mathbf{0}_{1\times7}} \end{array}\right), \mathbf{\Lambda}_{42}=\left(\begin{array}{ccccccc} 0 & 0 & 0 & 0 & 0.9026 & 0 & 0 \\ 0 & 0 & 0 & 0 & 0 & 0 & 0 \\ 0 & 0 & 0 & 0 & 0 & 0 & 0 \\ 0 & 0 & 0 & 1 & -81 & 0 & 0 \\ 0 & 0 & 0 & 0 & 0 & 0 & 0 \\ 0 & 0 & 0 & 0 & -331 & 1 & 0 \\ \hline \multicolumn{7}{c}{\mathbf{0}_{1\times7}} \end{array}\right), \mathbf{\Lambda}_{43}=\left(\begin{array}{ccccccc} 0 & 0 & 0 & 0 & -0.9026 & 0 & 0 \\ 0 & 0 & 0 & 0 & 0 & 0 & 0 \\ 0 & 0 & 0 & 0 & 0 & 0 & 0 \\ 0 & 0 & 0 & 0 & 81 & 0 & 0 \\ 0 & 0 & 0 & 0 & 0 & 0 & 0 \\ 0 & 0 & 0 & 0 & 331 & 0 & 0 \\ \hline \multicolumn{7}{c}{\mathbf{0}_{1\times7}} \end{array}\right),$$

$$\mathbf{\Lambda}_{51}=\left(\begin{array}{ccccccc} 0.2756 & 0 & 0 & 0 & 0 & 0 & 0 \\ 0 & 0 & 0.9613 & 0 & 0 & 0 & 0 \\ 0 & 0 & 0.2756 & 0 & 0 & 0 & 0 \\ -86.59 & 0 & 0 & 0 & 0 & 0 & 0 \\ -31 & 0 & -34.09 & 0 & 1 & 0 & 0 \\ 0 & 0 & -86.59 & 0 & 0 & 0 & 0 \\ \hline \multicolumn{7}{c}{\mathbf{0}_{1\times7}} \end{array}\right), \mathbf{\Lambda}_{52}=\left(\begin{array}{ccccccc} 0 & 0 & 0 & 0 & -0.9613 & 0 & 0 \\ 0 & 0 & 0 & 0 & 0 & 0 & 0 \\ 0 & 0 & 0 & 0 & 0 & 0 & 0 \\ 0 & 0 & 0 & 1 & 34.09 & 0 & 0 \\ 0 & 0 & 0 & 0 & 0 & 0 & 0 \\ 0 & 0 & 0 & 0 & -31 & 1 & 0 \\ \hline \multicolumn{7}{c}{\mathbf{0}_{1\times7}} \end{array}\right), \mathbf{\Lambda}_{53}=\left(\begin{array}{ccccccc} 0 & 0 & 0 & 0 & 0.9613 & 0 & 0 \\ 0 & 0 & 0 & 0 & 0 & 0 & 0 \\ 0 & 0 & 0 & 0 & 0 & 0 & 0 \\ 0 & 0 & 0 & 0 & -34.09 & 0 & 0 \\ 0 & 0 & 0 & 0 & 0 & 0 & 0 \\ 0 & 0 & 0 & 0 & 31 & 0 & 0 \\ \hline \multicolumn{7}{c}{\mathbf{0}_{1\times7}} \end{array}\right),$$

The translational deviation of surface can be calculated by $-\mathbf{A}_{jd}(k)\mathbf{J}^{-1}(k)\mathbf{\Phi}(k)\mathbf{E}\mathbf{\Psi}(\mathbf{0}_{1\times3} \quad {}^{F}x_P \quad {}^{F}y_P \quad {}^{F}z_P \quad \mathbf{0}_{1\times4} \quad {}^{F}x_P \quad {}^{F}y_P \quad {}^{F}z_P \quad \mathbf{0}_{1\times4} \quad {}^{F}x_P \quad {}^{F}y_P \quad {}^{F}z_P \quad 0)^T$. We denote this expression as a column vector $\mathbf{\Lambda}_{j4}$. The calculation results are $\mathbf{\Lambda}_{54}=\mathbf{\Lambda}_{44}=(\mathbf{0}_{1\times3}$ -19.25 -131 -81.25 $0)^T$.

The state equation can be assembled as

$$\underbrace{\begin{pmatrix}\mathbf{x}_1(2)\\ \mathbf{x}_2(2)\\ \mathbf{x}_3(2)\\ \mathbf{x}_4(2)\\ \mathbf{x}_5(2)\\ 1\end{pmatrix}}_{(\mathbf{x}(2)^T \;\; 1)^T} = \underbrace{\left(\begin{array}{c|c|c|c|c|c} \mathbf{I}_{7\times7} & \mathbf{0} & \mathbf{0} & \mathbf{0} & \mathbf{0} & \mathbf{0}_{7\times1} \\ \hline \mathbf{0} & \mathbf{I}_{7\times7} & \mathbf{0} & \mathbf{0} & \mathbf{0} & \mathbf{0}_{7\times1} \\ \hline \mathbf{0} & \mathbf{0} & \mathbf{I}_{7\times7} & \mathbf{0} & \mathbf{0} & \mathbf{0}_{7\times1} \\ \hline \mathbf{\Lambda}_{41} & \mathbf{\Lambda}_{42} & \mathbf{\Lambda}_{43} & \mathbf{0}_{7\times7} & \mathbf{0}_{7\times7} & \mathbf{\Lambda}_{44} \\ \hline \mathbf{\Lambda}_{51} & \mathbf{\Lambda}_{52} & \mathbf{\Lambda}_{53} & \mathbf{0}_{7\times7} & \mathbf{0}_{7\times7} & \mathbf{\Lambda}_{54} \\ \hline \mathbf{0} & \mathbf{0} & \mathbf{0} & \mathbf{0} & \mathbf{0} & 1 \end{array}\right)}_{diag(\mathbf{A}(1)\;\; 1)} \underbrace{\begin{pmatrix}\mathbf{x}_1(1)\\ \mathbf{x}_2(1)\\ \mathbf{x}_3(1)\\ \mathbf{x}_4(1)\\ \mathbf{x}_5(1)\\ 1\end{pmatrix}}_{(\mathbf{x}(1)^T \;\; 1)^T} + \underbrace{\left(\begin{array}{c|c} \mathbf{B}_1(2) & \\ \mathbf{B}_2(2) & \\ \mathbf{B}_3(2) & \mathbf{0}_{35\times1} \\ \mathbf{B}_4(2) & \\ \mathbf{B}_5(2) & \\ \hline \mathbf{0}_{1\times35} & 0 \end{array}\right)}_{diag(\mathbf{B}(2)\;\; 1)} \begin{pmatrix} \Delta f_{1z}(2)+\Delta m_{1z}(2) \\ \Delta f_{2z}(2)+\Delta m_{2z}(2) \\ \Delta f_{3z}(2)+\Delta m_{3z}(2) \\ \Delta f_{4y}(2)+\Delta m_{4y}(2) \\ \Delta f_{5y}(2)+\Delta m_{5y}(2) \\ \Delta f_{6x}(2)+\Delta m_{6x}(2) \\ \mathbf{0}_{2\times1} \end{pmatrix} + \begin{pmatrix}\zeta\ (2)\\ 0\end{pmatrix}.$$

Solving the state equation for two operations, the model for root cause identification is given by $\mathbf{y} = \begin{pmatrix} \left(\mathbf{y}^T(1) \quad 0\right)^T \\ \hline \left(\mathbf{y}^T(2) \quad 0\right)^T \end{pmatrix} = \mathbf{C}\left(\begin{array}{c|c} \mathbf{B}(1) & \mathbf{0} \\ \hline \mathbf{A}(1)\mathbf{B}(1) & \mathbf{B}(1) \end{array}\right)\begin{pmatrix} \left(\mathbf{u}^T(1) \quad 0\right)^T \\ \hline \left(\mathbf{u}^T(2) \quad 0\right)^T \end{pmatrix} + \begin{pmatrix} \left(\zeta^T(1) \quad 0\right)^T \\ \hline \left(\zeta^T(2) \quad 0\right)^T \end{pmatrix}$.

Output matrix **C** is determined by the selection of measured features. An optimized selection of measured features for root cause identification must maximize the rank of matrix $\mathbf{\Gamma}$, while minimize number of rows in matrix **C**, i.e., the minimum number of components in vector **y**. In this example, the number of errors to be determined is 12 and the minimum number of feature components to be measured should be 12. Each feature component is selected as one entry in vector $\mathbf{x}_j(k)$, e.g., $\mathbf{v}_j(k)$ in $\mathbf{x}_j(k)$ can be chosen as a feature component. Thus, the entry "1" appears at most once in each row of feature selection matrix **C**. The position of "1" is determined by non-zero entry in $\left(\begin{array}{c|c} \mathbf{B}(1) & \mathbf{0} \\ \hline \mathbf{A}(1)\mathbf{B}(1) & \mathbf{B}(2) \end{array}\right)$. For this case study, 4 features are selected and the output matrix **C** is

chosen as: $\mathbf{C}_{12\times 72}=\begin{pmatrix}\mathbf{0} & \mathbf{C}_1 & \mathbf{C}_2 & \mathbf{0} & \mathbf{0} & \mathbf{0} & \mathbf{0} & \mathbf{0} & \mathbf{0} & \mathbf{0}\\ \mathbf{0} & \mathbf{0} & \mathbf{0} & \mathbf{0} & \mathbf{0} & \mathbf{0} & \mathbf{0} & \mathbf{0} & \mathbf{C}_3 & \mathbf{C}_4\end{pmatrix}$, where

$\mathbf{C}_1=\left(\begin{array}{ccc|c} 1 & 0 & \mathbf{0}_{1\times 4} & \\ \mathbf{0}_{4\times 1} & \mathbf{0}_{4\times 1} & \mathbf{I}_{4\times 4} & \mathbf{0}_{6\times 1}\\ 0 & 0 & \mathbf{0}_{1\times 4} & \end{array}\right)$, $\mathbf{C}_2=\left(\begin{array}{cc|c} \mathbf{0}_{5\times 5} & & \\ & 1 & \mathbf{0}_{6\times 1}\end{array}\right)$, $\mathbf{C}_3=\left(\begin{array}{ccc|c} 1 & 0 & \mathbf{0}_{1\times 4} & \\ \mathbf{0}_{4\times 1} & \mathbf{0}_{4\times 1} & \mathbf{I}_{4\times 4} & \mathbf{0}_{6\times 1}\\ 0 & 0 & \mathbf{0}_{1\times 4} & \end{array}\right)$, and

$\mathbf{C}_4=\left(\begin{array}{cc|c} \mathbf{0}_{5\times 5} & & \\ & 1 & \mathbf{0}_{6\times 2}\end{array}\right)$. The size of other zero block matrices in $\mathbf{C}$ is 7×7.

After removing the zero rows in $\mathbf{u}$ and corresponding columns in $\mathbf{C}\left(\begin{array}{c|c}\mathbf{B}(1) & \mathbf{0}\\ \hline \mathbf{A}(1)\mathbf{B}(1) & \mathbf{B}(2)\end{array}\right)$, we obtain the equation $\mathbf{y}=\begin{pmatrix}\mathbf{y}(1)\\ \hline \mathbf{y}(2)\end{pmatrix}=\mathbf{\Gamma}\begin{pmatrix}\Delta\mathbf{f}(1)+\Delta\mathbf{m}(1)\\ \hline \Delta\mathbf{f}(1)+\Delta\mathbf{m}(1)\end{pmatrix}+\boldsymbol{\varepsilon}$ for diagnosis of errors that occur at each operation, where $\boldsymbol{\varepsilon}$ is the noise term composing of $\zeta(1)$ and $\zeta(2)$ in the first and second operations and

$$\mathbf{\Gamma}^*=\begin{pmatrix}
0 & 0 & 0 & -0.0025 & 0.0025 & 0 & 0 & 0 & 0 & 0 & 0 & 0\\
0.0083 & -0.0042 & -0.0042 & 0 & 0 & 0 & 0 & 0 & 0 & 0 & 0 & 0\\
0 & -0.1963 & 0.1963 & -0.3275 & 0.3275 & -1 & 0 & 0 & 0 & 0 & 0 & 0\\
-0.6771 & 0.3385 & 0.3385 & -0.9519 & -0.0481 & 0 & 0 & 0 & 0 & 0 & 0 & 0\\
0.1833 & -1.0283 & -0.1551 & 0 & 0 & 0 & 0 & 0 & 0 & 0 & 0 & 0\\
0.1833 & -0.3036 & -0.8797 & 0 & 0 & 0 & 0 & 0 & 0 & 0 & 0 & 0\\
0 & 0 & 0 & -0.678 & 0.678 & 0 & 0 & 0.001 & -0.001 & -0.0023 & 0.0023 & 0\\
0.0036 & -0.0018 & -0.0018 & 0 & 0 & 0 & 0.0036 & -0.0018 & -0.0018 & 0 & 0 & 0\\
0 & -0.1963 & 0.1963 & 60.6183 & -60.6183 & -1 & 0 & -0.1892 & 0.1892 & 0.2025 & -0.2025 & -1\\
0.675 & -0.3375 & -0.3375 & -0.1725 & -0.8275 & 0 & 1.5833 & -0.6801 & 0.0248 & 0 & 0 & 0\\
-0.4692 & -0.702 & 0.1712 & 248.25 & -248.25 & 0 & -0.6526 & 0.3263 & 0.3263 & -0.1725 & -0.8275 & 0\\
-0.5383 & -0.6675 & 0.2057 & 23.25 & -23.25 & 0 & -0.7216 & 0.3608 & 0.3608 & -0.9225 & -0.0775 & 0
\end{pmatrix}.$$

It can be observed that the rank of $\mathbf{\Gamma}^*$ is 12. The least square estimation can thus be performed. Therefore, measuring 4 features makes it possible to identify 12 error components. Only 12 components in quality characteristic $\mathbf{y}$ are needed for identifying if there are errors. The proposed approach identifies location of root cause without having to find out every potential error. Compared with quality characteristic components (at

least 24) and 6 features measured based on the previous model, reduction on the model dimension and measurements by the proposed approach is significant. If fixture and machine tool errors should be further distinguished, the strategy of sequential root cause identification suggests that additional in-process measurement only needs to be taken on the faulty (equivalent) locator(s). Therefore, the proposed strategy generally requires less features and in-process measurement for root cause identification.

2.6 Summary

This chapter presents a mathematical formulation of error equivalence and prediction of process variations. The error equivalence formulation, based on a novel concept of error equivalence transformation, helps to understand and model the mechanism that different error sources result in the identical variation pattern on part features. The derived quality prediction model (causal model) embedded with error equivalence mechanism can reveal more physical insights into the process variation.

As an application of error equivalence model in a multi-operational machining processes, this chapter presents a variation propagation modeling that facilitates root cause identification and measurement strategy. The benefit of introducing equivalent errors in the process modeling is that the process errors can be grouped with the base error (in the machining process, datum error and machine tool error can be grouped with fixture error). As a result, the dimension of model inputs is significantly reduced compared with previous modeling methodologies.

The feasibility of error grouping is discussed. It is shown that the symmetry of HTM in the infinitesimal analysis is the key factor for error grouping since the coordinate

transformation may possibly violate the symmetry in HTM multiplication. The modeling results indicate that HTM between the PCS and the FCS does not affect the symmetry in HTM multiplication. This grouping approach requires merging the MCS and the FCS during modeling to satisfy the condition of grouping. The requirement can easily be satisfied in the modeling stage.

The case studies demonstrated the validity of error equivalence model in the machining process, modeling procedure, and its implementation in measurement reduction. The modeling work presented in this chapter establishes the basis for root cause identification of multiple error sources and error-canceling-error automatic process adjustment.

Chapter 3

Error Cancellation Modeling and Its Application in Process Control*

Due to the error equivalence mechanism, the impacts of errors on part features may cancel one another. Error cancellation may hinder the error information from being identified and therefore increase the complexity of root cause identification. However, we can maneuver one error to cancel other errors and reduce process variation. By considering such dual effects of error cancellation, this chapter intends to study the implications of error cancellation based on the derived error equivalence model.

Section 3.1 analyzes error cancellation and its theoretical implications from the perspectives of process monitoring and control, including root cause diagnosis and error compensation. Using error cancellation, a sequential root cause identification procedure and error-canceling-error methodology are developed to reduce the time invariant process errors. In Section 3.2, the proposed diagnostic procedure is demonstrated by a machining experiment and the error compensation is also illustrated with a simulation study. A summary is given in Section 3.3.

*The work in this chapter has appeared in Wang, H. and Huang, Q , 2006, "Error Cancellation Modeling and Its Application in Machining Process Control," *IIE Transactions on Quality and Reliability,* 38, pp.379-388.

3.1 Error Cancellation and Its Theoretical Implications

It has been widely noted that the impact of multiple error sources on product features may cancel out one another. This phenomenon may have the drawback that it is possible for it to conceal the fact that multiple errors have occurred in the process, however, there is the opportunity for us to purposely use one type of error to counteract or compensate another error and thereby reduce variation.

Error equivalence can model the error cancellation and the impact of errors on feature deviation. By Eq. (2.6), we have

$$E(\mathbf{x})=\mathbf{\Gamma}E(\mathbf{u}^*)=\mathbf{\Gamma}^*E(\Sigma_{i=1}^{p}\mathbf{u}_i^*)=\mathbf{\Gamma}^*E(\Sigma_{i=1}^{p}\mathbf{K}_i\mathbf{u}_i), \text{ and} \quad (3.1a)$$

$$Cov(\mathbf{x})=\mathbf{\Gamma}^*Cov(\mathbf{u}^*)\mathbf{\Gamma}^{*T}+Cov(\boldsymbol{\varepsilon})=\mathbf{\Gamma}^*Cov[\Sigma_{i=1}^{p}\mathbf{K}_iCov(\mathbf{u}_i)\mathbf{K}_i^T]\mathbf{\Gamma}^{*T}+Cov(\boldsymbol{\varepsilon}), \quad (3.1b)$$

where E(.) and Cov(.) represent expectation and variance-covariance matrix of random variables in the parentheses.

Eq. (3.1a) indicates that the cancellation effect of three types of errors can be modeled as a linear combination of mean shift of equivalent amount of base errors, i.e., $E(\Sigma_{i=1}^{p}\mathbf{u}_i^*)$,. Their impacts on feature deviation are described by mapping matrix $\mathbf{\Gamma}^*$ in Eq. (2.6). For a special case that three types of errors completely cancel each other, i.e., $E(\Sigma_{i=1}^{p}\mathbf{u}_i^*)$ is statistically insignificant, the mean of process output is within control. It should be noticed that the variances caused by three types of errors cannot be cancelled (see Eq. (3.1b)). In the machining process, Eq. (2.6) becomes

$$\mathbf{x}=\left(\mathbf{\Gamma}^* \mid \mathbf{\Gamma}^* \mid \mathbf{\Gamma}^*\right)\left(\Delta\mathbf{d}^T \mid \Delta\mathbf{f}^T \mid \Delta\mathbf{m}^T\right)^T+\boldsymbol{\varepsilon}=\mathbf{\Gamma}^*(\Delta\mathbf{d}+\Delta\mathbf{f}+\Delta\mathbf{m})+\boldsymbol{\varepsilon} \quad (3.2)$$

and error cancellation is modeled by $E(\Delta\mathbf{d}+\Delta\mathbf{f}+\Delta\mathbf{m})$.

Modeling of error cancellation has many theoretical implications on machining process control. This section discusses the implications on three issues: diagnosability analysis, root cause identification, and error compensation.

3.1.1 Diagnosability Analysis of Manufacturing Process with Error Equivalence

This chapter studies the diagnosability of the process that is governed by a general linear causal model as follows, which relates the errors to the feature deviation **x**,

$$\mathbf{x} = \mathbf{\Gamma u} + \boldsymbol{\varepsilon} = \mathbf{\Gamma}\left(\mathbf{u}_1^T \quad \mathbf{u}_2^T \quad \cdots \quad \mathbf{u}_p^T\right)^T + \boldsymbol{\varepsilon}. \tag{3.3a}$$

where matrix $\mathbf{\Gamma}$ is determined by the part specification. Its relationship with $\mathbf{\Gamma}^*$ will be discussed in Proposition 3.1. In the machining process, the model becomes

$$\mathbf{x} = \mathbf{\Gamma}\left(\mathbf{x}_{\mathrm{D}}^T \quad \Delta\mathbf{f}^T \quad \delta\mathbf{q}_m^T\right)^T + \boldsymbol{\varepsilon}. \tag{3.3b}$$

Under a certain measurement strategy, diagnosability study aims to determine whether all the process errors $\mathbf{u}_i$'s are estimable. If the process is diagnosable, the least square estimation (LSE) can be performed, i.e.,

$$\left(\mathbf{u}_1^T \quad \mathbf{u}_2^T \quad \cdots \quad \mathbf{u}_p^T\right)^T = (\mathbf{\Gamma}^T\mathbf{\Gamma})^{-1}\mathbf{\Gamma x}. \tag{3.4}$$

The diagnosability depends on the rank of $\mathbf{\Gamma}$ (Zhou, *et al.*, 2003). We can see that Eq. (3.4) requires $\mathbf{\Gamma}^T\mathbf{\Gamma}$ to be full rank, or equivalently, all the columns in $\mathbf{\Gamma}$ to be independent. Proposition 1 addresses the structure of $\mathbf{\Gamma}$ for a machining process.

Proposition 3.1. If error equivalence holds for process errors $\left(\mathbf{u}_1^T \quad \mathbf{u}_2^T \quad \cdots \quad \mathbf{u}_p^T\right)^T$, the process will not be diagnosable with measurement of quality characteristic **x**. In the machining process, block matrices in matrix $\mathbf{\Gamma}$ (see Eq. (3.4)) corresponding to three

types of errors are dependent and matrix $\mathbf{\Gamma}^T\mathbf{\Gamma}$ is always not full rank, i.e., fixture, datum, and machine tool errors cannot be distinguished by measuring the part features only.

Proof. If we use transformation matrices $\mathbf{K}_i$ to transform errors $\mathbf{u}_i$ to base error $\mathbf{u}_1$, Eq. (2.6) becomes

$$\mathbf{x}=\left[\mathbf{\Gamma}^* \mid \mathbf{\Gamma}^*\mathbf{K}_2 \mid \cdots \mid \mathbf{\Gamma}^*\mathbf{K}_p\right]\left(\mathbf{u}_1^T \mid \mathbf{u}_2^T \mid \cdots \mid \mathbf{u}_p^T\right)^T+\boldsymbol{\varepsilon}. \tag{3.5a}$$

In the machining process, matrices $\mathbf{K}_2$ (from Eq. (2.8)) and $\mathbf{K}_3$ (Eq. (2.9)) transform datum error $\mathbf{x}_\mathrm{D}$ to $\Delta\mathbf{d}$ and machine tool error $\delta\mathbf{q}_m$ to $\Delta\mathbf{m}$, respectively. Eq. (2.6) becomes

$$\mathbf{x}=[\mathbf{\Gamma}^*\mathbf{K}_2 \mid \mathbf{\Gamma}^* \mid \mathbf{\Gamma}^*\mathbf{K}_3]\left(\mathbf{x}_\mathrm{D}^T \mid \Delta\mathbf{f}^T \mid \delta\mathbf{q}_m^T\right)^T+\boldsymbol{\varepsilon}. \tag{3.5b}$$

Comparing Eq. (3.5a) with Eq. (3.4), we obtain matrix $\mathbf{\Gamma}=\left[\mathbf{\Gamma}^* \quad \mathbf{\Gamma}^*\mathbf{K}_2 \quad \cdots \quad \mathbf{\Gamma}^*\mathbf{K}_p\right]$. However, the columns corresponding to fixture and machine tool errors in matrix $\mathbf{\Gamma}$ are dependent because columns of $\mathbf{\Gamma}^*\mathbf{K}_i$'s are the linear combination of columns of $\mathbf{\Gamma}^*$. Therefore, rank of $\mathbf{\Gamma}$ equals the rank of $\mathbf{\Gamma}^*$. This also implies that the system is not diagnosable.

An implication of this proposition is that LSE of $\left(\mathbf{u}_1^T \mid \mathbf{u}_2^T \mid \cdots \mid \mathbf{u}_p^T\right)^T$ in Eq. (3.4) cannot be obtained. However, the causal model (3.2) with error grouped eliminates the linearly dependent columns in matrix $\mathbf{\Gamma}$ and therefore $\mathbf{\Gamma}$ can be full rank. This fact leads to sequential root cause identification in Section 3.1.2.

3.1.2 Sequential Root Cause Identification

Using Eq. (3.2), the grouped errors $\mathbf{u}$ can be estimated as

$$\hat{\mathbf{u}}^{*(n)}=\sum_{i=1}^{p}\hat{\mathbf{u}}_i^{*(n)}=(\mathbf{\Gamma}^{*T}\mathbf{\Gamma}^*)^{-1}\mathbf{\Gamma}^{*T}\mathbf{x}^{(n)},\ n=1, 2, \ldots, N, \tag{3.6a}$$

where $\hat{\mathbf{u}}_i^{*(n)}$ is the LSE of $\mathbf{u}_i$ for the *n*th replicate of measurement. In a machining process, $\sum_{i=1}^{p} \hat{\mathbf{u}}_i^{*(n)}$ becomes $\Delta\hat{\mathbf{d}}^{(n)} + \Delta\hat{\mathbf{f}}^{(n)} + \Delta\hat{\mathbf{m}}^{(n)}$. Each row of $\mathbf{\Gamma}^*$ corresponds to output feature while each column of $\mathbf{\Gamma}^*$ corresponds to component of error vectors. Hence, the number of rows of $\mathbf{\Gamma}^*$ must be larger than the number of its columns to ensure that sufficient features are measured for LSE. The mean and variance-covariance of the detected errors are

$$\mathrm{E}(\hat{\mathbf{u}}) = \sum_{i=1}^{p} \mathbf{K}_i \mathrm{E}(\hat{\mathbf{u}}_i) \text{ and } \mathrm{Cov}(\hat{\mathbf{u}}) = \sum_{i=1}^{p} \mathbf{K}_i \mathrm{Cov}(\mathbf{u}_i) \mathbf{K}_i^T. \quad (3.6b)$$

Proposition 3.1 indicates that measurement other than quality characteristics **x** is necessary to distinguish error sources. However, it will not be economical to take the additional measurement if no process error occurs. A sequential procedure is thus proposed for root cause identification:

- Necessary error information (e.g., off-line measurement on workpieces) is collected first to identify the occurrence of error sources using Eq. (3.6a). The process error information can be analyzed by conducting hypothesis test on $\{\hat{\mathbf{u}}^{(n)}\}_{n=1}^{N}$. Since the estimated **u** is a mixture of noise and errors, a proper test statistic should be developed to detect the errors from process noise. Hypothesis testing for mean and variance can then be used to find out if the errors are mean shift or large variance.
- Additional measurement (e.g., in-line measurement on process errors) is then conducted to distinguish different types of errors $\left(\mathbf{u}_1^T \mid \mathbf{u}_2^T \mid \cdots \mid \mathbf{u}_p^T\right)^T$. E($\hat{\mathbf{u}}$) and Cov($\hat{\mathbf{u}}$) will be estimated with the in-process measurement of (*p*-1) error sources. By Eq. (3.6b) the remaining unmeasured errors can be obtained. The detailed procedures for the machining process will be given in the Section 3.2.1.

3.1.3 Error-Canceling-Error Compensation Strategy

We can use the effect of error cancellation to compensate process errors. An adjustment algorithm based on error equivalence mechanism can be designed to adjust the base error $\mathbf{u}_1$ to compensate the other process errors $\{\mathbf{u}_i\}_{i=2}^{p}$. With the development of adjustable fixture whose locator length is changeable, it is feasible to compensate errors only by changing the length of locators. We use index i to represent the ith adjustment period. During period i, N part feature deviations $\{\mathbf{x}^{(i),(n)}\}_{n=1}^{N}$ are measured to determine the amount of locator adjustment. Such compensation is only implemented at the beginning of the period. Denote $\mathbf{c}^{(i)}$ as the accumulative amount of locator length adjusted after the ith period and the beginning of period i+1. The compensation procedure can be illustrated with Fig. 3.1. One can see that a nominal machining process is disturbed by errors $\Delta\mathbf{d}$, $\Delta\mathbf{f}$ and $\Delta\mathbf{m}$, and the observation noise $\boldsymbol{\varepsilon}$. Error sources, noise, and machining process constitute a disturbed process, as marked in the dash line block. Using the feature deviation $\mathbf{x}^{(i)}$ for the ith period as input ($\mathbf{x}^{(i)}$ can be estimated by the average of N measured parts in the period i, i.e., $\hat{\mathbf{x}}^{(i)} = \overline{\mathbf{x}}^{(i)}$), an adjustment algorithm is introduced to generate signal $\mathbf{c}^{(i)}$ to manipulate adjustable fixture locators to counteract the errors for the (i+1)th machining period. The amount of compensation at period i+1 should be $\mathbf{c}^{(i)}$-$\mathbf{c}^{(i-1)}$. The error compensation model can then be

$$\mathbf{x}^{(i+1)}=\mathbf{S}^{(i+1)}+\boldsymbol{\Gamma}^{*}\mathbf{c}^{(i)} \quad \text{and} \quad \mathbf{S}^{(i+1)}=\boldsymbol{\Gamma}^{*}\mathbf{u}^{(i+1)}+\boldsymbol{\varepsilon}^{(i+1)}, \tag{3.7}$$

where $\mathbf{S}^{(i+1)}$ is the output of the disturbed process for time i+1. This term represents the feature deviation measured without any compensation being made.

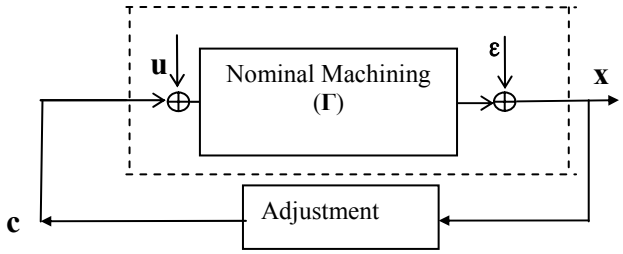

Figure 3.1 Error-Canceling-Error Strategy

The adjustment using equivalent errors can be illustrated with an example in Fig. 3.2, where a prismatic part is set up in a fixture with locators $\mathbf{f}_1$, $\mathbf{f}_2$, and $\mathbf{f}_3$. We expect to perform a parallel cutting on the top plane of the part. If the tool path tilts due to thermal effect, the yielded top plane will also tilt the same angle. However, under the adjustable fixture where the length of locator pin is adjustable, we may find out the adjustment amount (black bar in right panel of Fig. 3.2) for $\mathbf{f}_1$, $\mathbf{f}_2$, and $\mathbf{f}_3$ such that the part tilts the same angle as the deviated tool path. Obviously, a conforming part can still be obtained. Similarly, we can also adjust fixture locators to compensate the datum error. The amount of adjustment can be determined by EFE using Eq. (2.9). With this concept, the feature deviation caused by machine tool thermal error (tilted tool path) can also be generated by EFE ($\Delta m_1\ \Delta m_2\ \Delta m_3$) alone. In order to compensate this error, we must apply the amount of adjustment ($-\Delta m_1\ -\Delta m_2\ -\Delta m_3$) to these locating pins.

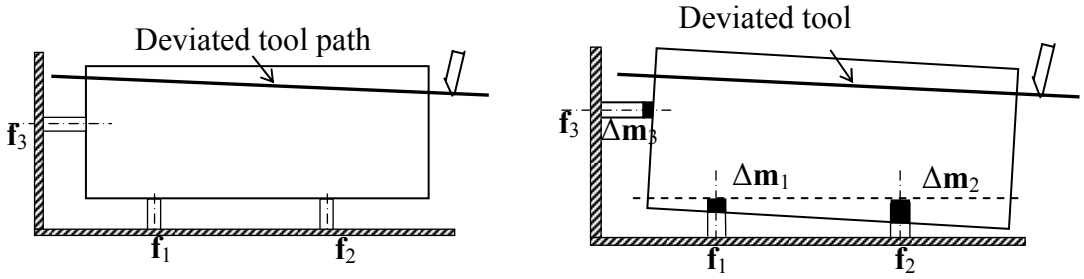

Figure 3.2 Process Adjustment Using EFE Concept

In this chapter, the compensation focuses on time invariant error because they account for the majority of overall machining errors (Zhou, Huang, and Shi, 2003). The negative value of predicted equivalent errors can be used to adjust locators. From Eq. (3.7), it is clear that if we set $\mathbf{\Gamma}^{*}\mathbf{c}^{(i)}=-\mathbf{\Gamma}^{*}\mathbf{u}^{(i+1)}$, then the adjustment can cancel out the process errors and deviation is $\mathbf{x}^{(i+1)}=\boldsymbol{\varepsilon}^{(i+1)}$. The adjustment $\mathbf{c}^{(i)}$ can be the LSE of $\mathbf{u}^{(i+1)}$, i.e.,

$$\mathbf{c}^{(i)}=\hat{\mathbf{u}}^{(i+1)}=-[(\mathbf{\Gamma}^{*T}\mathbf{\Gamma}^{*})^{-1}\mathbf{\Gamma}^{*T}\mathbf{x}^{(i)}-\mathbf{c}^{(i-1)}], \text{ and } \mathbf{c}^{(1)}=-(\mathbf{\Gamma}^{*T}\mathbf{\Gamma}^{*})^{-1}\mathbf{\Gamma}^{*T}\mathbf{x}^{(1)}. \tag{3.8}$$

By solving the recursive Eq. (3.8), we derive an integral adjustment that can minimize mean square error (MSE) of the feature deviation, i.e.,

$$\mathbf{c}^{(i)}=-(\mathbf{\Gamma}^{*T}\mathbf{\Gamma}^{*})^{-1}\mathbf{\Gamma}^{*T}\sum_{t=1}^{i}\mathbf{x}^{(t)}=-\sum_{t=1}^{i}(\Delta\hat{\mathbf{d}}^{(t)}+\Delta\hat{\mathbf{f}}^{(t)}+\Delta\hat{\mathbf{m}}^{(t)}). \tag{3.9}$$

Eq. (3.9) shows that the accumulative amount of compensation for the next period is equal to the sum of the LSE of EFE of all current and previous time periods of machining. The accumulative compensation $\mathbf{c}^{(i)}$ is helpful for evaluation of adjustment performance such as stability and robustness analysis. The amount of compensation for the i+1th period is $\mathbf{c}^{(i)}-\mathbf{c}^{(i-1)}$,

$$\mathbf{c}^{(i)}-\mathbf{c}^{(i-1)}=-(\mathbf{\Gamma}^{*T}\mathbf{\Gamma}^{*})^{-1}\mathbf{\Gamma}^{*T}\mathbf{x}^{(i)}. \tag{3.10}$$

The compensation accuracy can be estimated by $\mathbf{x}^{(i)}-\mathbf{\Gamma}^{*}(\mathbf{\Gamma}^{*T}\mathbf{\Gamma}^{*})^{-1}\mathbf{\Gamma}^{*T}\mathbf{x}^{(i)}$, i.e., the difference between $\mathbf{x}^{(i)}$ and its LSE. Denote range space of $\mathbf{\Gamma}^{*}$ as $R(\mathbf{\Gamma}^{*})$ and null space of $\mathbf{\Gamma}^{*T}$ as $N(\mathbf{\Gamma}^{*T})$. Spaces $R(\mathbf{\Gamma}^{*})$ and $N(\mathbf{\Gamma}^{*T})$ are orthogonal and constitute the whole vector space $\mathbf{R}^{q\times 1}$, where q is the number of rows in $\mathbf{x}^{(i)}$ (or $\mathbf{\Gamma}^{*}$). By the property of LSE, we know that the estimation error vector $\mathbf{x}^{(i)}-\mathbf{\Gamma}^{*}(\mathbf{\Gamma}^{*T}\mathbf{\Gamma}^{*})^{-1}\mathbf{\Gamma}^{*T}\mathbf{x}^{(i)}$ is orthogonal to $R(\mathbf{\Gamma}^{*})$. Therefore, the compensation accuracy of Eq. (3.9) can be estimated by projection of

observation (feature deviation) vector $\mathbf{x}^{(i)}$ onto $N(\mathbf{\Gamma}^{*T})$. This conclusion also shows the components of observation that can be compensated. The projection of observation vector $\mathbf{x}^{(i)}$ onto space $R(\mathbf{\Gamma}^{*})$ can be fully compensated with Eq. (3.9) whereas the projection onto $N(\mathbf{\Gamma}^{*T})$ cannot be compensated.

In practice, the accuracy that the adjustable locator can achieve must be considered. Suppose the standard deviation of locator's movement is σ_f. We can set the stopping region for applying error compensation with 99.73% confidence

$$-3\sigma_f \leq \mathbf{c}^{(i)} - \mathbf{c}^{(i-1)} \leq 3\sigma_f. \tag{3.11}$$

It should be noted that the error-canceling-error strategy in Eq. (3.9) is valid for compensation of time invariant process errors. Compensation strategy for dynamic errors will be studied in Chapter 5.

3.2 Applications of Error Cancellation in a Milling Process

Discussion in Section 3.1 implies the application of equivalent errors in sequential root cause identification and error compensation. The diagnostic algorithms are proposed in this section and demonstrated with a machining experiment. EFE compensation for process control is illustrated with a simulation.

3.2.1 Diagnosis Based on Error Equivalence

There are several diagnostic approaches (Ceglarek and Shi, 1996; Apley and Shi, 1998; and Rong, Shi, and Ceglarek, 2001) that have achieved considerable success in fixture errors detection. The approach proposed by Apley and Shi (1998) can effectively identify multiple fixture errors. By extending this approach, we use it for sequential root cause identification:

Step 1: Conduct measurement on features and datum surfaces of raw workpiece to estimate error sources $\hat{\mathbf{u}}^{*(n)}$ for the *n*th replicate by Eq. (3.6). The grouped error can be estimated by the average of $\hat{\mathbf{u}}^{(n)}$ over *N* measured workpieces, i.e., $\hat{\mathbf{u}}^{*} = \frac{1}{N}\sum_{n=1}^{N}\hat{\mathbf{u}}^{*(n)}$, *n*=1,2, …*N*. As mentioned in Section 3.2, the error vector $\hat{\mathbf{u}}^{(n)}$ is the mixture of error sources and process noise.

Step 2: To detect the errors from the process noise, we can use *F* test statistic introduced by Apley and Shi (1998):

$$F_i = \frac{\hat{S}_i^2}{[(\mathbf{\Gamma}^{*T}\mathbf{\Gamma}^{*})^{-1}_{i,i}]\hat{S}_\varepsilon^2},\ i=1, 2, \ldots, 6, \tag{3.12}$$

where $\hat{S}_i^2 = \frac{1}{N}\sum_{n=1}^{N}[\hat{u}_i^{(n)}]^2$, and $\hat{u}_i^{(n)}$ represents the *i*th component in vector $\hat{\mathbf{u}}^{(n)}$. $(\mathbf{\Gamma}^{*T}\mathbf{\Gamma}^{*})^{-1}_{i,i}$ is the *i*th diagonal entry of matrix $(\mathbf{\Gamma}^{*T}\mathbf{\Gamma}^{*})^{-1}$. The estimator for variance of noise is $\hat{S}_\varepsilon^2 = \frac{1}{N(q-6)}\sum_{n=1}^{N}\hat{\boldsymbol{\varepsilon}}^{(n)T}\hat{\boldsymbol{\varepsilon}}^{(n)}$, and $\hat{\boldsymbol{\varepsilon}}^{(n)} = \mathbf{x}^{(n)} - \mathbf{\Gamma}^{*}\hat{\mathbf{u}}^{(n)}$ is for noise terms. When $F_i > F_{1-\alpha}(N, N(q-6))$, we conclude that the *i*th error significantly occurs with confidence of 100(1-α)%. By investigating $\{\hat{u}_i^{(n)}\}_{n=1}^{N}$ for mean u_i (H_0: $u_i=0$ vs. H_1: $u_i\neq 0$), and variance σ_{ui}^2 (H_0: $\sigma_{ui}^2 \le \sigma_0^2$ vs. H_1: $\sigma_{ui}^2 > \sigma_0^2$), one can determine whether the pattern of the errors is mean shift or variance. σ_0^2 is a small value. In the case study, we choose $\sigma_0^2 = 0.1\text{mm}^2$. Under the normality assumption of EFEs ($\Delta\mathbf{d}$, $\Delta\mathbf{f}$, and $\Delta\mathbf{m}$), we can use the *T* test statistic $T = u_i / \sqrt{\frac{1}{N(N-1)}\sum_{n=1}^{N}(u_i^{(n)} - u_i)^2}$ and compare it with $t_{1-\alpha/2}(n-1)$ to test mean shift.

$\chi^2 = \sum_{n=1}^{N}(u_i^{(n)} - u_i)^2 / \sigma_0^2$ is used and compared with $\chi^2_{1-\alpha}(n-1)$ to test variance. α is the

significance level. If $F_i<F_{1-\alpha}(N, N(q\text{-}6))$, no errors occur at the ith locator, or the errors cannot be distinguished from process noise.

Step 3: Apply the additional measurement on locators and datum surfaces to distinguish errors whenever errors are identified. Denote $\Delta f_i^{(n)}$, $\Delta d_i^{(n)}$, and $\Delta m_i^{(n)}$ as the ith component in vector $\Delta\mathbf{f}^{(n)}$, $\Delta\mathbf{d}^{(n)}$, and $\Delta\mathbf{m}^{(n)}$, respectively. Locator deviation $\{\Delta f_i^{(n)}\}_{n=1}^{N}$ and datum surfaces $\{\mathbf{X}_j^{(n)}\}_{n=1}^{N}$ are measured. The EFE $\{\Delta d_i^{(n)}\}_{n=1}^{N}$ caused by datum error can be calculated by Eq. (2.8). The mean shift of the errors can be estimated using the sample mean of $\Delta d_i^{(n)}$, $\Delta f_i^{(n)}$, and $\Delta m_i^{(n)}=u_i^{(n)}-\Delta d_i^{(n)}-\Delta f_i^{(n)}$. The variance can then be estimated by the sample variance for $\Delta d_i^{(n)}$, $\Delta f_i^{(n)}$, and $\Delta m_i^{(n)}$. If the errors turn out to be the mean shift ($u_i\neq 0$ for certain i), machine tool error in terms of EFE is $\Delta\hat{m}_i=\hat{u}_i-\Delta d_i-\Delta f_i$, where Δd_i and Δf_i are the average EFE over all N parts. Machine tool error $\delta\mathbf{q}_m$ is then determined by the inverse of Eq. (2.9)

$$\delta\mathbf{q}_m=\mathbf{K}_3^{-1}\Delta\mathbf{m}. \tag{3.13}$$

The variance of grouped error (σ_{ui}^2) can then be decomposed as

$$\sigma_{ui}^2=\sigma_{di}^2+\sigma_{fi}^2+\sigma_{mi}^2. \tag{3.14}$$

If $\sigma_{ui}^2>\sigma_0^2$, variances caused by three types of errors σ_{di}^2, σ_{fi}^2, and σ_{mi}^2 can be estimated by the sample variance of $\{\Delta d_i^{(n)}\}_{n=1}^{N}$, $\{\Delta f_i^{(n)}\}_{n=1}^{N}$, and $\{\Delta\hat{m}_i^{(n)}\}_{n=1}^{N}$. The 100(1-2$\alpha$)% confidence interval (CI) of $\Delta\mathbf{m}$ is ($\Delta\hat{\mathbf{m}}\pm\mathbf{L}$), where $z_{1-\alpha}$ follows the cumulative standard normal distribution such that $\int_{-\infty}^{z_{1-\alpha}}\frac{1}{\sqrt{2\pi}}e^{-u^2/2}du=1-\alpha$ and

$\mathbf{L}=\left|(z_{1-\alpha}\sqrt{(\mathbf{\Gamma}_u^T\mathbf{\Gamma}_u)_{1,1}^{-1}}\hat{\sigma}_\varepsilon \quad \ldots z_{1-\alpha}\sqrt{(\mathbf{\Gamma}_u^T\mathbf{\Gamma}_u)_{6,6}^{-1}}\hat{\sigma}_\varepsilon)^T\right|_{6\times 1}$. The corresponding CI vector for $\delta\mathbf{q}_m$ is

($\mathbf{K}_3^{-1}\Delta\mathbf{m} \pm \mathbf{K}_3^{-1}\mathbf{L}$). The CI for $\Delta\mathbf{d}$ and $\Delta\mathbf{f}$ can be obtained by ($\Delta d_i \pm S_{di} t_{1-\alpha/2}(n-1)/\sqrt{n}$) and ($\Delta f_i \pm S_{fi} t_{1-\alpha/2}(n-1)/\sqrt{n}$), where S_{di} and S_{fi} are the sample variance for $\{\Delta d_i^{(n)}\}_{n=1}^{N}$ and $\{\Delta f_i^{(n)}\}_{n=1}^{N}$. This approach can effectively identify the machine tool errors.

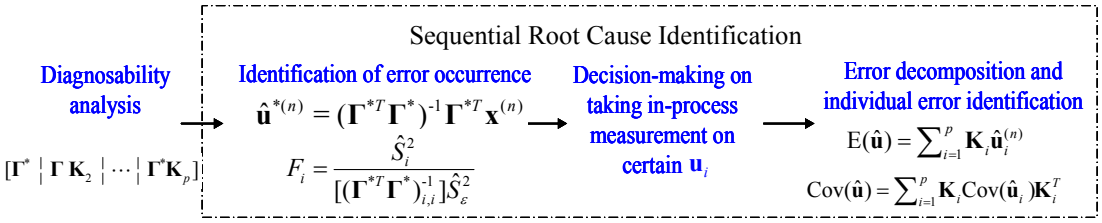

Figure 3.3 Sequential Root Cause Identification Procedures

Fig. 3.3 shows the sequential diagnostic methodology under the error equivalence mechanism. It can be seen that the sequential diagnostic methodology includes diagnosability analysis (Proposition 3.1) and sequential root cause identification.

To demonstrate the model and the diagnostic procedure, we intentionally introduced datum and machine tool errors to mill 5 block workpieces. We use the same setup, raw workpiece, and fixturing scheme as Fig. 2.10. Coordinate system *xyz* fixed with nominal fixture is also introduced to represent the plane. Top plane $\mathbf{X}_1$ and side plane $\mathbf{X}_2$ are to be milled. All 8 vertices are marked as 1~8 and their coordinates in the coordinate system *xyz* are measured to help to determine $\mathbf{X}_1$ and $\mathbf{X}_2$. In this chapter, the unit is mm for the length and radian for the angle. Under the coordinate system in the Fig. 2.9, surface specifications are $\mathbf{X}_1$=(0 0 1 0 0 15.24)^T, and $\mathbf{X}_2$=(0 1 0 0 96.5 0)^T. From model (3.2) and Eq. (2.23), we get $\mathbf{x}^i = \begin{pmatrix} \mathbf{\Gamma}_1^* \\ \mathbf{\Gamma}_2^* \end{pmatrix}(\Delta\mathbf{d}^i + \Delta\mathbf{f}^i + \Delta\mathbf{m}^i) + \boldsymbol{\varepsilon}^i$, where

$$\mathbf{\Gamma}_1=\begin{pmatrix} 0 & -0.0263 & 0.0263 & 0 & 0 & 0 \\ -0.0158 & 0.0079 & 0.0079 & 0 & 0 & 0 \\ 0 & 0 & 0 & 0 & 0 & 0 \\ 0 & -0.1379 & 0.1379 & 1.3368 & -1.3368 & -1 \\ -0.0828 & 0.0414 & 0.0414 & -1.5 & 0.5 & 0 \\ -1.3033 & -0.8483 & 1.1517 & 0 & 0 & 0 \end{pmatrix},\ \mathbf{\Gamma}_2=\begin{pmatrix} 0 & 0 & 0 & -0.0263 & 0.0263 & 0 \\ 0 & 0 & 0 & 0 & 0 & 0 \\ 0.0158 & -0.0079 & -0.0079 & 0 & 0 & 0 \\ 0 & 0.2632 & -0.2632 & -1.2026 & 1.2026 & -1 \\ 0.158 & -0.079 & -0.079 & -1.5 & 0.5 & 0 \\ 0.2212 & -1.6106 & 0.3894 & 0 & 0 & 0 \end{pmatrix}.$$

The number of rows q in $\mathbf{\Gamma}$ is 12. We set fixture error to be zero ($\Delta\mathbf{f}$=0). The primary datum plane I is pre-machined to be $\mathbf{X}_I$=(0 0.018 -0.998 0 0.207 -1.486)^T and its corresponding EFE is $\Delta\mathbf{d}$=(1.105 0 0 0 0 0)^{T}mm. The machine tool error is set to be $\delta\mathbf{q}_m$=(0 0.175 -1.44 0.0175 0 0)^T by adjusting the orientation and position of tool path. Based on coordinates of the vertices 1~8 measured, the feature deviations are given in Table 3.1. Since $\mathbf{X}_1$ and $\mathbf{X}_2$ are all planes, the deviations Δr_j's of surface size are all zero. Following steps 1-3, the identified EFEs are given in Tables 3.2 and 3.3.

Table 3.1 Measured Features (mm)

	$\mathbf{X}_1$					$\mathbf{X}_2$				
n	1	2	3	4	5	1	2	3	4	5
Δv_x	-0.001	-0.000	0.000	-0.000	0.001	0.000	-0.000	0.000	0.000	0.000
Δv_y	-0.033	-0.034	-0.039	-0.034	-0.035	0.000	0.000	0.000	0.000	0.000
Δv_z	0.000	-0.000	0.000	0.000	0.000	0.032	0.034	0.032	0.036	0.035
Δp_x	0.000	-0.000	0.000	0.000	0.000	0.000	0.000	0.000	0.000	0.000
Δp_y	-0.145	-0.163	-0.119	-0.185	-0.153	0.347	0.379	0.253	0.307	0.268
Δp_z	-3.877	-2.749	-2.329	-3.509	-2.459	0.579	0.358	0.479	0.539	0.429

Table 3.2 Estimation of u for 5 Replicates (mm)

$\hat{\mathbf{u}}^{(1)}$	$\hat{\mathbf{u}}^{(2)}$	$\hat{\mathbf{u}}^{(3)}$	$\hat{\mathbf{u}}^{(4)}$	$\hat{\mathbf{u}}^{(5)}$	$\hat{\mathbf{u}}$	T	χ^2
2.937	2.133	1.775	2.697	1.902	2.289	10.119	10.247
0.050	0.090	-0.064	0.057	0.002	0.027	-	-
0.002	0.090	-0.0562	0.057	0.020	0.023	-	-
0.055	-0.031	0.003	0.039	0.015	0.016	-	-
0.047	-0.031	0.004	0.039	0.018	0.015	-	-
0.004	0.000	-0.001	0.000	-0.001	0.001	-	-

We choose α to be 0.01. The threshold value $F_{0.99}(5,5(12\text{-}6))=F_{0.99}(5,30)=3.699$. In Table 3.2, we can see that F_1>3.699, which indicates that error occurs at locator 1. Using the data in the first row of Table 3.2 to conduct T and χ^2 tests for mean and

variance, respectively, we find that $T>t_{1-0.01/2}(5-1)= t_{0.995}(4)=4.604$ and $\chi^2<\chi^2_{1-0.01}(4)=13.277$. Hence, we conclude that there is significant mean shift while the variance is not large. If we make the additional measurement, by Eq. (3.13), the 98% confidence interval for the detected mean shift of machine tool error is $\delta\mathbf{q}_m$=(0.006 0.167 -1.540 0.018 -0.000 0.000)^T ± (0.008 0.001 0.000 0.000 0.001 0.000)^T, which is consistent with the pre-introduced errors. The EFE causal model and diagnostic algorithm is experimentally validated.

Table 3.3 Error Decomposition (mm)

Locators	$\hat{\mathbf{u}}$	F_i	$\Delta\mathbf{f}$	$\Delta\mathbf{d}$	$\Delta\mathbf{m}$
1	2.289	19.525	0	1.105	1.184
2	0.027	0.051	0	0	0.027
3	0.023	0.005	0	0	0.023
4	0.016	0.613	0	0	0.016
5	0.015	0.073	0	0	0.015
6	0.001	0.002	0	0	0.003

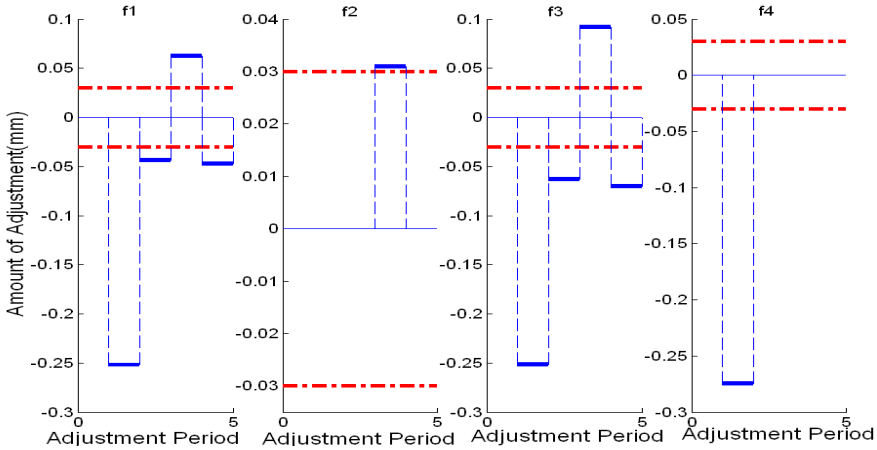

Figure 3.4 Error Compensation for Each Locator

3.2.2 Error Compensation Simulation

Using the same machining process as in Section 3.2.1, we can simulate error compensation for 5 adjustment periods. Total 5 parts are sampled during each period. The fixture error is set to be $\Delta\mathbf{f}$=(0.276 0 0 0.276 0 0)^{T}mm. The machine tool error is set to be

$\delta\mathbf{q}_m$=(-0.075 -0.023 0.329 -0.0023 0.0075 0)^T and its EFE is $\Delta\mathbf{m}$=(0 0 0.286 0 0 0)^{T}mm. We assume the measurement noise to follow $N(0, (0.002\text{mm})^2)$ for displacement and $N(0, (0.001\text{rad})^2)$ for orientation. The compensation values can be calculated by Eqs. (3.9) and (3.10). In this case study, the accuracy of the locator movement is assumed to be σ_f=0.01mm and the criterion for stopping the compensation is $-0.03 \le \mathbf{c}^{(i)} - \mathbf{c}^{(i-1)} \le 0.03$mm (see Eq. (3.11)). Fig. 3.4 shows the compensation ($\mathbf{c}^{(i)}$-$\mathbf{c}^{(i-1)}$) for locators f_1~f_4. The values of adjustment periods 2~5 are given by the solid line in the figure. The dash dot line represents the value of $\pm 3\sigma_f$. The adjustments for locators f_5 and f_6 are all zero and not shown in the figure. One can see that the effect of compensation in the second period is dominant. The compensation for the subsequent periods is relatively small because no significant error sources are introduced for these periods.

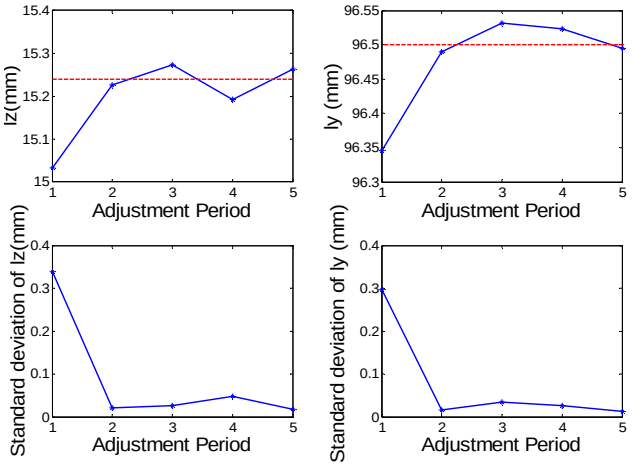

Figure 3.5 Mean and Standard Deviation of Two Features

The effect of error compensation can be illustrated with the quality improvement of two features, the plane distance along z axis (l_z) and y axis (l_y) as shown in Fig. 3.5. l_z can be estimated by the mean and standard deviation of length of edges l_{15}, l_{26}, l_{37} and l_{48} and l_y can be estimated by l_{14}, l_{23}, l_{67} and l_{58} for each machining period, where l_{mn} is the

distance between the vertices *m* and *n* and is estimated by the edge length of 5 parts in each period. Milling of planes $\mathbf{X}_1$ and $\mathbf{X}_2$ impacts the plane distance along *z* and *y* axes. The nominal part should have the same length of edges along *z* and *y* directions (15.24 and 96.5mm, see the dash line in Fig. 3.5), respectively. However, in the first adjustment period (i=1) without error compensation, the errors of edge lengths are beyond specified tolerance. In the periods 2~5 when compensation algorithm has been applied, deviation of l_z and l_y is significantly reduced.

3.3 Summary

This chapter investigates error cancellation among multiple errors (datum, fixture, and machine tool errors) for improving quality control in machining processes. As a summary, the implications of studying error cancellation are as follows:

First, process errors may cancel one another and conceal the error information. It has been proved that a machining process with datum, fixture, and machine tool errors cannot be diagnosable by only measuring the part features. To overcome this problem, a sequential procedure is therefore proposed, i.e., first identify error occurrence based on measurement of product deviation **x** and an *F* test statistics, and then discriminate error sources using in-process measurements (not product features) and hypothesis test only if process error is detected. This procedure can detect the mean shift as well as the variance of process errors from the process noise. A case study for a milling process of block parts has shown that the proposed approach can effectively identify the error sources.

Second, an error-canceling-error process adjustment strategy can be developed. Study of error cancellation also suggests that errors (machine tool and datum errors) can

be compensated by adjusting the base error (the length of fixture locators). An integral adjustment algorithm is presented in this chapter for compensation of time invariant error. It has been shown that the accumulative amount of compensation is equal to the sum of the LSE of EFE of all previous time periods of machining. The procedure has been demonstrated with a simulation study.

Chapter 4

Dynamic Error Equivalence Modeling and In-Line Monitoring of Dynamic Equivalent Fixture Errors*

This chapter studies the error equivalence of dynamic errors and thereby establishes a process model for the purpose of APC based on the dynamic equivalent errors. Considering process monitoring and data collection, this chapter presents a new concept, in addition to the widely recognized error avoidance and error compensation approaches, to control the effects of dynamic errors by in-line monitoring of process dynamic errors. This chapter selects the thermal effect of machine tool errors as an example to demonstrate the modeling and monitoring of dynamic equivalent errors.

The remainder of the chapter includes 4 sections. Section 4.1 introduces the problems in dynamic process modeling. In Section 4.2, based on an experiment, latent variable modeling (LVM) method is applied to build an ARX model for dynamic errors (thermal errors). Variable selection strategy is also discussed for the situation that high accuracy is required for model prediction. Using the latent variable model, the in-line monitoring of thermal error and control chart design are presented in Section 4.3. Section 4.4 discusses the isolation of lagged variables and sensors responsible for out-of-control signals. A summary is given in Section 4.5.

*This work will appear in Wang, H., Huang, Q., and Yang, H., 2007, "Latent Variable Modeling and In-Line Monitoring of Machine Tool Thermal Errors," accepted by *Journal of Manufacturing System*.

Nomenclature

N	number of observations
A	number of latent variables
p	number of part characteristics required by design specification
c	number of thermal sensors mounted onto a machine tool
t	time index
l	time lag l
$\mathbf{Z}^T$	transpose of matrix $\mathbf{Z}$
$\boldsymbol{\delta}_{p\times 1}^{(n)}$	thermal errors at time period n
$\boldsymbol{\Delta}_{N\times p}$	thermal error history from $t = 1$ to $t = N$, $[\boldsymbol{\delta}^{(1)}\ \boldsymbol{\delta}^{(2)} \ldots \boldsymbol{\delta}^{(N)}]^T$
$\mathbf{s}_{c\times 1}^{(n)}$	readings of c thermal sensors at time t, $[s_1^{(n)}\ s_2^{(n)} \ldots s_c^{(n)}]^T$
$\mathbf{S}_{N\times c}$	temperature history of machine tool from $t = 1$ to $t = N$, $[\mathbf{s}^{(1)}\ \mathbf{s}^{(2)} \ldots \mathbf{s}^{(N)}]^T$
$\mathbf{X}_{N\times k}$	descriptor data
$\mathbf{Y}_{N\times m}$	response data
$\mathbf{LV}$	latent variables of $\mathbf{X}$ and $\mathbf{Y}$, $[LV_1 \ldots LV_A]^{\mathrm{T}}$ ($A \ll k+m$)
$\mathbf{T}_{N\times A}$	common scores of $\mathbf{X}$ and $\mathbf{Y}$
$\mathbf{S}_{\mathbf{LV}}$	sample covariance matrix of latent variables $\mathbf{LV}$
$\mathbf{P}_{k\times A}$	$\mathbf{X}$ loadings
$\mathbf{Q}_{m\times A}$	$\mathbf{Y}$ loadings

$\mathbf{W}_{k\times A}$ weights of variables in **X**

$\mathbf{E}_{N\times k}$ **X** residuals

$\mathbf{F}_{N\times m}$ **Y** residuals

q back shift operator

$\mathbf{D}(q)$ difference operator with d_j = 1 or 2 (j=1,2,…,c or p), $Diag[(1-q^{-1})^{d1}$, $(1-q^{-1})^{d2},\ldots]$

$\mathbf{S}(i,j)$ a matrix $[\mathbf{D}(q)\mathbf{s}^{(i)}\ \mathbf{D}(q)\mathbf{s}^{(i+1)}\ \ldots\ \mathbf{D}(q)\mathbf{s}^{(j)}]^T$

$\mathbf{\Delta}(i,j)$ a matrix $[(\mathbf{D}(q)\boldsymbol{\delta}^{(i)}\ \mathbf{D}(q)\boldsymbol{\delta}^{(i+1)}\ldots,\ \mathbf{D}(q)\boldsymbol{\delta}^{(j)}]^T$

4.1 Introduction to Modeling of Dynamic Errors

Since dynamic errors may have great impact on part quality, in-line monitoring of dynamic errors is a very important issue for quality improvement. For example, thermally induced errors account for a large percentage of machine tool errors and hence in-line monitoring and compensation of thermal errors are critical to reduce process variations.

Although as shown in Chapter 1, the SI based dynamic modeling methodology shows significant advantages over the static one in terms of model accuracy and robustness, several barriers still remain when applying SI theory to the thermal error modeling:

- how to determine the number of temperature measurements that is sufficient to build an adequate SI model, in order to avoid excess amount of sensors to be mounted onto a machine tool.
- how to select appropriate lagged variables when a large number of thermal sensors are available. The stepwise regression is commonly applied for variable selection

(Chen, *et al.*, 1993). However, this method has certain limitations when being applied to model strongly correlated historical data. Thus a systematic approach for the selection of appropriate lagged variables is necessary for determining the structure of the dynamic model.

- how to effectively estimate machine thermal status and predict machine performance when the sensing resource is limited.

The purpose of this chapter is to overcome aforementioned difficulties. It presents a new concept of controlling machining thermal effects by in-line monitoring of machine thermal status based on SPC. Limited number of thermal sensors are employed to track the temperature distribution of machine tools and to detect out-of-control machine thermal status as the results of environment change, machine degradation, or process parameters change. The recently developed LVM method (Shi and MacGregor, 2000) provides a powerful tool for variable selection and model order determination. This method will be employed in both dynamic modeling and in-line monitoring.

4.2 Latent Variable Modeling of Machine Tool Dynamic Errors

4.2.1 Description of Data

In thermal error modeling, the collected information includes machine tool temperature and thermal error (provided by in-line probing system). Suppose c thermal sensors are mounted on a machine tool. Let $\mathbf{s}_{c\times 1}{}^{(n)} = [s_1{}^{(n)} \;\; s_2{}^{(n)} \; \ldots \; s_c{}^{(n)}]^T$ denote the c sensor readings at time t and $\mathbf{S}_{N\times c} = [\mathbf{s}^{(1)} \;\; \mathbf{s}^{(2)} \; \ldots \; \mathbf{s}^{(N)}]^T$ denote temperature history of machine tool from time $t = 1$ to $t = N$. Suppose p characteristics are probed and the measured readings for thermal error $\delta\mathbf{q}_m{}^{(n)}$ are denoted by $\boldsymbol{\delta}_{p\times 1}{}^{(n)}$. Then $\boldsymbol{\Delta}_{N\times p} = [\boldsymbol{\delta}^{(1)}$

$\boldsymbol{\delta}^{(2)}$ … $\boldsymbol{\delta}^{(N)}]^T$ represents thermal error history. $\mathbf{S}_{N\times c}$ and $\boldsymbol{\Delta}_{N\times p}$ are nonstationary multivariate time series data. This fact can be illustrated by an example. As shown in Fig. 4.1, 11 sensors are mounted onto a CNC machine tool, where S #*i* denotes sensor *i* (*i*=1, 2, …, 11). Under certain working conditions, the sensor readings over time index are shown in the left panel of Fig. 4.2. At the same time, in-line probing system provides the thermal errors in *z* direction of machine tool spindle (right panel of Fig. 4.2). The nonstationary nature of the data is obvious.

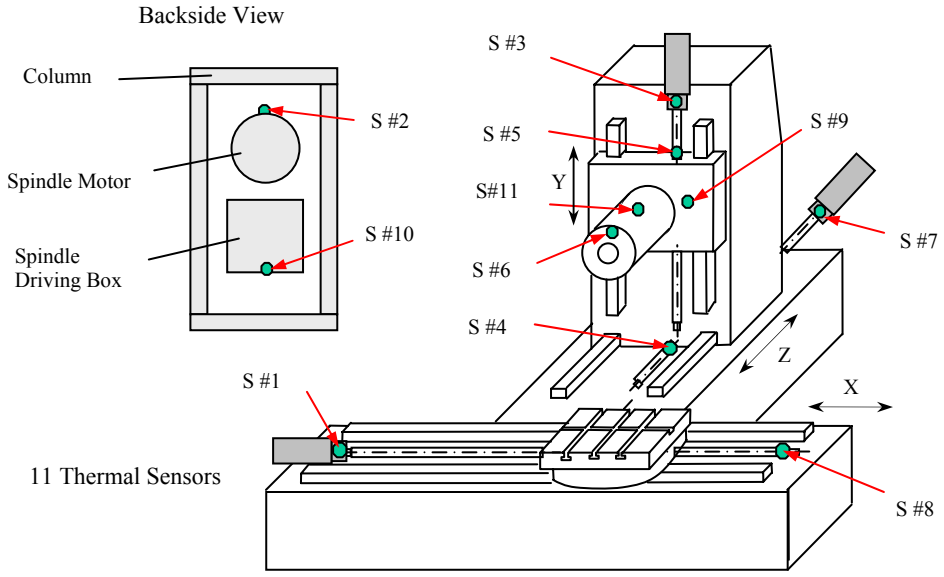

Figure 4.1 Thermal Sensor Locations on a Machine Tool

For engineering processes, the common treatment on nonstationarity is to take the first or second order difference on original data and check the first two moments for adequacy test (Box and Jenkins, 1970). Define a difference operator $\mathbf{D}_{c\times c}(q) = Diag[(1-q^{-1})^{d_1}, (1-q^{-1})^{d_2},\ldots, (1-q^{-1})^{d_j,\ldots}]$, where $d_j = 1$ or 2 (j=1,2,…,c or p) and q^{-1} is the back shift operator, i.e., $(1-q^{-1})z^{(t)}=z^{(t)}-z^{(t-1)}$. Therefore, to obtain stationary time series, the temperature and thermal error data are transformed as

$$\mathbf{D}(q)(\mathbf{S}_{N\times c}) = [\mathbf{D}(q)\mathbf{s}^{(1)} \;\; \mathbf{D}(q)\mathbf{s}^{(2)} \;\ldots\; \mathbf{D}(q)\mathbf{s}^{(N)}]^T, \tag{4.1}$$

$$\mathbf{D}(q)(\mathbf{\Delta}_{N\times p}) = [\mathbf{D}(q)\boldsymbol{\delta}^{(1)} \;\; \mathbf{D}(q)\boldsymbol{\delta}^{(2)} \;\ldots\; \mathbf{D}(q)\boldsymbol{\delta}^{(N)}]^T. \tag{4.2}$$

For simplicity, denote $[\mathbf{D}(q)\mathbf{s}^{(i)} \;\; \mathbf{D}(q)\mathbf{s}^{(i+1)} \ldots \mathbf{D}(q)\mathbf{s}^{(j)}]^T$ as $\mathbf{S}(i,j)$ and $[\mathbf{D}(q)\boldsymbol{\delta}^{(i)}$ $\mathbf{D}(q)\boldsymbol{\delta}^{(i+1)} \ldots \mathbf{D}(q)\boldsymbol{\delta}^{(j)}]^T$ as $\mathbf{\Delta}(i,j)$ with $i<j$.

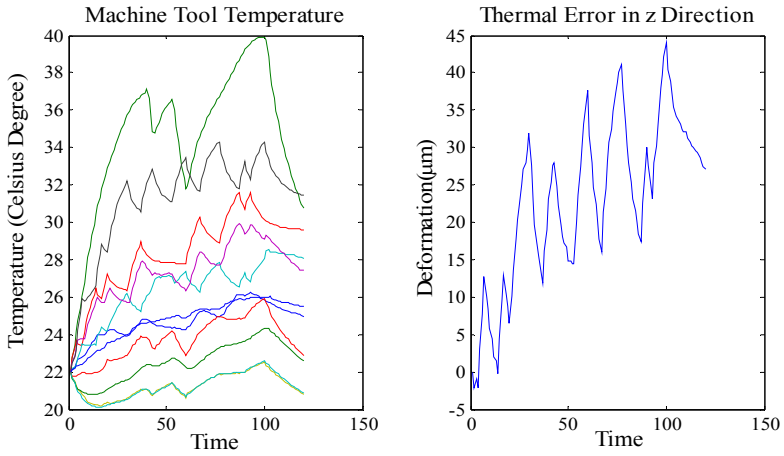

Figure 4.2 Machine Tool Temperature and Thermal Error Data

The order d_j in $\mathbf{D}(q)$ is determined by the nature of data. For the example data in Fig. 4.2, we can take the first and second order difference of the temperature and thermal error data. The first and second order differences of the temperature and thermal error data are shown in Fig. 4.3. We can also compute the mean and variance of these data differences. Among the total 120 observations (Fig. 4.2), two segments are randomly selected. Segment 1 contains observation No. 5 to 45 and Segment 2 contains the observation No. 50 to 90. The mean and variance of differences of these two segments are shown Tables A.1 and A.2 in Appendix D. We can see that the second order differences in two segments are very small and it is not necessary to consider the second order difference in the model (Box and Jenkins, 1970). Therefore, the first order difference is sufficient for the temperature and thermal error data in this example.

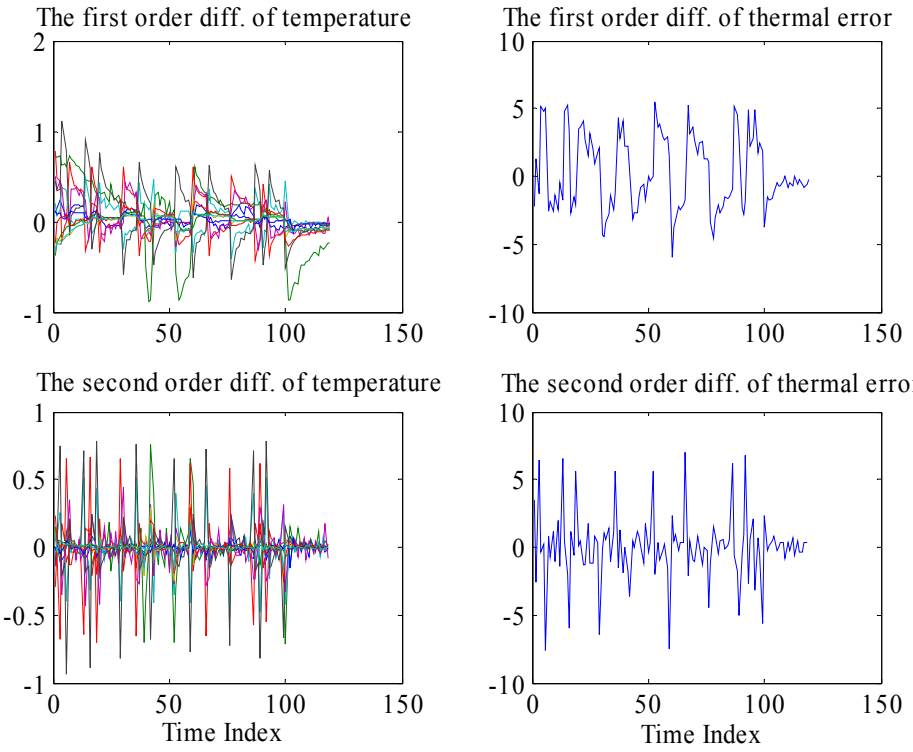

Figure 4.3 Stationarity Treatment

Rather than in a unique format presented in (Shi and MacGregor, 2000), construction of descriptor data **X** and response **Y** for the modeling study is depending upon whether in situ measurement of thermal deformation is sufficiently available during the process. There are commonly two situations. The first one is that thermal sensing information is sufficient and accurate model prediction can be achieved for real time thermal error compensation. Another situation is that thermal sensing information may be inadequate for model based compensation whereas in-line monitoring of machine thermal status and prediction of process degradation is important to continuous maintenance of product quality.

If the in situ measurements of thermal error are available, for example, using process intermittent probing, the lagged variables both in temperature and thermal error histories can be included in screening procedure of lagged input variable, and

determining the model structure. Suppose the speculated maximum time lag is l, where l can be chosen as a number large initially, the input vector **X** and output vector **Y** can be represented as

$$\mathbf{X} = [\mathbf{S}(1,N-l+1)\ \ \mathbf{S}(2, N-l+2) \ldots\ \ \mathbf{S}(l,N)\ \ \mathbf{\Delta}(1,N-l+1)\ \ \mathbf{\Delta}(2, N-l+2) \ldots\ \ \mathbf{\Delta}(l-1,N-1)], \quad (4.3)$$

$$\mathbf{Y} = \mathbf{\Delta}(l,N). \quad (4.4)$$

Here, block matrix $\mathbf{S}(i,N-l+i)$ is regarded as the data collection for variable difference $\mathbf{t}^{(i)}$-$\mathbf{t}^{(i-1)}$, where **t** is the variable vector of temperature. Matrix $\mathbf{\Delta}(i,N-l+i)$ contains data collection of the variable difference $\delta\mathbf{q}_m{}^{(i)}$-$\delta\mathbf{q}_m{}^{(i-1)}$. Eq. (4.3) enables the screening procedure to consider the lagged variables both in temperature history and thermal error history.

If the in situ measurement of thermal error is unavailable, the **X** can only be formed with time sequences of temperature measurements:

$$\mathbf{X} = [\mathbf{S}(1,N-l+1), \mathbf{S}(2, N-l+2),\ldots, \mathbf{S}(l,N)]. \quad (4.5)$$

When using data matrices (4.4) and (4.5), we can avoid stopping normal production and monitor thermal error in situ.

4.2.2 Latent Variable Modeling of Machine Tool Dynamic Error

Latent variable modeling is a method for constructing predictive models when the factors are many and highly collinear (Burnham, Viveros, and MacGregor, 1999). The general model structure is

$$\mathbf{X} = \mathbf{T}\mathbf{P}^T + \mathbf{E}, \quad (4.6)$$

$$\mathbf{Y} = \mathbf{T}\mathbf{Q}^T + \mathbf{F}, \quad (4.7)$$

where **P** is **X** loadings and **Q** is **Y** loadings. **X** and **Y** are assumed to have the common underlying latent variables **LV** with **LV**= $[LV_1,\ldots,LV_A]^T$ ($A \ll k+m$). **LV** reduces **X** and **Y** spaces into a low dimensional subspace spanned by **LV**. The subspace is expected to grasp the most relevant information and structures from **X** and **Y** spaces. **LV** has the nice property that its elements are orthogonal to each other. Each realization of **LV** forms the corresponding row of score matrix **T**, which can be directly computed from **X** as:

$$\mathbf{T} = \mathbf{X}\,\mathbf{W}(\mathbf{P}^T\mathbf{W})^{-1}, \tag{4.8}$$

where **W** is the weights of **X**. The unmodeled noise terms are **E** and **F**.

Y can be expressed in a regression form as

$$\mathbf{Y} = \mathbf{XG} + \mathbf{F} \tag{4.9}$$

with $\mathbf{G} = \mathbf{W}(\mathbf{P}^T\mathbf{W})^{-1}\mathbf{Q}^T$.

Among different model fitting approaches, such as principal component regression (PCR), partial least squares or projection to latent structures (PLS), canonical correlation analysis (CCA), and reduced rank analysis (RRA), PLS chooses **LV** by maximizing the covariance between historical information in **X** and **Y (**Shi and MacGregor, 2000) and it has been widely applied in chemical processes for process calibration and process monitoring (Nomikos and MacGregor, 1995). The PLS algorithm (Westerhuis, Kourti, and MacGregor, 1998) is adopted in this research. A variable screening procedure is then implemented to choose the number of sensors and maximum time lag for the model.

Training data matrices **X** and **Y** need to be mean centered and scaled to unit variance prior to fitting the model, while the new data matrices are still denoted as **X** and **Y** in this chapter. We add operator ~ on the top of the notation to represent the scaled variable or

data matrix (scale for each column). Hence, the input vector $\tilde{\mathbf{X}}$ and output vector $\tilde{\mathbf{Y}}$ can be represented as

$$\tilde{\mathbf{X}}=[\tilde{\mathbf{S}}(1,n\text{-}l\text{+}1)\ \tilde{\mathbf{S}}(2,\ n\text{-}l\text{+}2)\ \ldots\tilde{\mathbf{S}}(l,n)\ \ \tilde{\mathbf{\Delta}}(1,n\text{-}l\text{+}1)\ \tilde{\mathbf{\Delta}}(2,\ n\text{-}l\text{+}2)\ \ldots\tilde{\mathbf{\Delta}}(l\text{-}1,n\text{-}1)], \quad (4.10)$$

$$\tilde{\mathbf{Y}}=\tilde{\mathbf{\Delta}}(l,\ n).$$

$\tilde{\mathbf{X}}$ is an n-l+1 by rl+6(l-1) matrix consisting of the data collection of temperatures and thermal errors. Here, the block matrix $\tilde{\mathbf{S}}(i,n\text{-}l\text{+}i)$ contains n-l+1 scaled temperature data vectors for $\{\mathbf{s}^{(i)}\sim\mathbf{s}^{(n\text{-}l\text{+}i)}\}_{i=1,2,\ldots l}$ and can be regarded as the data collection of the variable difference $\tilde{\mathbf{t}}^{(i)}\text{-}\tilde{\mathbf{t}}^{(i\text{-}1)}$, i=1,2…l, over a period from i to n-l+I. Similarly, matrix $\tilde{\mathbf{\Delta}}(i,n\text{-}l\text{+}i)$ includes n-l+1 scaled thermal error vectors for $\{\boldsymbol{\delta}^{(i)}\sim\boldsymbol{\delta}^{(n\text{-}l\text{+}i)}\}_{i=1,2,\ldots l}$ and is an (n-l+1)-period (from i to n-l+i) data collection of the variable difference $\delta\tilde{\mathbf{q}}_m^{(i)}\text{-}\delta\tilde{\mathbf{q}}_m^{(i\text{-}1)}$. Temperatures will be used for input and thermal errors will be for autoregressive terms in the model. $\tilde{\mathbf{Y}}$ includes the data collection of thermal errors $\delta\tilde{\mathbf{q}}_m^{(n)}$. By LVM fitting procedure, we fit the regression coefficient **G** in Eq. (4.9) to the data in Eq. (4.10). Hence, the first order differences of errors at time period n can be represented as the function of error sources in the previous periods:

$$\delta\tilde{\hat{\mathbf{q}}}_m^{(n)}-\delta\tilde{\hat{\mathbf{q}}}_m^{(n-1)}=-\sum_{l=1}^{p_1}\tilde{\mathbf{A}}^{(l)}[\delta\tilde{\hat{\mathbf{q}}}_m^{(n-l)}-\delta\tilde{\hat{\mathbf{q}}}_m^{(n-l-1)}]+\sum_{l=1}^{p_2}\tilde{\mathbf{B}}^{(l)}[\tilde{\mathbf{t}}^{(n-l)}-\tilde{\mathbf{t}}^{(n-l-1)}], \quad (4.11)$$

where $\tilde{\mathbf{A}}^{(l)}$ is a 6×6 square coefficient matrix and its non-zero entries come from the entries in **G** corresponding to autoregressive terms. $\tilde{\mathbf{B}}^{(l)}$ is a 6×11 coefficient matrix and its non-zero entries come from the entries in **G** corresponding to the temperature variables (see the example of the coefficient matrices in the case study). p_1 and p_2 represent the maximum time lag for temperature and thermal error in the model. Time lag p_1 is for $\tilde{\mathbf{A}}$ and p_2 for $\tilde{\mathbf{B}}$, $n\geq n_0$. n_0 is the starting period when the adjustment applies.

Scaling the data back with the mean and variance from the training dataset, we have

$$\delta\mathbf{q}_m^{(n)} - \delta\mathbf{q}_m^{(n-1)} = -\sum_{l=1}^{p_1}\mathbf{A}^{(l)}[\delta\mathbf{q}_m^{(n-l)} - \delta\mathbf{q}_m^{(n-l-1)}] + \sum_{l=1}^{p_2}\mathbf{B}^{(l)}[\mathbf{t}^{(n-l)} - \mathbf{t}^{(n-l-1)}] + \mathbf{D}_0^{(n)} - \mathbf{D}_0^{(n-1)}, \tag{4.12}$$

where $\mathbf{D}_0(n)$ is the intercept term that is the linear combination of the means of the original data. $\mathbf{A}(l)$ and $\mathbf{B}(l)$ are the coefficient matrices after scaling back the data. Considering Eq. (2.9), we get

$$\begin{aligned}\Delta\mathbf{m}^{(n)} - \Delta\mathbf{m}^{(n-1)} = -\mathbf{K}\sum_{l=1}^{p_1}\mathbf{A}^{(l)}\mathbf{K}^{-1}[\Delta\mathbf{m}^{(n-l)} - \Delta\mathbf{m}^{(n-l-1)}] + \\ \mathbf{K}\sum_{l=1}^{p_2}\mathbf{B}^{(l)}[\mathbf{t}^{(n-l)} - \mathbf{t}^{(n-l-1)}] + \mathbf{K}[\mathbf{D}_0^{(n)} - \mathbf{D}_0^{(n-1)}].\end{aligned} \tag{4.13}$$

Denote q^{-1} as the backward operator, e.g., $q^{-1}\Delta\mathbf{m}^{(n)}$ represents $\Delta\mathbf{m}^{(n\text{-}1)}$. Canceling $(1\text{-}q^{-1})$ on both hand sides of Eq. (4.13) leads to

$$\Delta\mathbf{m}^{(n)} = -\mathbf{K}\sum_{l=1}^{p_1}\mathbf{A}^{(l)}\mathbf{K}^{-1}\Delta\mathbf{m}^{(n-l)} + \mathbf{K}\sum_{l=1}^{p_2}\mathbf{B}^{(l)}\mathbf{t}^{(n-l)} + \mathbf{K}_0^{(n)}, \tag{4.14}$$

where $\mathbf{K}_0^{(n)}$ is a matrix that is related to the initial condition $\mathbf{t}^{(n0)}$, $\Delta\mathbf{m}^{(n0)}$ and intercept term $\mathbf{D}_0^{(n)}$. Eq. (4.14) is the fitted model for the quasi-static EFE thermal error. It will predict the thermal error at the next period based on all the previous information such as the temperatures and thermal errors collected. It can also be applied to the equivalent error compensation (or automatic process adjustment) that has been discussed in Chapter 3. Design of process adjustment algorithm will be discussed in the next chapter.

Since the thermal errors in Fig. 4.2 are along *z* direction only, the equivalent amount of fixture error (EFE) is the same as thermal errors (see Fig. 4.4). We make the notations of EFE and thermal errors interchangeable in Section 4.3.

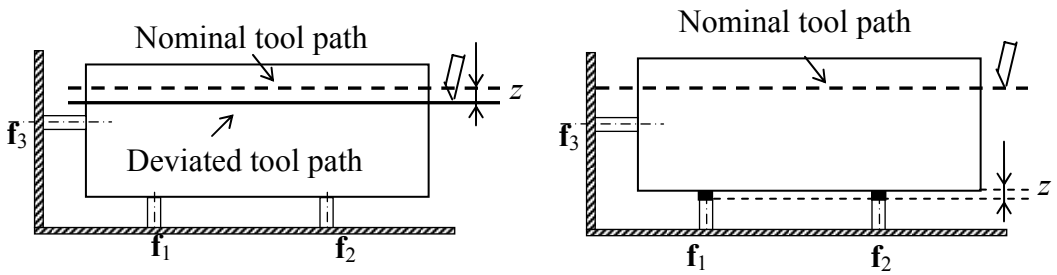

Figure 4.4 Equivalent Fixture Error of Fig. 4.2

As to the situation one mentioned in Section 4.2.1, we fit the model to data for variable screening. Given the 120 observations in Fig. 4.2, suppose the maximum time lag is 6 (or a larger number) for $\boldsymbol{\delta}^{(t)}_{1\times1}$ and $\mathbf{s}^{(t)}_{11\times1}$ (note: $\boldsymbol{\delta}$ is one dimensional for this case). Using the first 94 observations as training set and construct $\mathbf{X}$ and $\mathbf{Y}$ by Eqs. (4.3) and (4.4), we can see that after first order difference, l=6-1=5. So, according to Eq. (4.3), total $l\times c+l$-1=(6-1)×11+(6-1)-1=59 candidate variables in $\mathbf{X}_{90\times59}$ need to be screened to fit the corresponding thermal error data $\mathbf{Y}_{90\times1}$. The number of latent variables is determined by the percentage of variance they can explain. To start, just assume there are 30 latent variables and fit the model expressed by Eqs. (4.6) and (4.7). Based on the index of variable importance for projection (VIP: a variable with VIP greater than 0.8 is assumed to be significant) (Wold, 1994) and regression coefficients $\mathbf{G}$, 29 input variables in $\mathbf{X}$ are screened out (Table A.3 in the Appendix E).

Table A.3 suggests that sensor 9 seems to be insignificant in the thermal error model. However, in the experiment, sensor 9 is mounted onto the places near spindle motor and spindle bearing (Fig. 4.1), which appear to be major influencing heat sources. By further investigating the significant factors, $(1-q^{-1})\delta^{(t-2)}$ and $(1-q^{-1})\delta^{(t-1)}$, the lagged deformation information, which are related with temperature information from sensor 9, are found in the model.

The maximum time lag for temperature data and the thermal error is 5. The model could also be refitted with several larger time lags to be certain no significant lagged variables were missed. Sensors 1, 3, 4, 5, 7, 8, and 10 all appear at least 3 times with different lags in the model, which indicates that those 3 sensors might have more complicated thermal dynamic behaviors than the rest.

Since in-line probing is usually not easily accessible during production, LV modeling with only lagged temperature variables is a main focus in this chapter. For the rest of this section, a latent variable model will be built for in-line monitoring of machine tool thermal errors, in the case no sufficient information is available for error compensation.

We still use the first 94 observations for model fitting and assume 30 latent variables without autoregressive terms. The rest of data will be used for model testing. With the data matrices $\mathbf{X}_{90\times 55}$ (Eq. (4.5)) and $\mathbf{Y}_{90\times 1}$ (Eq. (4.4)), the model fitting procedure includes two steps, i.e.,

- Screen sensors and find A latent variables;
- Refit model with significant sensors and A latent variables.

The screening procedure remains the same and the result is given by Table A.4. Based on the percentage of variance explained by the latent variables (Table A.5 in Appendix E), choose 9 latent variables out of 30, i.e., $A = 9$, which explain 86.954% of variation in $\mathbf{X}$ and 96.6966% of variation in $\mathbf{Y}$ (see the ninth latent variable in Table A.5). Therefore, 24 input variables (denoted as $\mathbf{x}_{24\times 1}$) in Table A.4 are used to refit the model to get $\mathbf{LV}_{9\times 1}= \mathbf{x}^T\mathbf{W}(\mathbf{P}^T\mathbf{W})^{-1}$, $\mathbf{W}$, $\mathbf{T}$, $\mathbf{P}$, $\mathbf{Q}$ and $\mathbf{G}$.

To test model accuracy, first, we can use the temperature observations No. 95 to No. 119 as input for predicting thermal errors. After taking the first order difference, the new 25 observations are mean centered and scaled with the mean and variance obtained from training dataset. Denote the pre-processed data as $\mathbf{X}_{new}$. By Eq. (4.8), the new score $\mathbf{T}_{new}$ is obtained as $\mathbf{T}_{new} = \mathbf{X}_{new}\mathbf{W}(\mathbf{P}^T\mathbf{W})^{-1}$. By Eq. (4.9), the predicted $\mathbf{Y}$ is $\hat{\mathbf{Y}} = \mathbf{X}_{new}\mathbf{W}(\mathbf{P}^T\mathbf{W})^{-1}\mathbf{Q}^T$ and the residuals are $\mathbf{F}=\mathbf{Y}-\hat{\mathbf{Y}}$. The first 60 observations in another experiment are used to predict the thermal errors in a similar manner.

$\hat{\mathbf{Y}}$ needs to be added with mean and scaled back with the variance from the training dataset. Given the first new initial thermal error, we integrate the post-processed $\hat{\mathbf{Y}}$ and compare it with the observed thermal errors (Fig. 4.5). As can be seen, the residuals are small and this result is satisfactory.

If sensing information is sufficient, the prediction power of the model developed by SI theory is normally higher than the one obtained from LVM method. If not, LVM method is expected to have better performance. The reason is that LVM method is to model the underlying structure in $\mathbf{X}$ and $\mathbf{Y}$, rather than to model the impact of $\mathbf{X}$ on $\mathbf{Y}$. Therefore, reduced sensing information does not limit LVM's capability to find out some basic structures from the data, i.e., getting $\mathbf{T} = \mathbf{X}\mathbf{W}(\mathbf{P}^T\mathbf{W})^{-1}$ from $\mathbf{X}$ and $\mathbf{Y}$. The heat sources in a machine tool are abundant and more sensors are needed to well describe the temperature field. Thus LVM based in-line monitoring method is more appropriate for the given situation.

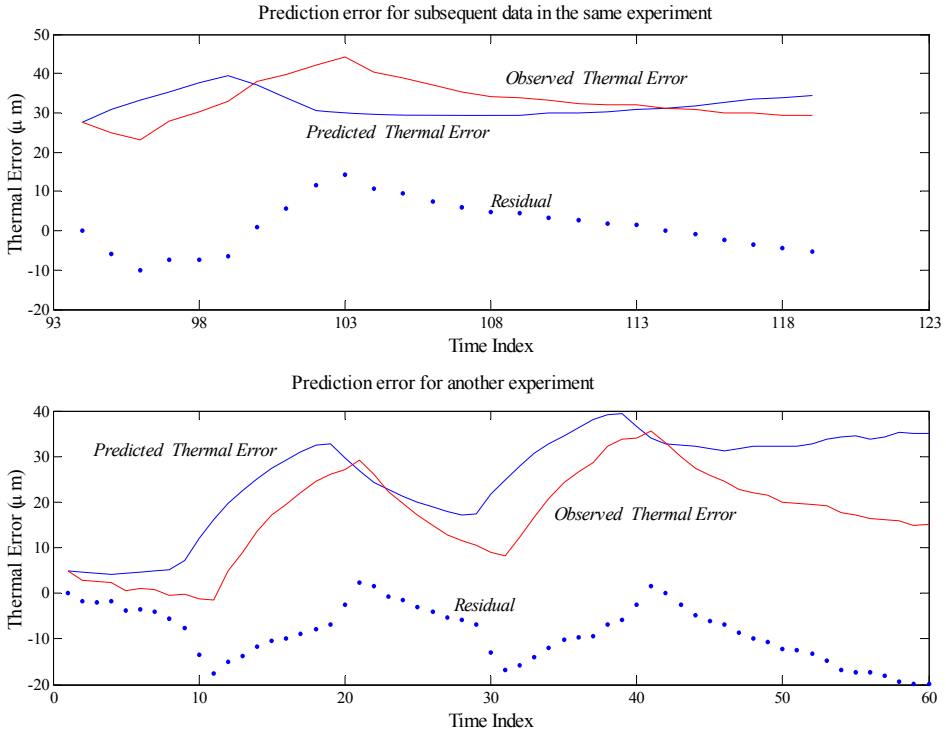

Figure 4.5 Model Prediction and Residuals

4.3 In-Line Monitoring of Dynamic Equivalent Errors of Machine Tool

The first step of in-line monitoring is to obtain historical temperature and thermal error data collected from a machine tool under normal working conditions. Then these data are used to fit a model using the same technique as introduced in Section 4.2. Its basic idea is to fit a latent variable model (Eqs. (4.6) and (4.7)) and monitor the process based on latent structures captured by utilizing the process information (e.g. temperature) and historical product information (e.g. thermal error) (Kourti and MacGregor, 1996). This section demonstrates the method to build control charts and to monitor machine tool thermal error.

We still use the data in Fig. 4.2 as an example. Suppose the first 94 observations on temperature and thermal error data are available for the training stage. During production, only temperature measurements are available. We need to find out whether the thermal behavior of the machine tool is changed to increase thermal errors.

With the model fitted in Section 4.2.2 (the second situation), we have **T**, **P**, **Q** and $\mathbf{LV}_{9\times1}$. If the 24 variables are denoted as vector $\mathbf{x}_{24\times1}$, then $\mathbf{LV}_{9\times1}$ can be expressed as

$$\mathbf{LV}^T = \mathbf{x}^T\mathbf{W}(\mathbf{P}^T\mathbf{W})^{-1}, \tag{4.15}$$

with $\mathbf{W}(\mathbf{P}^T\mathbf{W})^{-1}$ given in Table A.7 in Appendix E.

Use $\mathbf{t_a}$ to denote the one realization of **LV** (or one row in matrix **T**) and $\mathbf{t_a} = [t_1, t_2,\ldots, t_A]^T$ with $A = 9$ in the example. Define a Hostelling's T^2 statistic in terms of latent variables as

$$T^2 = \sum_{a=1}^{A} \frac{t_a^2}{s_a^2}, \tag{4.16}$$

where s_a^2 stands for the variance of t_a. It can be estimated from eigenvalues of the sample covariance matrix of **T**, i.e., $\mathbf{S_{LV}}$. Since $t_1, t_2,\ldots, t_A$ are orthogonal to each other, $\mathbf{S_{LV}}$ is a diagonal matrix and the estimator of s_a^2 is given by

$$s_a^2 = diag[\mathbf{S_{LV}}]_{aa}. \tag{4.17}$$

The control limit can be set by the F distribution (Johnson and Wichern, 1998),

$$T^2 \le \frac{A(n^2-1)}{n(n-A)} F_{A,n-A}(\alpha), \tag{4.18}$$

where $F_{A,\,n\text{-}A}(\alpha)$ is the upper 100(1-α)% critical point of F distribution with degree of freedom of (A, n-A).

In the example, *Diag*[$\mathbf{S_{LV}}$] = [7.6719, 3.1620, 2.5583, 1.0428, 1.0312, 1.2627, 0.3845, 0.2626, 0.5375], i.e., $s_1^2 = 7.6719$ and $s_9^2 = 0.5375$.

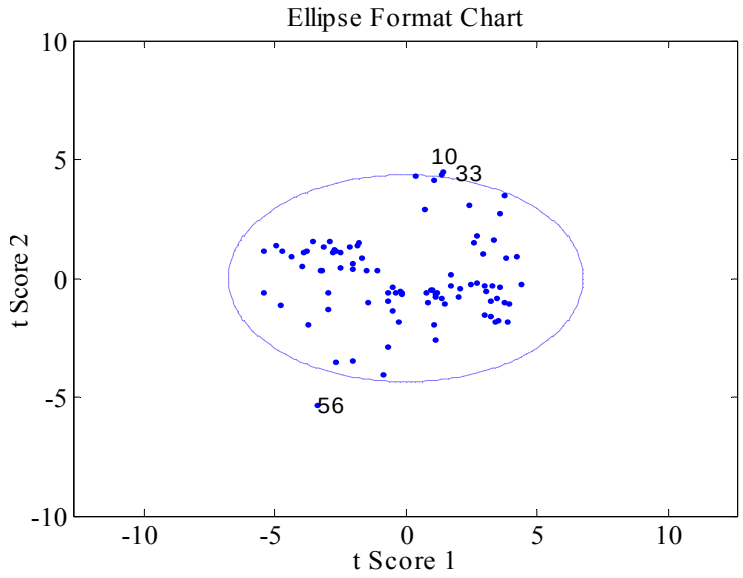

Figure 4.6 Ellipse Format Chart

We can see from Table A.5 that latent variable 1 accounts for the majority of the variance for the dependent variables. If only first two latent variables are considered, the elliptic control chart can be employed to monitor the stability of the machine tool. To build phase I control chart, the T^2 statistic is approximated by χ^2 distribution with 2 degrees of freedom (Johnson and Wichern, 1998), i.e.,

$$T^2 = \frac{t_1^2}{s_1^2} + \frac{t_2^2}{s_2^2} \le \chi_2^2(\alpha), \tag{4.19}$$

where $\chi_2^2(\alpha)$ is the upper 100(1-α)% critical point of χ^2 distribution with 2 degrees of freedom.

For level $\alpha = 0.05$ ($\chi_2^2(0.05) = 5.9915$), the ellipse format chart for the 90 observations is shown in Fig. 4.5 (after the first order difference, 90 data points are left for charting). In Fig. 4.6, points 10, 33, and 56 are beyond the limit. The scores of those 3

points need to be eliminated from **T** (not from **X**) before building phase II control chart. After the elimination, $Diag[\mathbf{S_{LV}}]$ = [7.7625, 2.4835, 2.6186, 1.0622, 1.0390, 1.1998, 0.3514, 0.2604, 0.5361]. This will be used for constructing phase II control limits.

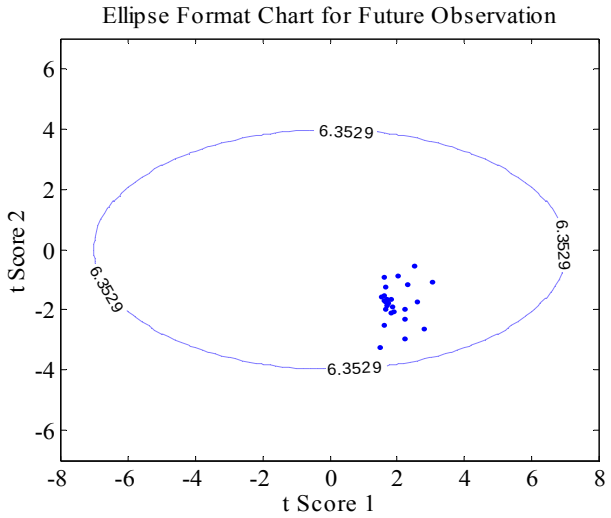

Figure 4.7 Control Ellipse for Future Observations

By Eq. (4.18), the phase II control chart is designed as

$$T^2 = \frac{\mathrm{t}_{\mathrm{new},1}^2}{s_1^2} + \frac{\mathrm{t}_{\mathrm{new},2}^2}{s_2^2} \le \frac{2(n^2-1)}{n(n-2)} F_{2,n-2}(\alpha), \tag{4.20}$$

where n is the number of observations for constructing the control limits (n = 90-3 = 87 in the example). s_1^2 and s_2^2 are computed from phase I, i.e., s_1^2 = 7.2636 and s_2^2 = 2.3244. $t_{\mathrm{new},1}^2$ and $t_{\mathrm{new},2}^2$ come from the future observations and they are the first two entries of $\mathbf{t}_{\mathrm{new}}$. For a new observation $(\mathbf{x}_{\mathrm{new}})_{24\times 1}$

$$(\mathbf{t}_{\mathrm{new}})^T = (\mathbf{x}_{\mathrm{new}})^T \mathbf{W}(\mathbf{P}^T\mathbf{W})^{-1}. \tag{4.21}$$

Suppose observations No. 95 to No. 119 are new measurements. The control ellipse based on Eq. (4.18) is shown in Fig. 4.7 (α = 0.05, and $F_{2,\,85}(0.05)$=3.1038), which suggests that the machine tool thermal condition is stable.

4.4 Isolation of Lagged Variables and Sensors Responsible for the Out-of-Control Signal

Although the control charts can identify out-of-control signals, they are unable to determine the root causes. Contribution plots have been suggested to isolate the variables responsible for the out-of-control signals (Kourti and MacGregor, 1996). The idea is to check the standardized scores (i.e., t_a/s_a) with high values and to further investigate the variables that have the large contributions to those scores.

In Section 4.3, points 10, 33, and 56 are identified to be out-of-control. The scores of these 3 points (the rows in **T** corresponding to these points) are listed in Table A.8. For each realization of **LV** (or each point), plot t_a/s_a with $a = 1,2,\ldots,9$ on the same graph (Fig. 4.8).

With 95% confidence of type I error, the Bonferroni limit for the graph in Fig. 4.8 is ±2.7 (Alt, 1985). We can see that the second score component (i.e., the second latent variable) of those 3 points is the main contributing factors to the out-of-control signal.

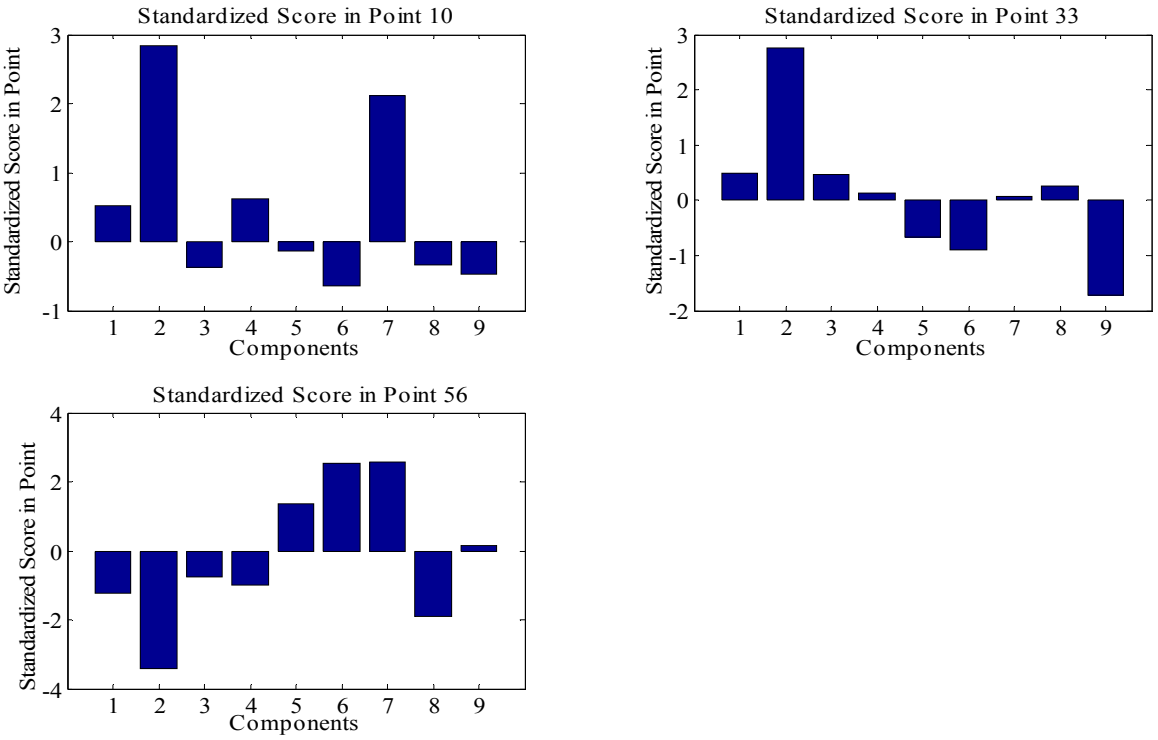

Figure 4.8 Standardized Scores in Points 10, 33, and 56

Since $\mathbf{t}^T = \mathbf{x}^T\mathbf{W}(\mathbf{P}^T\mathbf{W})^{-1}$ (refer to Table A.7 for $\mathbf{W}(\mathbf{P}^T\mathbf{W})^{-1}$), we can further investigate the contributions of lagged variable in $\mathbf{x}$ and contributing sensors responsible for the signals. For each realization of **LV**, the contribution of variable x_j (the jth component in $\mathbf{x}_{24\times1}$, j=1,2,..,24 and t=10, 33, and 56 for this example) to the score of the ath score component is defined to be (Kourti and MacGregor, 1996)

$$Contribution_{a,j} = x_j e_{aj}, \tag{4.22}$$

where e_{aj} is the jth component in the ath column (corresponding to ath score component) of matrix $\mathbf{W}(\mathbf{P}^T\mathbf{W})^{-1}$.

To the second latent variable in points 10, 33, and 56, the contributions of 24 variables (see Table A.4 for the variables) are shown in Fig. 4.9. Clearly, variable No.21, i.e. $(1-q^{-1})s_7^{(t)}$, makes the largest contributions to the signals.

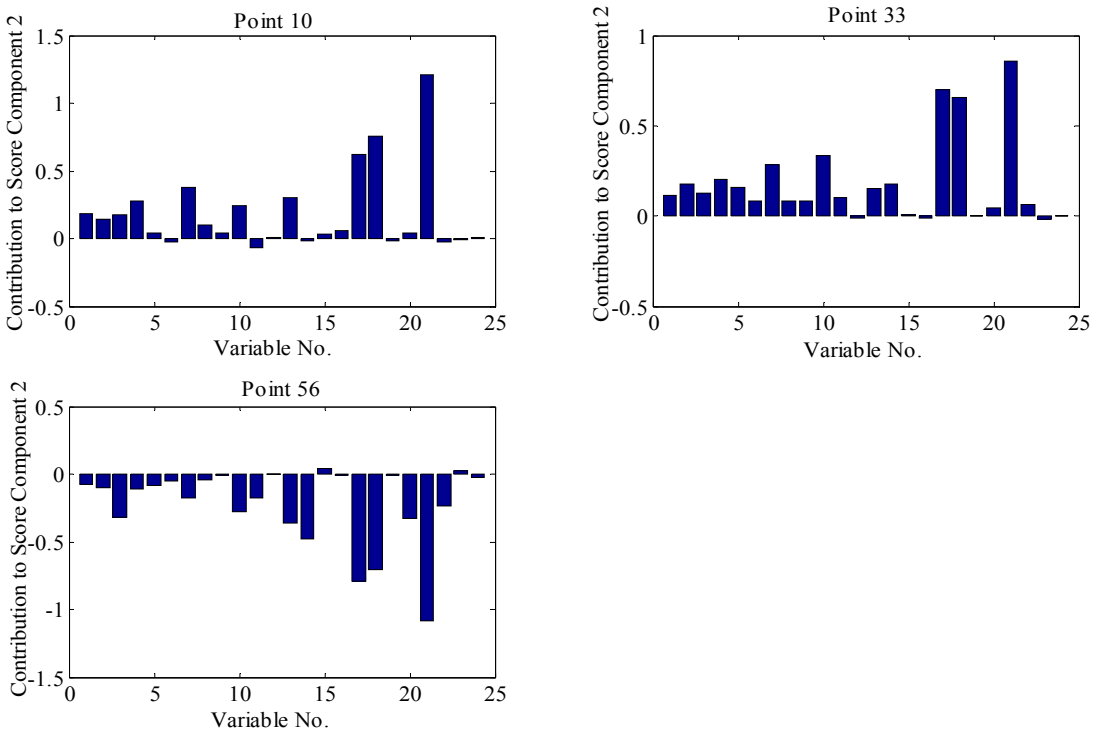

Figure 4.9 Lagged Variable Contributions to Score Component 2

Since the 24 lagged variables are from 10 sensors (sensor 9 is excluded by the screening procedure), study on the aggregated contributions from each sensor might provide valuable information for root cause determination, i.e., finding out the main heat sources that lead to thermal errors. The aggregated contribution can be found by summing up the contribution of lagged variables corresponding to each sensor (see the correspondence in Table A.6). Fig. 4.10 shows the contributions of 10 sensors to the second latent variable of points 10, 33, and 56. Although this latent variable is the main contributing factor to the out-of-control signal in these 3 points, the patterns in terms of sensor contributions are quite different. In these points the heat sources at sensors 3, 4, and 7 are the main factors causing the changes of machine tool thermal condition. Further investigation should be taken to find out the physical reasons, such as spindle bearing

overheating or coolant not functioning. All the sensor contributions for point 56 for score component 2 take negative values because the data was sampled at cooling down cycle.

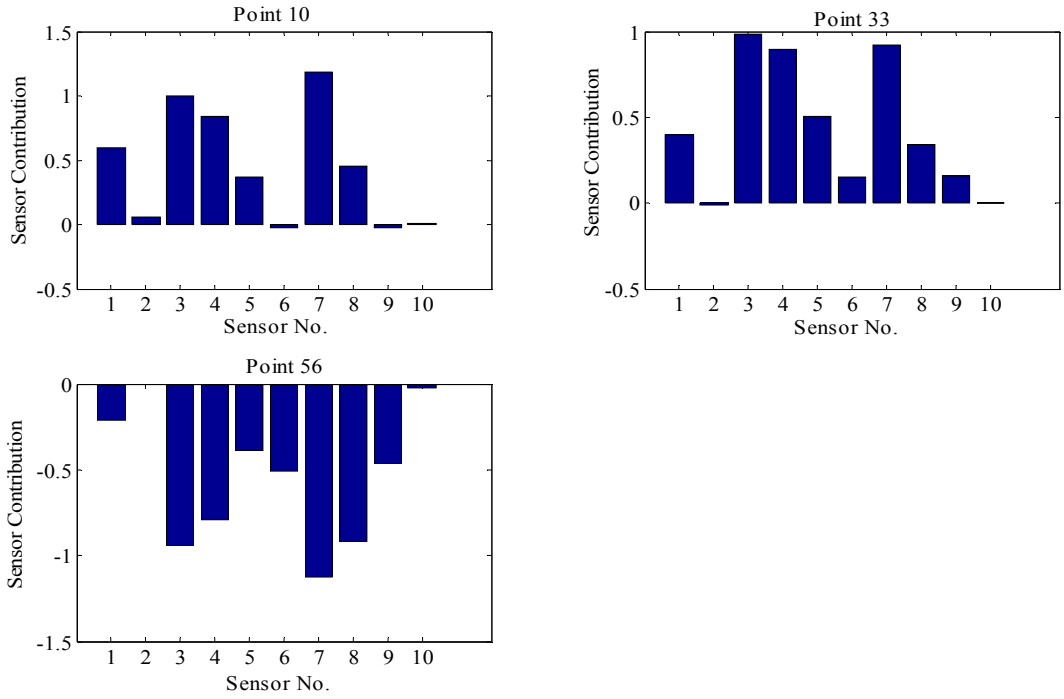

Figure 4.10 Sensor Contributions to Score Component 2

If more latent variables are beyond limits in Fig. 4.8, we can study the overall average lagged variable contribution and sensor contribution. The procedure of computing the overall average variable contribution is similar to that in Kourti and MacGregor (1996).

4.5 Summary

This chapter models the error equivalence for the dynamic process errors and develops the in-line monitoring of the equivalent dynamic process errors and process degradation caused by thermal errors. Machine tool thermal errors are selected as an example to demonstrate the dynamic error equivalence modeling and process monitoring

in machining. The thermal sensors and maximum time lag are chosen according to a screening procedure applied to results of LVM. The in-line monitoring of dynamic equivalent errors is achieved by theories of statistical quality control: first T^2 control chart is built to detect out of limit signal; then bar plots of normalized scores and contribution are created to identify the major contributing latent variables, the contribution of each lagged variable and sensor to the thermal errors. These procedures show that LVM method provides interesting results in variable screening, model prediction, and especially in in-line monitoring and root cause identification. LVM method is especially appropriate for multivariate measurements and ill-conditioned data, and it could also provide a benchmark to judge whether the sensing information is sufficient to perform dynamic error compensation.

The success of applying LVM method in monitoring is due to the property of LV model, i.e., finding out the latent variables that maximize the covariance between process variable (e.g., temperature) and product variable (e.g., thermal errors). LVM method captures the thermal patterns from the historical data collected from an in-control machine tool. Future observation is assumed to be out-of-control signal if the pattern changes are detected. Once an out-of-control signal is detected, the study shows that the lagged variable and sensor contribution plots are very helpful to determine the root causes.

Chapter 5

Error Compensation Based on Dynamic Error Equivalence for Reducing Dimensional Variation in Discrete Machining Processes*

Traditional SPC technique has been widely employed for the process monitoring in discrete manufacturing. However, SPC does not consider any adjustment that prevents the process drifting from the target. Furthermore, many in-line adjustment approaches, such as thermal error compensation and avoidance, are designed only for machine tool error reduction. This chapter intends to fully utilize the engineering process information and propose an alternative compensation strategy that could automatically reduce the overall process variations. Based on the model of dynamic equivalent errors developed in Chapter 4, a SPC integrated error-canceling-error APC methodology is derived to compensate for both time invariant and dynamic errors by adjusting the base error. The performance of the adjustment algorithm such as stability and sensitivity is then evaluated. A self updating scheme for the adjustment algorithm has been proposed to track the latest process information as well. This process adjustment has been simulated using the data collected from a real machining process. The results show that this algorithm can improve the machining accuracy and reduce the process variations.

* The work in this chapter has appeared in Wang, H. and Huang, Q., 2007, "Using Error Equivalence Concept to Automatically Adjust Discrete Manufacturing Processes for Dimensional Variation Reduction," *ASME Transactions, Journal of Manufacturing Science and Engineering*, 129, 644-652.

In Section 5.1, an error equivalence adjustment algorithm is derived to counteract the machining process variation. Its integration with SPC is discussed in Section 5.2. The adjustment algorithm is implemented via a case study in Section 5.3. Section 5.4 evaluates the performance of the APC methodology such as stability and sensitivity when a change in the dynamics of process occurs. Conclusions are given in Section 5.5.

5.1 Automatic Process Adjustment Based on Error Equivalence Mechanism

For a manufacturing process with causal relationship $\mathbf{x} = f(\mathbf{u}_1, \mathbf{u}_2, \ldots, \mathbf{u}_p) + \boldsymbol{\varepsilon}$, the traditional error compensation strategy is to minimize individual process errors $\mathbf{u}_i$'s so as to reduce output deviation $\mathbf{u}$. As pointed out in Chapter 3, since error equivalence also implies the cancellation among process errors, this allows us to develop a new compensation strategy, i.e., treating all process error sources as a system and using one error to compensate for the others. For instance, with the development of flexible fixture whose locator length is adjustable, it is feasible to compensate for the overall process errors in the machining process by changing locator length. In this new strategy, the outputs of the adjustment algorithm and process will be monitored using SPC methods. The main purpose is to monitor unexpected events such as adjustment device failure.

It should be noted that compensation cost is a critical factor to be considered in real applications. It is not discussed in this study because cost issue is often case dependent.

Using the observed feature deviation $\mathbf{x}^{(n)}$ at time period n as input, the proposed error equivalence based algorithm $\mathbf{G}_{\mathbf{u}_1}$ generates adjustment $\mathbf{c}^{(n)}$ to counteract $\Sigma_{i=2}^{p}\mathbf{u}_i^{*(n+1)}$ for the (n+1)th time period. Let $\mathbf{c}^{(n)}$ be the cumulative amount of adjustment. $\mathbf{x}^{(n+1)}$ is

$$\mathbf{x}^{(n+1)} = \mathbf{\Gamma}^* \mathbf{c}^{(n)} + \mathbf{\Gamma}^* \sum_{i=2}^{p} \mathbf{u}_i^{*(n+1)} + \boldsymbol{\varepsilon}^{(n+1)}. \tag{5.1}$$

The adjustment $\mathbf{c}^{(n)}$ should be able to cancel $\mathbf{E}(\mathbf{x})$ and reduce the process variation. The adjustment algorithm can be designed to reduce the mean squared deviation of product feature, i.e., min $\mathrm{E}[\mathbf{x}^{(n+1)}]^2$. As proposed by Capilla, *et al.*, (1999), we can treat a simpler problem of minimizing an instantaneous performance index, min $[\hat{\mathbf{x}}^{(n+1)}]^2$. Taking the first derivative of $[\hat{\mathbf{x}}^{(n+1)}]^2$ and equaling it to zero, the adjustment rule can be summarized as follows. When the process errors $\mathbf{u}_i^*$'s are all static, the adjustment to reduce the mean shift of the process output is

$$\mathbf{c}^{(n)} = -\sum_{j \in S} \hat{\mathbf{u}}_j^* = -(\mathbf{\Gamma}^{*T} \mathbf{\Gamma}^*)^{-1} \mathbf{\Gamma}^{*T} \sum_{k=1}^{n} \mathbf{x}^{(k)}. \tag{5.2}$$

where *S* is the set for the static errors. Eq. (5.2) is in fact the same as Eq. (3.9). Considering static and dynamic process errors, the process adjustment $\mathbf{c}^{(n)}$ using error equivalence turns out to be

$$\mathbf{c}^{(n)} = -\sum_{j \in S} \hat{\mathbf{u}}_j^* - \sum_{i \in D} \hat{\mathbf{u}}_i^{*(n+1)} = -\sum_{j \in S} \hat{\mathbf{u}}_j^* - g(\{\sum_{i \in D} \hat{\mathbf{u}}_i^{*(k)}\}_{\{k|k<n\}}),$$

$$\sum_{i \in D} \hat{\mathbf{u}}_i^{*(n)} = -\mathbf{c}^{(n-1)} + (\mathbf{\Gamma}^{*T} \mathbf{\Gamma}^*)^{-1} \mathbf{\Gamma}^{*T} \mathbf{x}^{(n)} - \sum_{j \in S} \mathbf{u}_j^*, \tag{5.3}$$

where *D* is the set for dynamic errors. $\sum_{j \in S} \hat{\mathbf{u}}_j^*$ and $\sum_{i \in D} \hat{\mathbf{u}}_i^{*(n+1)}$ are the process static and dynamic equivalent errors based on the least square estimation, respectively. Dynamic errors can be represented by $\sum_{i \in D} \hat{\mathbf{u}}_i^{*(n+1)} = g(\{\sum_{i \in D} \hat{\mathbf{u}}_i^{*(k)}\}_k)$, where *g*(.) is the fitted dynamic model of process errors. Since the process will compensate for the same amount of error $\sum_{j=2}^{p} \hat{\mathbf{u}}_j^*$ at each time period, the proposed sequential root cause identification procedure can be applied to identify the error sources.

In the machining processes, the dynamic machine tool error can be represented by an ARX model with the temperatures of machine tool as input (see Eq. (4.13)). Substituting process model (4.13) into Eq. (5.1), the prediction for feature deviation at period n+1 is

$$\hat{\mathbf{x}}^{(n+1)} = \mathbf{\Gamma}^{*}\mathbf{c}^{(n)} - \mathbf{\Gamma}^{*}\mathbf{K}_3\sum_{l=1}^{p_1}\mathbf{A}^{(l)}\mathbf{K}^{-1}\Delta\mathbf{m}^{(n-l)} + \mathbf{\Gamma}^{*}\mathbf{K}_3\sum_{l=0}^{p_2}\mathbf{B}^{(l)}\mathbf{t}^{(n-l)} + \mathbf{\Gamma}^{*}[\sum_{j\in S}\hat{\mathbf{u}}_j^{*} + \mathbf{K}_0^{(n)}]. \quad (5.4)$$

The adjustment rule for machining process is then

$$\mathbf{c}^{(n)} = \mathbf{K}_3\sum_{l=1}^{p_1}\mathbf{A}^{(l)}\mathbf{K}^{-1}\Delta\mathbf{m}^{(n-l)} - \mathbf{K}_3\sum_{l=0}^{p_2}\mathbf{B}^{(l)}\mathbf{t}^{(n-l)} - \sum_{j\in S}\hat{\mathbf{u}}_j^{*} - \mathbf{K}_0^{(n)}\text{, } \mathbf{c}^{(n0)}=0\text{, and}$$

$$\Delta\hat{\mathbf{m}}^{(n-l)} = -\mathbf{c}^{(n-l-1)} + (\mathbf{\Gamma}^{*T}\mathbf{\Gamma}^{*})^{-1}\mathbf{\Gamma}^{*T}\mathbf{x}^{(n-l)} - \sum_{j\in S}\hat{\mathbf{u}}_j^{*}\text{.} \quad (5.5)$$

Static error is obtained by direct measurement or by equation

$$\sum_{j\in S}\hat{\mathbf{u}}_j^{*} = (\mathbf{\Gamma}^{*T}\mathbf{\Gamma}^{*})^{-1}\mathbf{\Gamma}^{*T}\mathbf{x} - \sum_{i\in D}\mathbf{u}_i^{*}\text{,} \quad (5.6)$$

where $\mathbf{x}$ and $\sum_{i\in D}\mathbf{u}_i^{*}$ are the measurements of feature deviation and dynamic errors when fitting the error model g(.).

Applicable conditions of compensation strategy. The base error $\mathbf{u}_1$ is not random because of the adjustment. Although the adjustment $\mathbf{c}$ is expected to compensate for the remaining process errors $\Sigma_{i=2}^{p}\mathbf{x}_i^{*}$, it becomes a new random error source because of the variability in the actuator. Therefore, the adjusted total process error $\mathbf{u}_a^{*}$ has

$$\mathrm{E}(\hat{\mathbf{u}}_a^{*}) = \mathrm{E}(\mathbf{c}) + \Sigma_{i=2}^{p}\mathbf{K}_i\mathrm{E}(\hat{\mathbf{u}}_i) \text{ and } \mathrm{Cov}(\hat{\mathbf{u}}_a^{*}) = \mathrm{Cov}(\mathbf{c}) + \Sigma_{i=2}^{p}\mathbf{K}_i\mathrm{Cov}(\hat{\mathbf{u}}_i)\mathbf{K}_i^{T}\text{.} \quad (5.7)$$

$\mathbf{G}_{\mathbf{x}_1}$ normally aims to keep the process output $\mathbf{x}$ on the target and with the minimum variation. The commonly used adjustment algorithm is to let $\mathrm{E}(\mathbf{c}) = -\Sigma_{i=2}^{p}\mathbf{K}_i\mathrm{E}(\hat{\mathbf{u}}_i)$ or $\mathrm{E}(\hat{\mathbf{u}}^{*}) = 0$. However, the generalized variance of error $\mathbf{u}_a^{*}$ or $\mathrm{Det}(\mathrm{Cov}(\hat{\mathbf{u}}_a^{*}))$ is not necessary to be smaller than the one without adjustment, where Det(.) represents the

determinant of the matrix in the parentheses. Cleary, if $\mathrm{Det}(\mathrm{Cov}(\mathbf{c})) \le \mathrm{Det}(\mathrm{Cov}(\hat{\mathbf{u}}_1))$, the new compensation strategy will uniformly reduce process variation. If $\mathrm{Det}(\mathrm{Cov}(\mathbf{c})) > \mathrm{Det}(\mathrm{Cov}(\hat{\mathbf{u}}_1))$ but the increase of total process variation $(\mathrm{Det}(\mathrm{var}(\hat{\mathbf{u}}_a^*))-\mathrm{Det}(\mathrm{Cov}(\hat{\mathbf{u}}^*)))/\mathrm{Det}(\mathrm{Cov}(\hat{\mathbf{u}}^*))$ is insignificant, the compensation might be acceptable as well. For instance, the precision of fixture is usually much higher than the workpiece and machine tool. An adjustable fixture equipped could have lower precision or larger $\mathrm{Det}(\mathrm{Cov}(\mathbf{c}))$. The minor percentage of fixture variation in the tool process errors might justify the application of error compensation because it brings the process on the target. Compensation is normally not effective if $\mathrm{Det}(\mathrm{Cov}(\mathbf{c}))>\mathrm{Det}(\mathrm{Cov}(\hat{\mathbf{u}}_1))$ and $(\mathrm{Det}(\mathrm{Cov}(\hat{\mathbf{u}}_a^*))-\mathrm{Det}(\mathrm{Cov}(\hat{\mathbf{u}}^*)))/\mathrm{Det}(\mathrm{Cov}(\hat{\mathbf{u}}^*))$ is appreciable.

The conventional compensation strategy aims to offset $\mathrm{E}(\hat{\mathbf{u}}_i)$ and reduce $\mathrm{Cov}(\hat{\mathbf{u}}_i)$ individually. It will be effective if there are only a few process errors dominating in $\mathrm{E}(\hat{\mathbf{u}})$ and $\mathrm{Cov}(\hat{\mathbf{u}})$. Otherwise, a large number of adjustments are needed to compensate for all error sources in order to keep the process output **x** on target. Under this condition, these two compensation strategies can be applied complementarily. The error sources with the largest variations can be counteracted using conventional methods to reduce $\mathrm{Cov}(\hat{\mathbf{u}})$, whereas the new compensation strategy is to achieve $\mathrm{E}(\hat{\mathbf{u}}_a^*) = 0$.

5.2 SPC Integrated Process Adjustment Based on Error Equivalence

In real application, process adjustment as shown in Eq. (5.5) has to consider the following practical problems:

Over Adjustment. Over adjustment may increase the production cost and process variation. However, the adjustment does not need to be implemented in the periods when:

- The process errors are not significant compared to the assigned tolerance of base errors (denoted by $\pm\sigma_{\mathbf{u}_1^*}$). We can predict the process errors in the next period and test if the predicted errors are within tolerance.
- The adjustment is beyond the accuracy limit of the device. Therefore, in the early stage of adjustment system design, we should choose the device whose accuracy limit matches the assigned tolerance of base errors.

Fast varying errors. The adjustment in Eq. (5.5) only compensates for the slow varying dynamic errors (quasi-static errors), which are relatively constant between the adjacent periods. Large process variation within one period can lead to large adjustment errors in $\mathbf{x}$. In order to identify such process change, the samples of outputs $\{\mathbf{x}^{(n)}\}$ of the manufacturing process within one period can be monitored by quality control charts.

Unexpected process errors. On some occasions, unexpected process errors (e.g., variation of adjustable fixture locator, hot chips during machining) have not been considered in $\{\mathbf{u}_i\}$ and thus the adjusted process could show a large variation. Integration of SPC and APC is an economic way to reduce the variation of adjusted process though it has been rarely applied in a discrete manufacturing process. Monitoring the estimated noise, i.e., $\hat{\boldsymbol{\varepsilon}}^{(n)}=\mathbf{x}^{(n)}-\boldsymbol{\Gamma}^*\Sigma_{i=2}^{p}\mathbf{u}_i^{*(n)}-\boldsymbol{\Gamma}^*\mathbf{c}^{(n-1)}$ can help to detect if unexpected errors impact the process output. When the unexpected errors take place, we can also update the process error model to track the latest information about errors and make a closer prediction. With the updating scheme, the coefficients in function $g(.)$ also change with period n. In the machining process, suppose we measure the temperature and thermal error every period,

and the measurement data are available at the period 1~n_0. The updating adjustment procedure can be proposed as follows:

- At the beginning of period n_0+k, data, including part features (measured by CMM) $\{\mathbf{x}^{(n0+k-l)}\}$, thermal errors (measured by in-line probes) $\{\delta\mathbf{q}_m{}^{(n0+k-l)}\}$, and temperatures (measured by thermal sensors) $\{\mathbf{t}^{(n0+k-l)}\}$, are collected to compute the locator adjustment $\mathbf{c}^{(n0+k-1)}$-$\mathbf{c}^{(n0+k-2)}$. k=1, 2, 3,…(Eq. (5.5)). Then cut the parts after the adjustment. With the updating scheme, the fitted coefficient matrices $\{\mathbf{A}^{(l)}\}$ and $\{\mathbf{B}^{(l)}\}$ in Eq. (5.5) also change with period n (or equivalently, updating iteration). So, it is reasonable to denote them as $\{\mathbf{A}_n{}^{(l)}\}$ and $\{\mathbf{B}_n{}^{(l)}\}$.
- At the end of period n_0+k, measure the parts and take the average of measurement results to estimate $\mathbf{x}^{(n0+k)}$.
- Increase k and repeat the above procedures.

Since SPC is an effective tool to enhance the process robustness, we can develop a SPC strategy for the adjusted process by collecting the information of process output $\mathbf{x}^{(n)}$ and adjustment output $\mathbf{c}^{(n)}$ for each sample product. Then we can do the following:

- Monitor samples of feature deviation $\mathbf{x}$ within one period to determine whether the period length is appropriate for quasi-static error assumption. Shorter period duration might be necessary when quality control chart signals an alarm.
- Monitor the part features $\mathbf{x}^{(n)}$ by multivariate control charts, $\mathbf{c}^{(n)}$ by multivariate EWMA chart and the noise estimation $\hat{\boldsymbol{\varepsilon}}^{(n)}$ for all the samples to identify whether unexpected errors or process change occurs.
- Update the adjustment algorithm when the control chart indicates out-of-control of $\mathbf{x}^{(n)}$, $\mathbf{c}^{(n)}$, or systematic trend of $\hat{\boldsymbol{\varepsilon}}^{(n)}$.

- Within the device accuracy limit, the incremental adjustment $\mathbf{c}^{(n)}$-$\mathbf{c}^{(n-1)}$ should be applied (to compensate for the quasi-static errors) only when cumulative adjustment $\mathbf{c}^{(n)}$ exceeds control limits determined by the tolerance of the base error $\mathbf{u}_1^*$ and meanwhile incremental adjustment $\mathbf{c}^{(n)}$-$\mathbf{c}^{(n-1)}$ exceeds device accuracy limits. Both error tolerance and device accuracy limits define a dead band for the adjustment.

The SPC integrated adjustment based on error equivalence can be shown by Fig. 5.1. To simplify the representation, the figure only shows the adjustment scheme for compensating static errors.

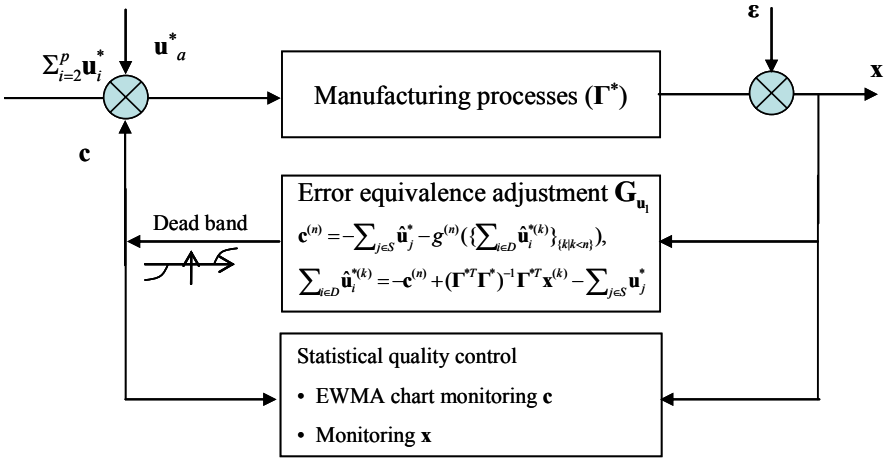

Figure 5.1 Adjustment Based on Error Equivalence

5.3 Simulation of Error Equivalence Process Adjustment

We use the same single stage milling process to implement the process adjustment as in Chapter 2. The process performs cutting on two planes $\mathbf{X}_1$ and $\mathbf{X}_2$ as shown in Fig. 2.9 in Chapter 2. Thickness along the z direction l_z and y direction l_y are the part features to be controlled (the nominal thickness of the finished part is $l_z = 15.24 \pm 0.1$mm and $l_y = 96.5 \pm 0.1$mm).

In this simulation, we use the data (Fig. 5.2(a)) from the experiment. There are 11 thermal sensors mounted on the CNC milling machine to collect data (r=11). The thermal deviation is measured along two directions: the angular deviation α around x axis and translational deformation along z direction of the tool head (see Fig. 5.2(b)). The left panel of Fig. 5.2(a) shows the readings from 11 thermal sensors. The middle and right panels show the measurement of thermal errors. The data are collected in each adjustment period.

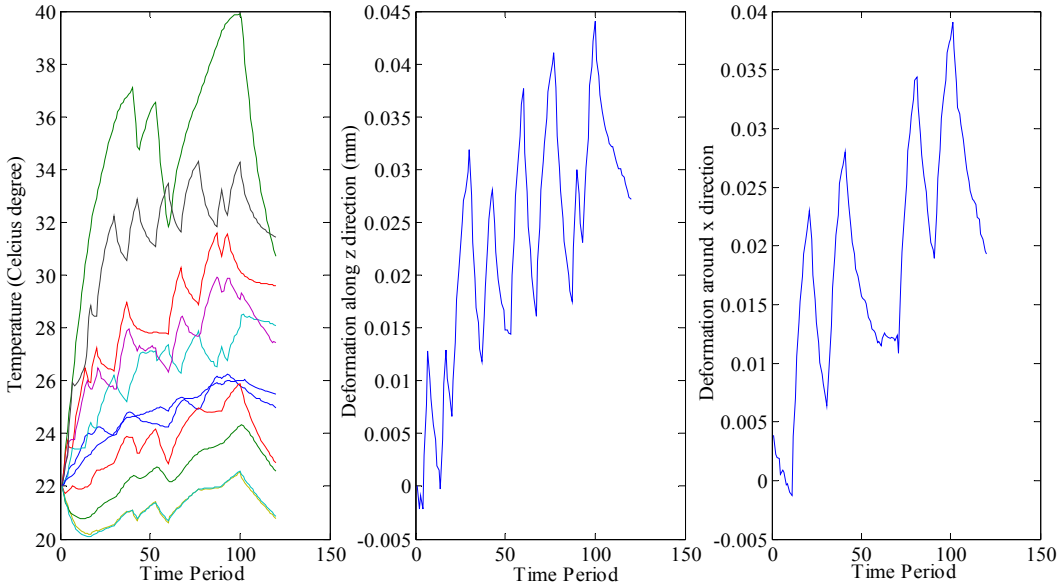

Figure 5.2 (a) Machine Tool Temperature and Error Data

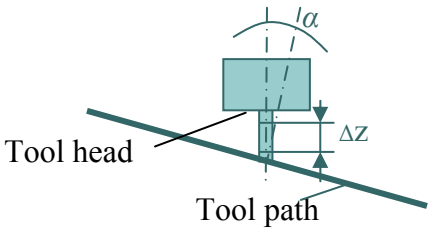

Figure 5.2 (b) Thermal Error Measurements

We have derived $\mathbf{\Gamma}^*$ in Chapter 3 to be:

$$\mathbf{\Gamma} = \begin{pmatrix} 0 & -0.0263 & 0.0263 & 0 & 0 & 0 \\ -0.0158 & 0.0079 & 0.0079 & 0 & 0 & 0 \\ 0 & 0 & 0 & 0 & 0 & 0 \\ 0 & -0.1379 & 0.1379 & 1.3368 & -1.3368 & -1 \\ -0.0828 & 0.0414 & 0.0414 & -1.5 & 0.5 & 0 \\ -1.3033 & -0.8483 & 1.1517 & 0 & 0 & 0 \\ 0 & 0 & 0 & -0.0263 & 0.0263 & 0 \\ 0 & 0 & 0 & 0 & 0 & 0 \\ 0.0158 & -0.0079 & -0.0079 & 0 & 0 & 0 \\ 0 & 0.2632 & -0.2632 & -1.2026 & 1.2026 & -1 \\ 0.158 & -0.079 & -0.079 & -1.5 & 0.5 & 0 \\ 0.2212 & -1.6106 & 0.3894 & 0 & 0 & 0 \end{pmatrix}. \tag{5.8}$$

Suppose the maximum time lag in the model is 5, and N=95, the fitted coefficient matrix **G** is

$$\mathbf{G} = \left(\begin{array}{ccc|c|ccc|cc|c|cc} v_1^{(4)} & \cdots & v_{11}^{(4)} & \cdots & v_1^{(0)} & \cdots & v_{11}^{(0)} & a_1^{(4)} & 0 & \cdots & a_1^{(1)} & 0 \\ w_1^{(4)} & \cdots & w_{11}^{(4)} & \cdots & w_1^{(0)} & \cdots & w_{11}^{(0)} & 0 & a_2^{(4)} & \cdots & 0 & a_2^{(1)} \end{array} \right)^T$$

where $v_i(l)$ and $a_i(l)$ are fitted coefficients. Then coefficient matrices $\widetilde{\mathbf{A}}^{(l)}$ and $\widetilde{\mathbf{B}}^{(l)}$ are

$$\tilde{\mathbf{A}}^{(l)} = \begin{pmatrix} 0 & 0 & 0 & 0 & 0 & 0 \\ 0 & 0 & 0 & 0 & 0 & 0 \\ 0 & 0 & -a_1^{(l)} & 0 & 0 & 0 \\ 0 & 0 & 0 & -a_2^{(l)} & 0 & 0 \\ 0 & 0 & 0 & 0 & 0 & 0 \\ 0 & 0 & 0 & 0 & 0 & 0 \end{pmatrix} \text{ and } \tilde{\mathbf{B}}^{(l)} = \begin{pmatrix} 0 & 0 & 0 & \cdots & 0 \\ 0 & 0 & 0 & \cdots & 0 \\ v_1^{(l)} & v_2^{(l)} & v_3^{(l)} & \cdots & v_{11}^{(l)} \\ w_1^{(l)} & w_2^{(l)} & w_3^{(l)} & \cdots & w_{11}^{(l)} \\ 0 & 0 & 0 & \cdots & 0 \\ 0 & 0 & 0 & \cdots & 0 \end{pmatrix}_{6\times 11}. \tag{5.9}$$

The static kinematic errors, after being transformed to equivalent fixture error, are assumed to be $\sum_{j\in S} \hat{\mathbf{u}}_j^* = [0.4\ 0\ 0.35\ 0\ 0\ 0]^T$ mm. The measurement noise $\boldsymbol{\varepsilon}^{(n)}$ is assumed to follow $N(0, (0.002\text{mm})^2)$ for displacement and $N(0, (0.001\text{rad})^2)$ for orientation. For each adjustment period, 5 parts go through the cutting operation. We use average of 5

measurements to estimate the real feature deviation for each period. Thermal error and temperature for 95 periods (So, n_0=95) are available before the adjustment is applied. The measurements of temperature from i~95+i periods and thermal error from i~94+i are used to estimate the adjustment of locator pins for the (95+i)th period, i=1,2,…,20. The adjustment algorithm is updated after measuring the parts at the (95+i)th period.

The accuracy of the locator movement is assumed to be σ_f=0.003mm and the criterion for stopping the compensation is $-0.01 \le \mathbf{c}^{(n)} - \mathbf{c}^{(n-1)} \le 0.01$mm. The values of adjustments for 6 locators are given by the solid line in the Fig. 5.3. The dash dot line represents the value of $\pm 3\sigma_f$. The adjustments for locators 4, 5, and 6 are zero since the EFEs of errors introduced on these locators are zero in this example.

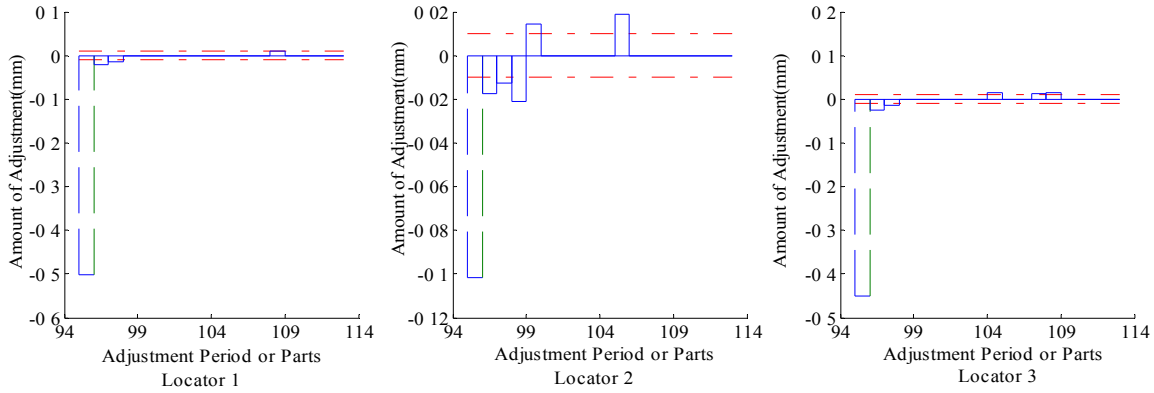

Figure 5.3 EFE Adjustment

The effect of the automatic process adjustment can be evaluated by monitoring the thickness of the part l_y and l_z. The mean of such distance (in each period) is estimated by the average of 4 edge lengths along y and z directions at that period. The variance in each period is estimated by the variance of the 4 edge lengths.

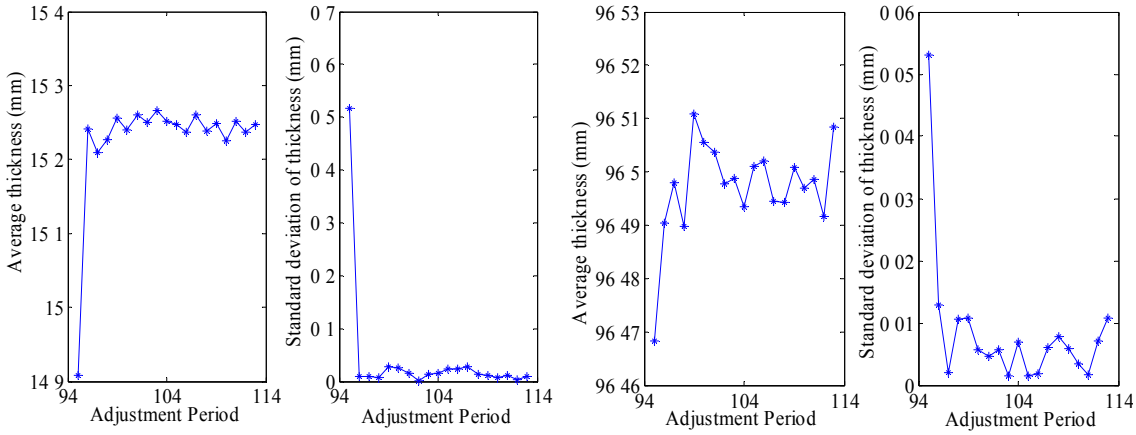

Figure 5.4 Monitoring Thickness and Standard Deviation of Edge Length

Fig. 5.4 shows the mean and standard deviation of the thickness for 20 adjustment periods (periods 95~114). There is no adjustment applied in period 95. We can see that, after the process adjustment, the mean of the thickness is within specification limit ($\pm$ 0.01mm) and variance is greatly reduced. We conclude that the proposed adjustment algorithm can significantly increase the product quality. It should be noticed that the thickness l_y has less mean shift than that l_z. This is because plane $\mathbf{X}_2$ tilts around x axis and the distances between edges l_y are smaller along z direction. Such edge layout leads to edge lengths with less variance and mean shift.

5.4 Adjustment Algorithm Evaluation

Since the adjustment algorithm may have unstable modes, it is necessary to estimate the performance such as stability and sensitivity. The stability of the adjustment algorithm means that an error in the output can be cancelled by an adjustment sequence that converges to zero. One can obtain the stability of the algorithm by inspecting the poles of the transfer function of Eq. (5.5). Sensitivity refers to how the quality could be

affected whenever moderate changes occur in the algorithm parameters. This can be analyzed by differentiating Eq. (5.5) with respect to coefficients in function $g(.)$.

Introducing backward operator q^{-1}, Eq. (5.5) can be represented as

$$\begin{aligned}&[\mathbf{I}+\mathbf{K}_3\textstyle\sum_{l=1}^{p_1}\mathbf{A}_n^{(l)}\mathbf{K}_3^{-1}q^{-l-l}]\mathbf{c}^{(n)}\\&=\mathbf{K}\textstyle\sum_{l=1}^{p_1}\mathbf{A}_n^{(l)}\mathbf{K}^{-1}(\mathbf{\Gamma}^{*T}\mathbf{\Gamma}^{*})^{-1}\mathbf{\Gamma}^{*T}q^{-l}\mathbf{x}^{(n)}-\mathbf{K}_3\textstyle\sum_{l=0}^{p_2}\mathbf{B}_n^{(l)}q^{-l}\mathbf{t}^{(n)}-\mathbf{K}_3\textstyle\sum_{l=1}^{p_1}\mathbf{A}_n^{(l)}\mathbf{K}_3^{-1}\sum_{j\in S}\hat{\mathbf{u}}_j^{*}-\sum_{j\in S}\hat{\mathbf{u}}_j^{*}-\mathbf{K}_0^{(n)}\end{aligned} \tag{5.10}$$

The stability of the algorithm is governed by the entries in 6×6 matrix $[\mathbf{I}+\mathbf{K}_3\sum_{l=1}^{p_1}\mathbf{A}_n^{(l)}\mathbf{K}_3^{-1}q^{-l-1}]^{-1}$. If the roots of denominator of each entry contain the poles inside the unit circle in q plane, the algorithm is stable.

It clear that the adjustment algorithm is always stable if the thermal error model does not contain autoregressive term, i.e., $\mathbf{A}_n^{(l)}=\mathbf{0}$. When autoregressive terms are included in the model, the algorithm may be unstable though the prediction accuracy may increase. The designed algorithm at certain periods may contain unstable poles (poles outside unit circle). This may cause the adjustment exhibit fluctuation and large output if the parameters $\mathbf{A}_n^{(l)}$ and $\mathbf{B}_n^{(l)}$ in the algorithm had been unchanged as n increase. The solution for unstable output can be to use the model without autoregressive term since such algorithm is always stable. Another solution is to introduce the updating scheme which makes the adjustment output capture the latest process information. In this case, Eq. (5.10) is not strictly proper to evaluate the stability for only one adjustment period because model for $\Delta m^{(n-l-1)}$ is different from $\Delta m^{(n-l)}$. In practice, the proposed algorithm can achieve satisfactory results. This has been validated by the results from the simulation study in Section 5.3.

Another important issue is the sensitivity of the algorithm to the modeling errors that can feasibly occur. If there are moderate changes of modeling parameters (entries in matrices $\mathbf{A}_n^{(l)}$) and $\mathbf{B}_n^{(l)}$), we are more interested in how the quality of the product could be affected. Such change may be due to several reasons, including sensor reading errors and change of lubrication condition. To study sensitivity, expand Eq. (5.5) as

$$\begin{aligned} c_j^{(n)} &= -\sum_{l=1}^{p_1}\sum_{i=1}^{3}[a_1^{(l)} + a_2^{(l)} f_{jy}]h_i \Delta m_i^{(n-l)}, \\ &\quad -\sum_{l=0}^{p_2}\sum_{i=1}^{11}[v_i^{(l)} + w_i^{(l)} f_{1y}]t_i^{(n-l)} - u_i - k_{0i}^{(n)}, j = 1,2,3, \\ c_j^{(n)} &= -\sum_{l=1}^{p_1}\sum_{i=1}^{3} a_2^{(l)} f_{jz} h_i \Delta m_i^{(n-l)} - \sum_{l=0}^{p_2}\sum_{i=1}^{11} w_i^{(l)} f_{jz} t_i^{(n-l)} - u_i - k_{0i}^{(n)}, j = 4,5, \\ c_6^{(n)} &= 0, \end{aligned} \tag{5.11}$$

where h_i is the function of fixture coordinates $f_1, \ldots, f_6$. Differentiating both hand sides of Eq. (5.11) leads to

$$\begin{aligned} \Delta c_j^{(n)} &= -\sum_{l=1}^{p_1}\sum_{i=1}^{3} h_i \Delta m_i^{(n-l)} \Delta a_1^{(l)} - \sum_{l=1}^{p_1}\sum_{i=1}^{3} h_i \Delta m_i^{(n-l)} f_{jy} \Delta a_2^{(l)} \\ &\quad -\sum_{l=0}^{p_2}\sum_{i=1}^{11} t_i^{(n-l)} \Delta v_i^{(l)} - \sum_{l=0}^{p_2}\sum_{i=1}^{11} f_{1y} t_i^{(n-l)} \Delta w_i^{(l)}, j = 1,2,3, \\ \Delta c_j^{(n)} &= -\sum_{l=1}^{p_1}\sum_{i=1}^{3} f_{jz} h_i \Delta m_i^{(n-l)} \Delta a_2^{(l)} - \sum_{l=0}^{p_2}\sum_{i=1}^{11} f_{jz} t_i^{(n-l)} \Delta w_i^{(l)}, j = 4,5, \\ \Delta c_6^{(n)} &= 0. \end{aligned} \tag{5.12}$$

$\Delta\mathbf{m}^{(n-l)}$ is only related to the previously fitted model and is not affected by the fitting error of $\mathbf{A}_n^{(l)}$ and $\mathbf{B}_n^{(l)}$. It can be considered as a constant when we conduct the sensitivity analysis. For the example in Section 5.3, substituting the values of coordinates yields

$$\begin{aligned} \Delta c_1^{(n)} &= \sum_{l=1}^{p_1}(25\Delta m_1 + 16.3\Delta m_2 - 22.1\Delta m_3)\Delta a_2 + \sum_{l=1}^{p_1}(1.3\Delta m_1 + 0.8\Delta m_2 - 1.2\Delta m_3)\Delta a_1 \\ &\quad -\sum_{l=0}^{p_2}\sum_{i=1}^{11} t_i \Delta v_i - 19.2\sum_{l=0}^{p_2}\sum_{i=1}^{11} t_i \Delta w_i, \\ \Delta c_j^{(n)} &= \sum_{l=1}^{p_1}(107.5\Delta m_1 + 70\Delta m_2 - 95\Delta m_3)\Delta a_2 + \sum_{l=1}^{p_1}(1.3\Delta m_1 + 0.8\Delta m_2 - 1.2\Delta m_3)\Delta a_1 \\ &\quad -\sum_{l=0}^{p_2}\sum_{i=1}^{11} t_i \Delta v_i - 82.5\sum_{l=0}^{p_2}\sum_{i=1}^{11} t_i \Delta w_i, j = 2,3, \\ \Delta c_j^{(n)} &= \sum_{l=1}^{p_1}(-13.3\Delta m_1 - 8.4\Delta m_2 + 11.5\Delta m_3)\Delta a_2 - 10\sum_{l=0}^{p_2}\sum_{i=1}^{11} t_i \Delta w_i, j = 4,5, \\ \Delta c_6^{(n)} &= 0. \end{aligned} \tag{5.13}$$

To simplify the representation, time indices (n-l) and l are dropped in this equation. We can conclude the following about the adjustment algorithm at time period n,

- There is no adjustment on the locator 6.
- Deviation of coefficients $a_1^{(n-l)}$ and $v_i^{(n-l)}$ does not affect the adjustment $c_4^{(n)}$ and $c_5^{(n)}$; and $a_1^{(n-l)}$ has the same effect on the adjustment of $c_1^{(n)}$, $c_2^{(n)}$, and $c_3^{(n)}$.
- The adjustment for locators 2 and 3 are more likely to be affected by the fitting errors. Locators 4 and 5 are less sensitive to the fitting error. This is because the thermal error occurs is only around z and along x directions. The EFEs on locators 1, 2, and 3 have more impact on the feature deviation than on locators 4 and 5. Locator 6 never affects feature deviation along these two directions.

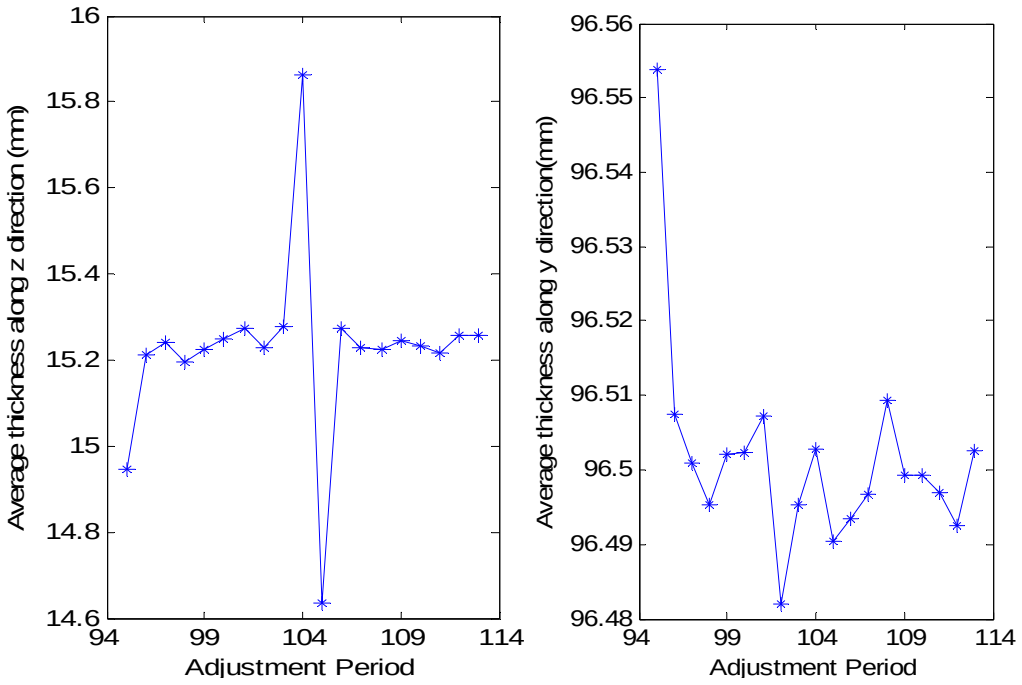

Figure 5.5 Effect of Parameters Change in Process Adjustment Algorithm

The updating scheme can effectively enhance the sensitivity robustness of the adjustment algorithm. We have simulated the feature deviation when there are changes of 50%, 200%, 350% and 500% in the coefficients $v_6^{(0)}$ and $w_6^{(0)}$ in matrix $\mathbf{B}_{105}^{(0)}$. Fig. 5.5 shows an example when there are changes up to 500% in the coefficients. We can notice a large variation of feature l_z at period 104 and 105. Feature l_y is not too much affected. After period 105, the feature l_z falls within the specification limit since the adverse effect of the fitting error has been counteracted by the updated model.

5.5 Summary

APC and its integration with traditional SPC have not been sufficiently addressed in discrete machining processes. Regarding the error compensation, the conventional method in machining processes is to compensate for the multiple errors individually. Based on the dynamic error equivalence model developed in Chapter 4, this chapter derives a novel SPC integrated error-canceling-error APC methodology to compensate for joint impact of errors in the machining process. As an alternative strategy, an APC methodology by using one type of error to compensate for others has been proposed. The method shows an advantage that it compensates for the overall process variation without interrupting production in the machining processes. The applicable condition of this new compensation strategy is also discussed.

This chapter first develops an error equivalence adjustment method based on the engineering process causal model and statistical model of dynamic equivalent errors. It uses prediction from the statistical process error model to compensate for the errors in the future periods. Second, SPC is applied to the adjusted process to identify the unexpected

process errors. When SPC signals an alert, the fitted model is updated to obtain the latest information of the dynamic process. The adjustment algorithm is implemented using the data collected from a milling process. It has been shown that the error equivalence adjustment can effectively improve the machining accuracy and reduce the variation. In addition, a discussion on the applicable condition of compensation strategy shows that the variation of adjustment to the base error must be relatively small compared with that of the base error itself. Finally, the performance of designed adjustment algorithm is analyzed. It has been demonstrated that the proposed updating scheme is effective to tune the parameters and stabilize its output. The sensitivity of adjustment output to the change of model parameters is also studied. It helps to find out the parameters that contribute most to the deviations in the adjustment outputs.

Chapter 6

Conclusions and Future Work

6.1 Conclusions

Process quality improvement usually relies on the modeling of process variations. Models that can reveal the physics of fundamental engineering phenomena could provide better insights into the process and significantly enhance the quality. The work in this dissertation aims to improve the understanding of error equivalence phenomenon, that is, different types of process errors can result in the same feature deviation on parts. The implication of error equivalence mechanism can greatly impact the prediction and quality control in manufacturing processes. The major contributions of this dissertation are summarized as follows

- *Error equivalence modeling*. A rigorous mathematical definition of error equivalence is introduced. An error transformation is proposed to establish the mathematical formulation of error equivalence phenomenon. By the kinematic analysis, equivalent errors are transformed into one base error. In machining processes, the base error is chosen to be fixture deviation and other types of errors, including datum and machine tool errors, are transformed to the fixture error. A process causal model is derived to depict how the base errors affect the features of parts. The error equivalence is investigated for both static and dynamic process errors. The model serves as the base for quality prediction and control.

- *Sequential root cause diagnosis strategy*. Due to the error equivalence mechanism, errors may cancel each other on the part features and may conceal the process information for process diagnosis. The proposed sequential diagnostic methodology based on error equivalence overcomes the difficulty by conducting diagnosability analysis, identifying the existence of process variations, and distinguishing the multiple error sources.
- *Error-canceling-error compensation strategy integrated with SPC*. The error cancellation is further explored and a novel error-canceling-error APC strategy is proposed, i.e., treating all error sources as one system and using the base error to automatically compensate or adjust the others for process variation reduction. An error equivalence adjustment algorithm is designed to compensate both time invariant and dynamic errors. By monitoring outputs from the manufacturing process as well as adjustment algorithm, SPC could enhance the robustness of the controlled process.

In this dissertation, the studies and analyses are based on a machining process. However, error equivalence methodology for process control is generic and can be easily extended to other discrete manufacturing processes.

6.2 Future Work

This study aims to establish error equivalence theory and obtain insights into this fundamental phenomenon for improved process variation control. In addition to the results obtained in the modeling, diagnosis and error compensation, we can further expand the impact of error equivalence on the life cycle of product design and manufacturing. The error equivalence can facilitate tolerance synthesis and optimal tolerance allocation in a complex manufacturing process. For example, process tolerance can be allocated only to the total amount of equivalent error at the initial design stage. This would lead to reducing the dimension of design space. Then the tolerance would be further distributed for individual error sources at late stages of process design when more process information becomes available.

Furthermore, since error equivalence phenomenon widely exists in different types of manufacturing processes, it could be expected to develop error equivalence based quality control strategy for certain advanced manufacturing processes such as micromachining.

References

Agapiou, J.S., Steinhilper, E., Gu, F., and Bandyopadhyay, P., 2003, "A Predictive Modeling Methodology for Part Quality from Machining Lines," *NAMRI/SME Transactions*, XXXI, pp. 629-636.

Agapiou, J.S., Steinhilper, E., Bandyopadhyay, P., and Xie, J., 2005, "A Predictive Modeling Methodology for Part Quality from Machining Lines," *2005 ASME Mechanical Engineering Congress and Exposition, IMECE2005-79352.*

Altintas, Y. and Lee, P., 1998, "Mechanics and Dynamics of Ball End Milling," *ASME Transactions, Journal of Manufacturing Science and Engineering*, 120, pp. 684-692.

Anjanappa, M., Anand, D.K., Kirk, J.A., and Shyam, S., 1988, "Error correction methodologies and control strategies for numerical machines," *Control Methods for Manufacturing Process*, 7, pp. 41-49.

Apley, D. and Shi, J., 1998, "Diagnosis of Multiple Fixture Faults in Panel Assembly," *ASME Transactions, Journal of Manufacturing Science and Engineering*, 120, pp. 793-801.

Apley, D. and Shi, J., 2001, "A Factor-Analysis Method for Diagnosing Variability in Multivariate Manufacturing Processes", *Technometrics*, 43, pp. 84-95.

Asada, H. and By, A.B., 1985, "Kinematic Analysis of Workpart Fixturing for Flexible Assembly with Automatically Reconfigurable Fixtures," *IEEE Transactions on Robotics and Automation*, RA-1, pp. 86-94.

Åström, K.J., 1970, *Introduction to Stochastic Control Theory*, Academic Press, NY.

Åström, K.J., 1988, *Automatic Tuning of PID Controllers*, Instrument Society of America, Research Triangle Park, NC.

Åström, K.J. and Wittenmark, B., 1990, *Computer Controlled Systems: Theory and Design*, 2nd edn., Prentice Hall, Englewood Cliffs, NJ.

Box, G.E.P., 1957, "Evolutionary Operation: A Method for Increasing Industrial Productivity," *Applied Statistics*, 6, pp. 81-101.

Box, G.E.P. and Jenkins, G.M., 1963, "Further Contributions to Adaptive Quality Control: Simultaneous Estimation of Dynamics: Non-zero Costs," *Bulletin of the International Statistics Institute*, *34th Session*, *Ottawa*, pp. 943-974.

Box, G.E.P. and Jenkins, G.M., 1970, *Time Series Analysis Forecasting and Control*, Holden-Day, Oakland, CA.

Box, G.E.P. and Kramer, T., 1992, "Statistical Process Monitoring and Feedback Adjustment- A Discussion," *Technometrics*, 34, pp. 251-285.

Box, G.E.P. and Draper, N.R., 1969, *Evolutionary operation: A statistical method for process improvement*, John Wiley & Sons, NY.

Bryan, J.B., 1990, "International Status of Thermal Error Research," *Annals of the CIRP*, 39, pp. 645-656.

Butler, S.W. and Stefani, J.A., 1994, "Supervisory Run-to-Run Control of Polysilicon Gate Etch Using in Situ Ellipsometry," *IEEE Transactions on Semiconductor Manufacturing*, 7, pp. 193-201.

Cai, W., Hu, S., and Yuan, J., 1997, "Variational Method of Robust Fixture Configuration Design for 3-D Workpiece," *ASME Transactions, Journal of Manufacturing Science and Engineering*, 119, pp. 593-602.

Camelio, J. and Hu, S., 2004, "Multiple Fault Diagnosis for Sheet Metal Fixtures Using Designated Component Analysis," *Transactions of the ASME, Journal of Manufacturing Science and Engineering*, 126, pp. 91-97.

Camelio, J., Hu, S. and Ceglarek, D., 2003, "Modeling Variation Propagation of Multi-Station Assembly Systems with Compliant Parts," *Transactions of the ASME, Journal of Mechanical Design*, 125, pp. 673-681.

Capilla, C., Ferrer, A., and Romero, R., 1999, "Integration of Statistical and Engineering Process Control in a Continuous Polymerization Process," *Technometrics*, 41, pp. 14-28.

Carlson, J. S. and Söderberg, R., 2003, "Assembly Root Cause Analysis: A Way to Reduce Dimensional Variation in Assembled Products," *International Journal of Flexible Manufacturing Systems*, 15, pp. 113-150.

Ceglarek, D. and Shi, J., 1996, "Fixture Failure Diagnosis for Auto Body Assembly Using Pattern Recognition," *ASME Transactions, Journal of Engineering for Industry*, 118, pp. 55-65.

Ceglarek, D., Shi, J., and Wu, S.M., 1994, "A Knowledge-Based Diagnostic Approach for the Launch of the Auto-Body Assembly Process," *ASME Transactions, Journal of Engineering for Industry*, 116, pp. 491-499.

Chang, M., and Gossard, D.C., 1998, "Computational Method for Diagnosis of Variation-Related Assembly Problem," *International Journal of Production Research*, 36, pp. 2985-2995.

Chen, J.S., Yuan, J.X., Ni, J., and Wu, S.M., 1993, "Real-Time Compensation for Time-Variant Volumetric Errors on a Machining Center," *ASME Transactions, Journal of Engineering for Industry*, 115, pp. 472-479.

Chou, Y-C., Chandru, V., and Barash, M., 1989, "A Mathematical Approach to Automatic Configuration of Machining Fixtures: Analysis and Synthesis," *ASME Transactions, Journal of Engineering for Industry*, 111, pp. 299-306.

Choudhuri, S.A. and De Meter, E.C., 1999, "Tolerance Analysis of Machining Fixture Locators," *ASME Transactions, Journal of Manufacturing Science and Engineering*, 121, pp. 273-281.

Del Castillo, E., 1996, "A Multivariate Self-Tuning Controller for Run-to-Run Process Control under Shift and Trend Disturbances," *IIE Transactions*, 28, pp. 22-28.

Del Castillo, E. and Hurwitz, A., 1997, "Run-to-Run Process Control: Literature Review and Extensions," *Journal of Quality Technology*, 29, pp. 184-196.

Ding, Y., Ceglarek, D., and Shi, J., 2002, "Fault Diagnosis of Multistage Manufacturing Processes by Using State Space Approach", *ASME Transactions, Journal of Manufacturing Science and Engineering*, 124, pp. 313-322.

Ding, Y., Jin, J., Ceglarek, D., and Shi, J., 2005, "Process-Oriented Tolerancing for Multi-Station Assembly Systems", *IIE Transactions*, 37, pp. 493-508.

Ding, Y., Shi, J., and Ceglarek, D., 2002, "Diagnosability Analysis of Multistage Manufacturing Processes", *ASME Transactions, Journal of Dynamics Systems, Measurement, and Control*, 124, pp. 1-13.

Djurdjanovic, D. and Ni, J., 2001, "Linear State Space Modeling of Dimensional Machining Errors," *NAMRI/SME*, XXIX, pp. 541-548.

Donmez, M.A., Blomquist, D.S., Hocken, R.J., Liu, C.R., and Barash, M.M., 1986, "A General Methodology for Machine Tool Accuracy Enhancement by Error Compensation," *Precision Engineering*, 8, pp. 187-196.

Ehmann, K.F., Kapoor, S.G., DeVor, R.E., and Lazogluo, 1991, "Machining Process Modeling: A Review," *ASME Transactions, Journal of Manufacturing Science and Engineering*, 119, pp. 655-663.

English, J.R. and Case, K.E., 1990, "Control Charts Applied as Filtering Devices within a Feedback Loop," *IIE Transactions*, 26, pp. 255-269.

Ferreira, P.M. and Liu, C.R., 1986, "A Contribution to the Analysis and Compensation of the Geometric Error of a Machining Center," *Annals of the CIRP*, 35, pp. 259-262.

Frey, D.D., Otto, K.N., and Pflager, W., 1997, "Swept Envelopes of Cutting Tools in Integrated Machine and Workpiece Error Budgeting," *Annals of the CIRP*, 46, pp. 475-480.

Harris, T.J. and Ross, W.H., 1991, "Statistical Process Control Procedures for Correlated Observations," *Canadian Journal of Chemical Engineering*, 69, pp. 48-57.

Hu, S.J., 1997, "Stream of Variation Theory for Automotive Body Assembly", *Annals of the CIRP*, 46/1, pp. 1-6.

Hu, S.J. and Wu, S.M., 1992, "Identifying Root Cause of Variation in Automobile Body Assembly Using Principal Component Analysis," *Transactions of NAMRI*, XX, pp. 311-316.

Huang, Q. and Shi, J., 2004, "Stream of Variation Modeling of Serial-Parallel Multistage Manufacturing Systems With Coupled Process Routes," *ASME Transactions*, *Journal of Manufacturing Science and Engineering*, 126, pp. 611-618.

Huang, Q. and Shi, J., 2004, "Variation Transmission Analysis and Diagnosis of Multi-Operational Machining Processes," *IIE Transactions on Quality and Reliability,* 36, pp. 807-815.

Huang, Q., Shi, J., and Yuan, J., 2003, "Part Dimensional Error and Its Propagation Modeling in Multi-Operational Machining Process," *ASME Transactions, Journal of Manufacturing Science and Engineering*, 125, pp. 255-262.

Huang, Q., Zhou, S., and Shi, J., 2002, "Diagnosis of Multi-Operational Machining Processes through Process Analysis," *Robotics and Computer-Integrated Manufacturing*, 18, pp. 233-239.

Huang, Y. and Liang, S.Y., 2005, "Modeling of Cutting Forces under Hard Turning Conditions Considering Tool Wear Effect," *ASME Transactions, Journal of Manufacturing Science and Engineering*, 127, pp. 262-270.

Jin, J. and Shi, J., 1999, "State Space Modeling of Sheet Metal Assembly for Dimensional Control", *ASME Transactions, Journal of Manufacturing Science and Engineering*, 121, pp. 756-762.

Kapoor, S.G., DeVor, R.E., Zhu, R., Gajjela, R., Parakkal, G., and Smithey, D., 1998, "Development of Mechanistic Models for the Prediction of Machining Performance: Model-Building Methodology," *Journal of Machining Science and Technology*, 2, pp. 215-238.

Kline, W.A., Devor, R.E., and Shareef, I., 1982, "Prediction of Surface Accuracy in End Milling," *ASME Transactions, Journal of Engineering for Industry*, 104, pp. 272-278.

Kurtoglu, A., 1990, "The Accuracy Improvement of Machine Tools," *Annals of CIRP*, 39, pp. 417-419.

Lawless, J.F., Mackay, R.J., and Robinson, J.A., 1999, "Analysis of Variation Transmission in Manufacturing Process-Part I," *Journal of Quality Technology*, 31, pp. 131-142.

Li, H. and Shin, Y.C., 2006, "A Comprehensive Dynamic End Milling Simulation Model," *ASME Transactions, Journal of Manufacturing Science and Engineering*, 128, pp. 86-95.

Li, Z. and Zhou, S., 2006, "Robust Method of Multiple Variation Sources Identification in Manufacturing Processes for Quality Improvement," *ASME Transactions, Journal of Manufacturing Science and Engineering*, 128, pp. 326-336.

Liu, X., Soshi, M., Sahasrabudhe, A., Yamazaki, K., and Mori, M., 2006, "A Geometrical Simulation System of Ball End Finish Milling Process and Its Application for the Prediction of Surface Micro Features," *ASME Transactions, Journal of Manufacturing Science and Engineering*, 128, pp. 74-85.

MacGregor, J.F., 1988, "Online-line Statistical Process Control," *Chemical Engineering Process*, 10, pp. 21-31.

MacGregor, J.F., 1991, "Discussion of Some Statistical Process Control Methods for Autocorrelated Data by D.C. Montgomery and C.M. Mastrangelo," *Journal of Quality Technology*, 23, pp. 198-199.

MacGregor, J.F. and Harris, T.J., 1990, "Discussion of Exponentially Weighted Moving Average Control Schemes: Properties and Enhancements," *Technometrics*, 32, pp. 1-29.

Mann, B.P, Young, K.A., Schmitz, T.L., and Dilley, D.N., 2005, "Simultaneous Stability and Surface Location Error Predictions in Milling," *ASME Transactions, Journal of Manufacturing Science and Engineering*, 127, pp. 446-453.

Mantripragada, R. and Whitney, D.E., 1999, "Modeling and Controlling Variation Propagation in Mechanical Assemblies Using State Transition Models," *IEEE Transaction on Robotics and Automation*, 15, pp. 124-140.

Marin, R.A. and Ferreira, P., 2001, "Kinematic Analysis and Synthesis of Deterministic 3-2-1 Locator Schemes for Machining Fixtures," *ASME Transactions, Journal of Manufacturing Science and Engineering*, 123, pp. 708-719.

Marin, R. and Ferreira, P., 2003, "Analysis of Influence of Fixture Locator Errors on the Compliance of the Work Part Features to Geometric Tolerance Specification," *ASME Transactions, Journal of Manufacturing Science and Engineering*, 125, pp. 609-616.

Martinsen, K., 1993, "Vectorial Tolerancing for All Types of Surfaces," *ASME Advances in Design Automation*, 2, pp. 187-198.

Messina, W.S., Montgomery, D.C., Keats, J.B., and Runger, G.C., 1996, "Strategies for Statistical Monitoring of Integral Control for the Continuous Process Industries," *Statistical Applications in Process Control*, pp. 193-215.

Moriwaki, T. and Shamoto, E., "Analysis of Thermal Deformation of an Ultraprecision Air Spindle System," *Annals of CIRP*, 37, pp. 315-319.

Mozumder, P.K., Saxena, S., and Collins, D.J., 1994, "A Monitor Wafer Based Controller for Semiconductor Processes," *IEEE Transactions on Semiconductor Manufacturing*, 7, pp. 400-410.

Rong, Q., Ceglarek, D., and Shi, J., 2000, "Dimensional Fault Diagnosis for Compliant Beam Structure Assemblies," *ASME Transactions, Journal of Manufacturing Science and Engineering*, 122, pp. 773-780.

Rong, Y. and Bai, Y., 1996, "Machining Accuracy Analysis for Computer-aided Fixture Design Verification," *ASME Transactions, Journal of Manufacturing Science and Engineering*, 118, pp. 289-299.

Sachs, E., Hu, A., and Ingolfsson, A., 1995, "Run-by-Run Process Control: Combining SPC and Feedback Control," *IEEE Transactions on Semiconductor Manufacturing*, 8, pp. 26-43.

Schultschik, R., 1977, "The Components of the Volumetric Accuracy," *Annals of CIRP*, 26, pp. 223-228.

Shawki, G.S.A. and Abdel-Aal, M.M., 1965, "Effect of Fixture Rigidity of and Wear on Dimensional Accuracy," *International Journal of Machine Tool Design and Research*, 5, pp. 183-202.

Smith, S. and Tlusty, J., 1991, "An Overview of Modeling and Simulation of the Milling Process," *ASME Transactions, Journal of Engineering for Industry*, 113, pp. 169-175.

Soons, J. A., Theuws, F.C., and Schellekens, P.H., 1992, "Modeling the Errors of Multi-Axis Machines: a General Methodology," *Precision Engineering*, 14, pp. 5-19.

Sutherland, J.W. and DeVor, R.E., 1986, "An Improved Method for Cutting Force and Surface Error Prediction in Flexible End Milling Systems," *ASME Transactions, Journal of Engineering for Industry*, 108, pp. 269-279.

Tsung, F., 2000, "Statistical Monitoring and Diagnosis of Automatic Controlled Processes Using Dynamic PCA", *International Journal of Production Research*, 38, pp. 625-637.

Tsung, F. and Shi, J., 1999, "Integrated Design of Run-to-Run PID Controller and SPC Monitoring for Process Disturbance Rejection," *IIE Transactions*, 31, pp. 517-527.

Tsung, F., Shi, J., and Wu, C.F.J., 1999, "Joint Monitoring of PID-Controlled Processes," *Journal of Quality Technology*, 31, pp. 275-285.

Tucker, W.T., Faltin, F.W., and Vander Wiel, S.A., 1993, "Algorithmic Statistical Process Control: An Elaboration," *Technometrics*, 35, pp. 363-375.

Vander Wiel, S.A., Tucker, W.T., Faltin, F.W., and Doganaksoy, N., 1992, "Algorithmic Statistical Process Control: Concepts and Application," *Technometrics*, 34, pp. 286-297.

Venugopal, R. and Barash, M, 1986, "Thermal Effects on the Accuracy of Numerically Controlled Machine Tools," *Annals of CIRP*, 35, pp. 255-258.

Wang, H., Huang, Q., and Katz, R., 2005, "Multi-Operational Machining Processes Modeling for Sequential Root Cause Identification and Measurement Reduction," *ASME Transactions, Journal of Manufacturing Science and Engineering*, 127, pp. 512-521.

Wang, H. and Huang, Q., 2006, "Error Cancellation Modeling and Its Application in Machining Process Control," *IIE Transactions on Quality and Reliability,* 38, pp. 379-388.

Wang, H. and Huang, Q., 2007, "Using Error Equivalence Concept to Automatically Adjust Discrete Manufacturing Processes for Dimensional Variation Reduction," *ASME Transactions, Journal of Manufacturing Science and Engineering*, 129, pp. 644-652.

Wang, M.Y., 2000, "Automated Fixture Layout Design for 3D Workpieces," *IEEE Transactions on Robotics and Automation*, 16, pp. 839-846.

Wang, Y. and Nagarkar, S.R., 1999, "Locator and Sensor Placement for Automated Coordinate Checking Fixtures," *ASME Transactions, Journal of Manufacturing Science and Engineering*, 121, pp. 709-719.

Weill, R., Darel, I., and Laloum, M., 1991, "The Influence of Fixture Positioning Errors on the Geometric Accuracy of Mechanical Parts," *Proceedings of CIRP Conference on PE & ME*, pp. 215-225.

Wu, D.W. and Liu, C.R., 1985, "An Analytical Model of Cutting Dynamics, Part 1: Model Building," *ASME Transactions, Journal of Engineering for Industry*, 107, pp. 107-111.

Yang, H. and Ni, J., 2003, "Dynamic Modeling for Machine Tool Thermal Error Compensation, ASME Transactions," *ASME Transactions, Journal of Manufacturing Science and Engineering*, 125, pp. 245-254.

Zhou, S., Ding, Y., Chen, Y., and Shi, J., 2003, "Diagnosability Study of Multistage Manufacturing Processes Based on Linear Mixed-Effects Models," *Technometrics*, 45, pp. 312-325.

Zhou, S., Huang, Q., and Shi, J., 2003, "State Space Modeling for Dimensional Monitoring of Multistage Machining Process Using Differential Motion Vector," *IEEE Transactions on Robotics and Automation*, 19, pp. 296-309.

Appendices

Appendix A: Infinitesimal Analysis of Workpiece Deviation Due to Fixture Errors

If there are small deviations on these 6 locators as $(f_{1z}\ \ f_{2z}\ \ f_{3z}\ \ f_{4y}\ \ f_{5y}\ \ f_{6x})^T$, the change of orientation and position of rigid workpiece in the 3-D space can be analyzed by (Cai, *et al.*, 1997).

$$\delta \mathbf{q}_f = \text{-}\mathbf{J}^{-1}\mathbf{\Phi}\mathbf{E}\Delta\mathbf{f}\ , \tag{A.1}$$

where for prismatic workpiece, Jacobian Matrix **J** is

$$\mathbf{J}=\begin{pmatrix} \neg\nu_{Ix} & \neg\nu_{Iy} & \neg\nu_{Iz} & -2(-f_{1z}\nu_{Iy}+f_{1y}\nu_{Iz}) & -2(f_{1z}\nu_{Ix}-f_{1x}\nu_{Iz}) & -2(-f_{1y}\nu_{Ix}+f_{1x}\nu_{Iy}) \\ \neg\nu_{Ix} & \neg\nu_{Iy} & \neg\nu_{Iz} & -2(-f_{2z}\nu_{Iy}+f_{2y}\nu_{Iz}) & -2(f_{2z}\nu_{Ix}-f_{2x}\nu_{Iz}) & -2(-f_{2y}\nu_{Ix}+f_{2x}\nu_{Iy}) \\ \neg\nu_{Ix} & \neg\nu_{Iy} & \neg\nu_{Iz} & -2(-f_{3z}\nu_{Iy}+f_{3y}\nu_{Iz}) & -2(f_{3z}\nu_{Ix}-f_{3x}\nu_{Iz}) & -2(-f_{3y}\nu_{Ix}+f_{3x}\nu_{Iy}) \\ \neg\nu_{IIx} & \neg\nu_{IIy} & \neg\nu_{IIz} & -2(-f_{4z}\nu_{IIy}+f_{4y}\nu_{IIz}) & -2(f_{4z}\nu_{IIx}-f_{4x}\nu_{IIz}) & -2(-f_{4y}\nu_{IIx}+f_{4x}\nu_{IIy}) \\ \neg\nu_{IIx} & \neg\nu_{IIy} & \neg\nu_{IIz} & -2(-f_{5z}\nu_{IIy}+f_{5y}\nu_{IIz}) & -2(f_{5z}\nu_{IIx}-f_{5x}\nu_{IIz}) & -2(-f_{5y}\nu_{IIx}+f_{5x}\nu_{IIy}) \\ \neg\nu_{IIIx} & \neg\nu_{IIIy} & \neg\nu_{IIIz} & -2(-f_{6z}\nu_{IIIy}+f_{6y}\nu_{IIIz}) & -2(f_{6z}\nu_{IIIx}-f_{6x}\nu_{IIIz}) & -2(-f_{6y}\nu_{IIIx}+f_{6x}\nu_{IIIy}) \end{pmatrix}, \tag{A.2}$$

where $\mathbf{v}_j=(v_{jx}\ \ v_{jy}\ \ v_{jz})^{\mathrm{T}}$ is the orientation vector of datum surface j and the index k is dropped in the equations in Appendix A. The Jacobian matrix **J** is definitely full rank because the workpiece is deterministically located. The inverse of Jacobian therefore exists. Matrix **Φ** is

$$\boldsymbol{\phi}=\begin{pmatrix} \nu_{Ix} & \nu_{Iy} & \nu_{Iz} & 0 & 0 & 0 & 0 & 0 & 0 & 0 & 0 & 0 & 0 & 0 & 0 & 0 & 0 & 0 \\ 0 & 0 & 0 & \nu_{Ix} & \nu_{Iy} & \nu_{Iz} & 0 & 0 & 0 & 0 & 0 & 0 & 0 & 0 & 0 & 0 & 0 & 0 \\ 0 & 0 & 0 & 0 & 0 & 0 & \nu_{Ix} & \nu_{Iy} & \nu_{Iz} & 0 & 0 & 0 & 0 & 0 & 0 & 0 & 0 & 0 \\ 0 & 0 & 0 & 0 & 0 & 0 & 0 & 0 & 0 & \nu_{IIx} & \nu_{IIy} & \nu_{IIz} & 0 & 0 & 0 & 0 & 0 & 0 \\ 0 & 0 & 0 & 0 & 0 & 0 & 0 & 0 & 0 & 0 & 0 & 0 & \nu_{IIx} & \nu_{IIy} & \nu_{IIz} & 0 & 0 & 0 \\ 0 & 0 & 0 & 0 & 0 & 0 & 0 & 0 & 0 & 0 & 0 & 0 & 0 & 0 & 0 & \nu_{IIIx} & \nu_{IIIy} & \nu_{IIIz} \end{pmatrix}. \tag{A.3}$$

When it is clear in the text, index k is dropped in the above equation. **E** is an 18× 6 matrix, that is, $\begin{pmatrix} \mathbf{E}_1 & \mathbf{0} & \mathbf{0} & \mathbf{0} & \mathbf{0} & \mathbf{0} \\ \mathbf{0} & \mathbf{E}_1 & \mathbf{0} & \mathbf{0} & \mathbf{0} & \mathbf{0} \\ \mathbf{0} & \mathbf{0} & \mathbf{E}_1 & \mathbf{0} & \mathbf{0} & \mathbf{0} \\ \mathbf{0} & \mathbf{0} & \mathbf{0} & \mathbf{E}_2 & \mathbf{0} & \mathbf{0} \\ \mathbf{0} & \mathbf{0} & \mathbf{0} & \mathbf{0} & \mathbf{E}_2 & \mathbf{0} \\ \mathbf{0} & \mathbf{0} & \mathbf{0} & \mathbf{0} & \mathbf{0} & \mathbf{E}_3 \end{pmatrix}_{18\times 6}$, where $\mathbf{E}_1=(0\ \ 0\ \ 1)^T$, $\mathbf{E}_2=(0\ \ 1\ 0)^T$, and $\mathbf{E}_3=(1\ \ 0\ \ 0)^T$.

Appendix B: Proof for Proposition in Chapter 2

Proof. If the variables u_1, u_2, ..., u_m can be grouped to Eq. (2.25), we can expand Eqs. (2.24) and (2.25) and make them equal. Then we get $k_j p_i = g_{ij}$. Substituting it into $\mathbf{\Gamma}$ yields

$$\mathbf{\Gamma}=\begin{pmatrix} k_1 p_1 & k_2 p_1 & \dots & k_m p_1 \\ k_1 p_2 & k_2 p_2 & \dots & k_m p_2 \\ \dots & & & \\ k_1 p_n & k_2 p_n & \dots & k_m p_n \end{pmatrix}$$

whose rank is not larger than 1. On the other hand, if rank($\mathbf{H}$) is less than 1, there exists at most one row that is linearly independent. The conclusion is obvious.

Appendix C: Proof for Corollary in Chapter 2

Proof. This can be proved by substituting Eq. (2.4) into the expression $\left(\mathbf{X}_j^T \quad 1\right)^T = {}^F\mathbf{H}_P^{-1}\mathbf{H}_d^{-1}\mathbf{H}_f^{-1\,F}\mathbf{H}_M\mathbf{H}_m{}^F\mathbf{H}_M^{-1\,F}\mathbf{H}_P\left(\mathbf{X}_j^{0T} \quad 1\right)^T$ and conducting a lengthy computation. It can be found that equalities among the coefficient matrices are determined by the symmetry of matrix $\mathbf{H}_d^{-1}\mathbf{H}_f^{-1\,F}\mathbf{H}_M\mathbf{H}_m^{-1\,F}\mathbf{H}_M^{-1}$. Since $\mathbf{H}_d$, $\mathbf{H}_f$, and $\mathbf{H}_m$ are skew-symmetric, $\mathbf{H}_d^{-1}\mathbf{H}_f^{-1\,F}\mathbf{H}_M\mathbf{H}_m^{-1\,F}\mathbf{H}_M^{-1}$ is also skew-symmetric if ${}^F\mathbf{H}_M=\mathbf{I}_{8\times 8}$. Non-identity matrix ${}^F\mathbf{H}_M$ can affect the symmetry of $\mathbf{H}_d^{-1}\mathbf{H}_f^{-1\,F}\mathbf{H}_M\mathbf{H}_m^{-1\,F}\mathbf{H}_M^{-1}$, which yields different coefficient matrices for $\Delta\mathbf{d}$, $\Delta\mathbf{f}$, and $\Delta\mathbf{m}$. Therefore, the MCS and the FCS must coincide with each other for the proposed grouping method.

Appendix D: Determine Difference Order for D(q)

Table A.1 First Order Difference

		Sensor 1	Sensor 2	Sensor 3	Sensor 4	Sensor 5	Sensor 6
Mean	Segment 1	0.046	0.257	0.111	0.107	0.089	-0.003
	Segment 2	0.042	0.078	0.072	0.004	0.053	0.018
Variance	Segment 1	0.007	0.126	0.080	0.035	0.045	0.007
	Segment 2	0.007	0.137	0.056	0.030	0.038	0.006

Table A.1 First Order Difference (Continued)

		Sensor 7	Sensor 8	Sensor 9	Sensor 10	Sensor 11	Thermal Error
Mean	Segment 1	0.194	0.059	0.030	0.039	0.000	0.481
	Segment 2	0.049	0.025	0.027	0.023	0.019	0.378
Variance	Segment 1	0.140	0.001	0.003	0.009	0.005	9.053
	Segment 2	0.106	0.001	0.003	0.015	0.004	9.191

Table A.2 Second Order Difference

		Sensor 1	Sensor 2	Sensor 3	Sensor 4	Sensor 5	Sensor 6
Mean	Segment 1	-0.0041	-0.0093	0.0003	-0.0079	-0.0025	0.0069
	Segment 2	-0.0003	-0.0003	-0.0054	0.0042	-0.008	-0.0013
Variance	Segment 1	0.0019	0.04	0.0764	0.043	0.0306	0.005
	Segment 2	0.0031	0.0353	0.0425	0.0331	0.0161	0.0051

Table A.2 Second Order Difference (Continued)

		Sensor 7	Sensor 8	Sensor 9	Sensor 10	Sensor 11	Thermal Error
Mean	Segment 1	-0.0317	0.0002	0.0024	0.0019	0.0066	-0.1921
	Segment 2	0.0107	-0.0008	-0.0007	-0.0018	-0.001	0.0716
Variance	Segment 1	0.1275	0.0006	0.0003	0.0056	0.0018	7.6983
	Segment 2	0.0763	0.001	0.0004	0.0045	0.0018	5.9466

Appendix E: Screened Variables

Table A.3 Screened Variables With Autoregressive Terms

No.	Predictor	B	VIP		No.	Predictor	B	VIP
1	$(1-q^{-1})s_1^{(t-4)}$	-0.01305	0.86065		16	$(1-q^{-1})s_8^{(t-1)}$	-0.09953	1.16198
2	$(1-q^{-1})s_4^{(t-4)}$	-0.03241	0.81609		17	$(1-q^{-1})s_{10}^{(t-1)}$	0.02845	0.92829
3	$(1-q^{-1})s_5^{(t-4)}$	-0.00634	0.83828		18	$(1-q^{-1})s_1^{(t)}$	0.08247	1.59173
4	$(1-q^{-1})s_8^{(t-4)}$	0.09179	0.86482		19	$(1-q^{-1})s_2^{(t)}$	-0.02080	0.83598
5	$(1-q^{-1})s_{10}^{(t-4)}$	-0.02364	0.80570		20	$(1-q^{-1})s_3^{(t)}$	-0.06807	2.47004
6	$(1-q^{-1})s_3^{(t-3)}$	-0.34848	0.80145		21	$(1-q^{-1})s_4^{(t)}$	0.05154	2.25059
7	$(1-q^{-1})s_3^{(t-2)}$	0.07769	0.95171		22	$(1-q^{-1})s_5^{(t)}$	-0.13403	1.91569
8	$(1-q^{-1})s_4^{(t-2)}$	-0.27098	0.90617		23	$(1-q^{-1})s_6^{(t)}$	-0.10494	1.22256
9	$(1-q^{-1})s_7^{(t-2)}$	0.56576	1.18210		24	$(1-q^{-1})s_7^{(t)}$	0.74162	2.85025
10	$(1-q^{-1})s_1^{(t-1)}$	-0.07559	0.87789		25	$(1-q^{-1})s_8^{(t)}$	-0.09977	1.86957
11	$(1-q^{-1})s_3^{(t-1)}$	-0.37920	1.63392		26	$(1-q^{-1})s_{10}^{(t)}$	0.05774	1.22009
12	$(1-q^{-1})s_4^{(t-1)}$	-0.21441	1.51635		27	$(1-q^{-1})s_{11}^{(t)}$	-0.05022	1.06204
13	$(1-q^{-1})s_5^{(t-1)}$	-0.04998	1.05582		28	$(1-q^{-1})\delta^{(t-2)}$	-0.20495	1.07594
14	$(1-q^{-1})s_6^{(t-1)}$	-0.49069	0.93271		29	$(1-q^{-1})\delta^{(t-1)}$	-0.66046	1.80827
15	$(1-q^{-1})s_7^{(t-1)}$	0.38506	1.79123					

Table A.4 Screened Variables Without Autoregressive Terms

No.	Predictor	B	VIP		No.	Predictor	B	VIP
1	$(1-q^{-1})s_1^{(t-4)}$	0.07546	0.87825		13	$(1-q^{-1})s_8^{(t-1)}$	0.01998	1.16039
2	$(1-q^{-1})s_5^{(t-4)}$	-0.14213	0.84481		14	$(1-q^{-1})s_{10}^{(t-1)}$	-0.06269	0.91400
3	$(1-q^{-1})s_8^{(t-4)}$	0.06449	0.86229		15	$(1-q^{-1})s_1^{(t)}$	0.05278	1.61400
4	$(1-q^{-1})s_3^{(t-2)}$	0.13863	0.94842		16	$(1-q^{-1})s_2^{(t)}$	0.07197	0.83951
5	$(1-q^{-1})s_4^{(t-2)}$	-0.20317	0.88582		17	$(1-q^{-1})s_3^{(t)}$	-0.13796	2.45840
6	$(1-q^{-1})s_7^{(t-2)}$	0.37119	1.21801		18	$(1-q^{-1})s_4^{(t)}$	-0.02998	2.24474
7	$(1-q^{-1})s_1^{(t-1)}$	-0.09405	0.85471		19	$(1-q^{-1})s_5^{(t)}$	-0.04362	1.94720
8	$(1-q^{-1})s_3^{(t-1)}$	-0.28725	1.64462		20	$(1-q^{-1})s_6^{(t)}$	-0.24511	1.22009
9	$(1-q^{-1})s_4^{(t-1)}$	-0.22753	1.54242		21	$(1-q^{-1})s_7^{(t)}$	0.75227	2.84803
10	$(1-q^{-1})s_5^{(t-1)}$	0.00147	1.06443		22	$(1-q^{-1})s_8^{(t)}$	-0.13120	1.88072
11	$(1-q^{-1})s_6^{(t-1)}$	-0.59538	0.92221		23	$(1-q^{-1})s_{10}^{(t)}$	0.24731	1.23607
12	$(1-q^{-1})s_7^{(t-1)}$	-0.03143	1.80960		24	$(1-q^{-1})s_{11}^{(t)}$	-0.03777	1.06831

Appendix F: Results of Partial Least Square Estimation

Table A.5 Percentage of Variance Explained by Latent Variables

Number of Latent Variables	Model Effects (%)		Dependent Variables (%)	
	Current	Total	Current	Total
1	15.5917	15.5917	76.1821	76.1821
2	20.1072	35.6989	7.7077	83.8898
3	9.3684	45.0672	6.9591	90.8489
4	12.616	57.6833	1.4366	92.2855
5	13.0862	70.7695	1.3161	93.6016
6	7.6245	78.394	0.8509	94.4525
7	2.5189	80.913	1.3834	95.836
8	5.0934	86.0064	0.2656	96.1016
9	0.9476	86.954	0.595	96.6966
10	0.9948	87.9488	0.395	97.0916

Table A.6 Regression Coefficient B

No.	Predictor	B		No.	Predictor	B
1	$(1-q^{-1})s_1^{(t-4)}$	-0.00295		13	$(1-q^{-1})s_8^{(t-1)}$	-0.03124
2	$(1-q^{-1})s_5^{(t-4)}$	-0.07369		14	$(1-q^{-1})s_{10}^{(t-1)}$	0.05272
3	$(1-q^{-1})s_8^{(t-4)}$	0.04627		15	$(1-q^{-1})s_1^{(t)}$	0.09544
4	$(1-q^{-1})s_3^{(t-2)}$	-0.02239		16	$(1-q^{-1})s_2^{(t)}$	0.03551
5	$(1-q^{-1})s_4^{(t-2)}$	-0.14135		17	$(1-q^{-1})s_3^{(t)}$	-0.25085
6	$(1-q^{-1})s_7^{(t-2)}$	0.19833		18	$(1-q^{-1})s_4^{(t)}$	-0.07654
7	$(1-q^{-1})s_1^{(t-1)}$	-0.06708		19	$(1-q^{-1})s_5^{(t)}$	-0.14277
8	$(1-q^{-1})s_3^{(t-1)}$	-0.00332		20	$(1-q^{-1})s_6^{(t)}$	-0.03152
9	$(1-q^{-1})s_4^{(t-1)}$	-0.13779		21	$(1-q^{-1})s_7^{(t)}$	0.63287
10	$(1-q^{-1})s_5^{(t-1)}$	0.00365		22	$(1-q^{-1})s_8^{(t)}$	-0.15118
11	$(1-q^{-1})s_6^{(t-1)}$	0.05853		23	$(1-q^{-1})s_{10}^{(t)}$	-0.02636
12	$(1-q^{-1})s_7^{(t-1)}$	0.13353		24	$(1-q^{-1})s_{11}^{(t)}$	-0.00588

Appendix F: Results of Partial Least Square Estimation (Continued)

Table A.7 Matrix $W(P^TW)^{-1}$

0.0981	0.1184	-0.2937	-0.0671	0.1614	0.0115	-0.1211	-0.1543	-0.2777
0.0853	0.1030	-0.3320	-0.1636	-0.0416	-0.2867	-0.2415	0.0031	-0.1945
0.0915	0.1248	-0.3311	-0.1683	0.0010	-0.1158	0.1513	0.4230	0.1306
-0.0976	0.2586	-0.1109	-0.2005	-0.1183	0.1166	-0.0912	-0.0588	0.2703
0.0797	-0.2724	-0.1579	-0.0732	-0.2737	-0.7027	0.0143	0.1231	0.1023
0.1446	-0.1463	0.0200	0.4585	0.4373	0.2628	0.3876	0.0295	-0.0456
-0.0982	0.2468	-0.1376	-0.0260	-0.0408	-0.0275	-0.0757	-0.3548	-0.7202
-0.2310	0.1041	0.1130	0.2678	-0.0693	-0.0939	0.1550	-0.0113	-0.2258
0.2093	-0.1019	-0.3140	-0.4380	-0.1832	-0.2984	-0.2134	-0.1396	0.1070
-0.1242	0.2688	-0.0965	-0.1842	-0.1653	-0.0548	0.0829	0.2448	0.3003
-0.0906	0.1443	0.3645	0.0643	0.1818	-0.0501	-0.0926	0.1017	-0.2684
0.2656	0.0230	-0.1141	0.1265	0.4077	0.4207	-0.0419	-0.3707	-0.1089
-0.1548	0.2160	0.0510	0.1519	-0.1224	-0.2794	-0.0759	-0.1968	0.1371
-0.0765	0.2734	0.3562	0.2578	0.2401	-0.2263	-0.4808	-0.1649	-0.0098
-0.2389	0.0403	-0.1355	0.1708	0.3586	0.5769	0.3515	0.1920	0.0056
-0.1083	0.0747	-0.1138	-0.0946	0.0687	-0.2293	0.3266	0.3766	0.5756
-0.3585	-0.3941	-0.3279	0.0025	0.0572	0.0339	-0.1391	-0.1223	-0.0245
0.3242	0.3285	0.0280	-0.2948	-0.5396	-0.7230	-0.1123	-0.5779	-0.4749
-0.2946	-0.0201	-0.1390	-0.0745	-0.2116	-0.2126	0.1252	0.0170	0.1537
-0.1731	-0.1173	0.0282	-0.2887	0.1699	0.2162	0.4279	0.0117	0.0748
0.3942	0.5384	0.4333	0.6301	0.6588	0.7654	0.4969	0.3907	0.4897
-0.2819	-0.1268	-0.1118	0.1892	0.1004	-0.0881	-0.1786	-0.3599	-0.0845
-0.1728	0.0233	0.1074	-0.0166	0.2916	-0.0056	-0.0537	-0.1426	-0.0017
-0.1526	-0.0162	0.1654	-0.1552	0.2400	0.1773	0.2017	-0.0706	-0.2082

Table A.8 Scores for Points 10, 33, and 56

$\mathbf{t}_{10}^T$	1.4300	4.4685	-0.5961	0.6465	-0.1329	-0.7059	1.2548	-0.1687	-0.3506
$\mathbf{t}_{33}^T$	1.3451	4.3501	0.7506	0.1393	-0.6887	-0.9764	0.0422	0.1284	-1.2530
$\mathbf{t}_{56}^T$	-3.3721	-5.3679	-1.2482	-1.0136	1.3881	2.7800	1.5272	-0.9628	0.1017

About the Author

Hui Wang received a Bachelor's Degree in Mechanical Engineering from Shanghai Jiao Tong University, Shanghai, China in 2001, and an M.S.E. in Mechanical Engineering at the University of Michigan, Ann Arbor in 2003. He is currently a Ph.D. student in the department of Industrial and Management Systems Engineering at the University of South Florida, Tampa.

While in the Ph.D. program at the University of South Florida, Hui Wang focuses on the research of modeling and quality control for manufacturing processes including traditional discrete manufacturing and micro/nano manufacturing. Currently, he has four publications in *ASME Transactions, Journal of Manufacturing Science and Engineering*, *IIE Transactions on Quality and Reliability*, and *Journal of Manufacturing Systems*. He also made paper presentations at annual meetings of ASME, IERC, and INFORMS. He is a member of INFORMS and IIE.